FACULDADE DE ENGENHARIA DA UNIVERSIDADE DO PORTO

INSTITUTO DE CIÊNCIAS BIOMÉDICAS ABEL SALAZAR

PEG-4MAL hydrogels functionalized with a laminin syndecan-binding peptide for 3D culture of neural stem cells

Andreia Patrícia Moura Gonçalves

THESIS SUBMITTED FOR THE DEGREE OF MASTER IN BIOENGINEERING

Supervisor: Dr. Isabel Freitas Amaral

Co-Supervisor: Dr. Ana Paula Pêgo

September 16, 2019

PEG-4MAL hydrogels functionalized with a laminin syndecan-binding peptide for 3D culture of neural stem cells

Author:
Andreia Gonçalves

Supervisor:
Isabel Freitas Amaral

Co-Supervisor:
Ana Paula Pêgo

Thesis submitted for the degree of Master in Bioengineering
(Molecular Biotechnology)

Faculdade de Engenharia da Universidade do Porto
Instituto de Ciências Biomédicas Abel Salazar

16 September, 2019

The work presented in this thesis was developed at the following institutions:

nBTT - nanoBiomaterials for Targeted Therapies Group

i3S - Instituto de Investigação e Inovação em Saúde

INEB - Instituto Nacional de Engenharia Biomédica

Universidade do Porto, Portugal

Confocal microscopy and quantitative image analysis were conducted at the Bioimaging i3S Scientific Platform, member of the PPBI (PPBI-POCI-01-0145-FEDER-022122), with the assistance of Maria Lázaro and Eduardo Conde-Sousa, respectively. This work was funded by projects NORTE-01-0145-FEDER-000008 and NORTE-01-0145-FEDER- 000012, supported by Norte Portugal Regional Operational Programme (NORTE 2020), under the PORTUGAL 2020 Partnership Agreement, through the European Regional Development Fund (ERDF) and FEDER - Fundo Europeu de Desenvolvimento Regional funds through the COMPETE 2020 - Operacional Programme for Competitiveness and Internationalisation (POCI), Portugal 2020; by Portuguese funds through FCT/MCTES in the framework of the project "Institute for Research and Innovation in Health Sciences" (POCI-01-0145-FEDER-007274), and by Santa Casa da Misericórdia de Lisboa through project COMBINE (Prémio Neurociências Melo e Castro 1068-2015).

Scientific Outputs:

1. Gonçalves, A.M., Barros, D., Amaral, I.F., Pêgo, A.P., A synthetic hydrogel functionalized with syndecan-binding motifs supports cell proliferation and neurite outgrowth of neural stem cells. Poster presented at: Interrogations at the Biointerface - Do organoids fill the in vivo/ in vitro gap?, 7th Advanced Summer School; 2019 Jun 27-28; Porto, Portugal.

2. Barros, D., Sousa, E.C., Gonçalves, A.M., Woojin, M.H., García, A.J., Amaral, I.F., Pêgo, A.P., Engineering Hydrogels with Affinity-Bound Laminin as 3D Neural Stem Cell Culture Systems, Biomaterials Science (2019).

Resumo

As lesões no sistema nervoso central (SNC), causadas por trauma ou doenças do foro neurológico, constituem um problema médico com elevada prevalência e alto impacto socioeconómico. Para melhorar a capacidade de regeneração do SNC, têm sido exploradas terapias celulares, particularmente as que se baseiam no transplante de células estaminais neurais (CEN). Contudo, a limitada sobrevivência celular, a diferenciação não controlada e a fraca integração no tecido hospedeiro, têm prejudicado a eficácia desta abordagem terapêutica.

Para superar estas barreiras, hidrogéis que mimetizam o microambiente dos nichos neurogénicos têm sido explorados como veículos para entrega de células, de modo a favorecer a sobrevivência, proliferação e diferenciação das CENs. Os hidrogéis sintéticos constituem uma opção atrativa para este propósito, uma vez que permitem o controlo independente sobre as suas propriedades bioquímicas e biofísicas; porém, o seu design requer a seleção de domínios promotores de adesão celular adequados. Dada a relevância da laminina nos nichos neurogénicos, vários péptidos derivados de laminina têm sido investigados. Em particular, ligandos adesivos de lamina que interagem com sindecanos são especialmente apelativos, dado o envolvimento destes recetores celulares na regulação da neurogénese e estaminalidade das CENs.

Neste trabalho, explorámos a sequência do péptido sindecano-ligante AG73 derivado da cadeia $\alpha 1$ da laminina de murganho com reconhecida capacidade de promover a extensão de neurites, de modo a conferir bioatividade a hidrogéis sintéticos baseados em poli(etileno glicol) de quatro braços com grupos maleimida terminais – PEG-4MAL. Com este propósito, o PEG-4MAL foi primeiramente funcionalizado com diferentes concentrações (0.01 – 2.00 mM) do péptido AG73 contendo um grupo tiol, e posteriormente reticulado usando uma combinação de "cross-linkers" degradáveis (péptido MMP2-sensitive) e não degradáveis (PEG-ditiol), com uma razão molar de 80:20.

Os hidrogéis PEG-4MAL funcionalizados com AG73 foram produzidos com sucesso e com uma elevada eficiência de imobilização do péptido ($> 96\%$), independentemente da concentração de AG73, de acordo com a medição dos tióis livres na solução da reação. Estudos reológicos subsequentes revelaram uma rigidez ($G' \approx 500$ Pa) comparável à do cérebro humano, para todos os hidrogéis biofuncionalizados. Mais ainda, a incorporação do péptido AG73 não influenciou significativamente os módulos de cisalhamento elástico (G') e viscoso (G''), para qualquer das concentrações testadas, preservando as propriedades viscoelásticas e mecânicas dos géis. A incorporação de uma sequência "scrambled" de AG73 resultou em géis PEG-4MAL com G' significativamente reduzido quando comparado com géis não modificados ou géis funcionalizados com igual concentração de AG73 bioativo.

O efeito da densidade do péptido AG73 no comportamento das CENs foi seguidamente explorado usando CENs humanas (hCEN) encapsuladas nos hidrogéis funcionalizados e cultivadas sob condições de diferenciação neuronal por um período de até 14 dias. Os hidrogéis de PEG-4MAL funcionalizados com AG73 mostraram uma maior capacidade para suportar a viabilidade e a diferenciação neuronal das hCEN, particularmente para as concentrações mais elevadas de péptido (1.00 e 2.00 mM). Isto foi verificado através da incubação dos géis celularizados com corantes vitais fluorescentes e de imuno-detecção de βIII-tubulina. Apesar disto, o número total de células ao dia 7 não foi variou significativamente com a incorporação de AG73.

Para ultrapassar a heterogeneidade da rede polimérica resultante da rápida cinética de gelificação dos hidrogéis de PEG-4MAL, e a fim de assegurar a integridade dos géis celularizados durante todo o período de cultura, procedeu-se à otimização da cinética de gelificação e da degradabilidade dos géis. A redução do pH da solução precursora de PEG-4MAL (até 6.5), e a subsequente redução da velocidade da reação tiol-MAL, permitiu aumentar o tempo de gelificação. Isto resultou num aumento da viabilidade e atividade metabólica das hCEN comparativamente a hidrogéis formados com soluções precursoras de PEG-4MAL a pH 7.4. Por outro lado, o uso de uma percentagem mais baixa de "cross-linker" degradável (razão molar de 60:40 de péptido MMP2-sensitive para PEG-ditiol) resultou em hidrogéis que mantiveram a sua integridade durante todo o tempo de cultura, sem afetar de forma negativa a diferenciação neuronal das hCEN. Por último, a cultura de hCEN nos hidrogéis AG73-PEG-4MAL otimizados revelou que o AG73 imobilizado é capaz de fornecer sinais de adesão celular favoráveis à viabilidade e diferenciação neuronal das hCEN. De facto, para géis funcionalizados com 1.00 mM de AG73 observou-se uma vasta distribuição de neurites com expressão de βIII-tubulina, contrariamente aos hidrogéis não modificados, onde não ocorreu extensão de neurites.

Em suma, este trabalho destaca o potencial de motivos adesivos sindecano-ligantes para a biofuncionalização de hidrogéis sintéticos quer para a cultura de hCEN, quer para a sua utilização como veículos de entrega de células estaminais neurais no contexto da regeneração do SNC. Por último, a estratégia de otimização estabelecida constitui um avanço no desenvolvimento de hidrogéis de PEG-4MAL mais reprodutíveis e homogéneos para utilização numa maior gama de aplicações em engenharia de tecidos.

Abstract

Central nervous system (CNS) damage, whether caused by trauma or neurological disorders, constitutes a highly prevalent condition with high socioeconomic burden. To improve the CNS limited capacity to spontaneously regenerate, cell-based therapies are being explored, with emphasis on the transplantation of neural stem cells (NSC); however, the limited cell survival, uncontrolled differentiation, and poor integration into the host tissue have hampered the efficacy of this therapeutic approach.

To surpass these hurdles, hydrogels mimicking the microenvironment of NSC niches have been explored as cell-delivery vehicles, to favor NSC survival, proliferation and differentiation. Synthetic-based engineered hydrogels constitute an attractive option for this purpose, by allowing an independent control over biochemical and biophysical properties. Given the key role of laminin in neurogenic niches, laminin-derived peptides have been investigated to render these hydrogels adhesive to NSC. Of these, laminin cell-binding ligands interacting with syndecans are particularly appealing due to the involvement of these receptors in the regulation of NSC stemness and neurogenesis.

In this work we explored the AG73 syndecan-binding peptide sequence from mouse laminin $\alpha 1$ chain with reported neurite promoting ability, to confer bioactivity to synthetic hydrogels based on a four-arm maleimide-terminated poly(ethylene glycol) – PEG-4MAL. To that end, PEG-4MAL was firstly functionalized with different input concentrations of a thiol-containing AG73 peptide (0.01 – 2 mM), and then crosslinked using a combination of protease degradable (MMP2-sensitive) and non-degradable (PEG-dithiol) cross-linkers, initially set at an 80:20 molar ratio.

AG73-functionalized PEG-4MAL hydrogels were successfully produced with a high ($> 96\%$) peptide binding efficiency, regardless of the input AG73 concentration, as determined by measuring unreacted/free thiols in the reaction buffer (AG73-PEG-4MAL precursor solution). Subsequently, rheological studies revealed a stiffness ($G' \approx 500$ Pa) comparable to that of human brain tissue, for all biofunctionalized hydrogels. Moreover, the tethering of AG73 peptide did not significantly impact the hydrogel's storage (G') and loss (G'') moduli, independently of the tested concentration, preserving the bulk mechanical and viscoelastic properties of the gels. Interestingly, the tethering of a scrambled sequence of AG73 resulted in PEG-4MAL gels with significantly reduced G', compared to plain gels or gels functionalized with an equal concentration of bioactive AG73.

The effect of AG73 density on NSC behavior was subsequently assessed using human NSC (hNSC) cultured under neuronal differentiation conditions within functionalized hydrogels for up to 14 days. PEG-4MAL hydrogels functionalized with AG73 showed a higher ability

to support hNSC viability and neuronal differentiation, particularly for the highest peptide concentrations tested (1.00 and 2.00 mM). This was verified by the incubation of the cell-laden gels with vital/dead dyes and immunolabelling of the early neuronal marker βIII-tubulin. In spite of this, total cell numbers at day 7 were not influenced by the grafting of AG73.

To overcome the polymer network heterogeneity resultant from the fast gelation kinetics of PEG-4MAL gels, and to ensure the overall integrity of cell-laden hydrogels over the entire culture period, the hydrogel gelation kinetics and degradability were subsequently optimized. By lowering the pH of the PEG-4MAL precursor solution (to 6.5), and thereby reducing the speed of the thiol-MAL reaction, slower gelation rates were achieved. This resulted in an increase in hNSC viability and metabolic activity compared to hydrogels prepared at a higher pH. In turn, the use of a lower percentage of degradable cross-linker (60:40 molar ratio of MMP2-sensitive peptide to PEG-dithiol) resulted in hydrogels maintaining their overall integrity throughout the culture, without negatively impacting hNSC neuronal differentiation. Finally, the culture of hNSC within the optimized AG73-PEG-4MAL hydrogels revealed that immobilized AG73 provides cell adhesiveness cues favoring hNSC cell viability and neuronal differentiation. In fact, when grafted at a concentration of 1.00 mM, a wide distribution of neurites expressing βIII-tubulin was observed, contrarily to plain hydrogels, which were not permissive to neurite extension.

Altogether, this work highlights the potential of syndecan-binding motifs for the functionalization of 3D synthetic hydrogel platforms designed for the culture of hNSC, and for use as vehicles of neural stem cells in the context of CNS regeneration. Also, the established optimization strategy constitutes a step forward for the development of more homogeneous and reproducible PEG-4MAL hydrogels, for use in a larger spectrum of tissue engineering applications.

Acknowledgements

This thesis has been a long and bumpy road. Despite teaching me how to become a scientist and appreciate the small eureka moments, it has also taught me that science is unexpected, and resilience is key. This journey, however, was not a lonely one. It counted with the continuous support of wonderful people to whom I owe a special word of appreciation.

First, I would like to express my gratitude to Dr Isabel Amaral, for always being an enthusiastic and inspiring supervisor, for all the patience and wisdom words, and above all, for always working alongside me. You have taught me a lot about the most diverse topics, and to that I am really thankful. Secondly, thanks to Dr Ana Paula Pêgo for giving me the opportunity to work in her laboratory and allowing me to put into practice much of the knowledge I have learned from her over the past years. Also, many thanks go to Daniela Barros, for allowing me to continue her work and for always helping, even with the most trivial questions.

To all the members of the i3S community which were somehow involved in the development of this work, particularly to María Lazaro for all the help regarding confocal microscopy, to Eduardo Conde-Sousa for all the assistance in image analysis, to Frederico Silva and Fátima Fonseca for the support in the HPLC studies, to Catarina Meireles and Emília Cardoso for all the guidance with flow cytometry, and also to Dalila and Ricardo for all the laboratory help.

To all the members of the nBTT group, thank you so much for all the fun, the friendly work environment, technical guidance and scientific advice. You are all wonderful people and hold a special place in my heart. A special mention to Sofia Guimarães, for making me believe I could overcome the small intricacies of life.

Besides all the people that worked directly with me during this thesis, I must also thank and spread my appreciation to friends and family. To Filipa for still putting up with me after 15 years and for always giving me the best advice and rides home. To Inês for all the continuous support and therapy sessions. To Sofia for all the hugs, vegan inspiration and confidence in my abilities. To Paula for all the silly talks and attempts to exercise. To Helena, Anabela, André, Mariana, Patrícia, Rafaela and other college friends, thank you for your partnership during this journey. You have been been part of my growth as both a person and a professional. And also, thank you to my family, without whom I certainly would not have achieved so much in my life. Specially to my mother, for unsurmountable support, love and undeserved patience. I cannot thank her enough for enduring endless days of stress and for making me feel loved even when I was too worried with work to be a good daughter.

Lastly, I want to thank the most important person in my life, António. Your patience, enthusiasm, love and encouragement have given me the strength to soldier through this process knowing you have my back. I look forward to sharing this great adventure of life with you. You are an inspiration to me every day.

Contents

List of Figures

List of Tables

Abbreviations

(b)FGF	(basic) Fibroblast Growth Factor
BBB	Blood Brain Barrier
BSA	Bovine Serum Albumin
BDNF	Brain Derived Neurotrophic Factor
CAMs	Cell Adhesion Molecules
CNS	Central Nervous System
CSF	Cerebrospinal Fluid
CS(PG)	Chondroitin Sulfate (Proteoglycans)
CNTF	Ciliary Neurotrophic Factor
G^*	Complex Modulus
CLSM	Confocal Laser Scanning Microscopy
DNA	Deoxyribonucleic acid
DRG	Dorsal root ganglia
ESC	Embryonic stem cell(s)
EGF	Epidermal growth factor
ECM	Extracellular matrix
FBS	Fetal bovine serum
PEG-4MAL	Four-arm maleimide-terminated poly(ethylene glycol)
GDNF	Glial cell-line-derived neurotrophic factor
GMEM	Glasgow Minimum Essential Medium
GAG	Glycosaminoglycan
HA	Hyaluronic acid
hNSC	Human Neural Stem Cell(s)
HS(PG)	Heparan sulfate (proteoglycans)
HPLC	High-Performance Liquid Chromatography
IF	Immunofluorescence
iPSC	Induced Pluripotent Stem Cell(s)
iNSC	Induced Neural Stem Cell(s)
LG	Laminin globular (domain)
LN	Laminin N-terminal (domain)

LVR	Linear Viscoelastic Region
G''	Loss Modulus
MAL	Maleimide
MMP	Matrix Metalloproteinase
MSC	Mesenchymal Stem Cell(s)
ξ	Mesh Size
NPC	Neural Progenitor Cell(s)
NSC	Neural Stem Cell(s)
NGF	Nerve Growth Factor
NOGO	Neurite Outgrowth inhibitor
NT-3	Neurotrophin-3
PNS	Peripheral Nervous System
δ	Phase Angle
PBS	Phosphate buffered saline
PEG	Poly(ethylene glycol)
SH-PEG-SH	Poly(ethylene glycol)- dithiol
PLA	Polylactic Acid
PLGA	Poly(lactic-co-glycolic) acid
PLG	Poly(lactide-co-glycolide)
PI	Propidium iodide
RT-qPCR	Reverse transcription quantitative polymerase chain reaction
RT	Room Temperature
SCI	Spinal Cord Injury
SD	Standard deviation
SEM	Standard error of the mean
G'	Storage Modulus
SGZ	Subgranular zone
SVZ	Subventricular zone
TBI	Traumatic Brain Injury
2D/3D	Two-dimensional/Three-dimensional
TCPS	Tissue culture polystyrene
w/v	Weight/Volume
E	Young's modulus

Chapter 1

Introduction

This chapter starts by briefly reviewing the most important components of the central nervous system (CNS), together with the main consequences of CNS damage and the challenges that it ensues. An overview of the current regenerative strategies being pursued to overcome tissue degeneration and promote CNS regeneration is provided, with emphasis on neural stem cell (NSC)-based therapies aimed at achieving tissue repair and functional recovery. A short introduction to the neurogenic niches, as well as to their most important biochemical and biophysical properties for mimicking the native NSC microenvironment *in vitro*, is also presented.

1.1 Central Nervous System: structure and function

The human **CNS** is a highly complex and specialized network of more than 100 billion individual nerve cells responsible for **crucial life functions** such as cognition, movement, senses, and emotions [1]. The CNS is comprised of the **brain**, and the **spinal cord**, with the brain coordinating higher-level functions, and the spinal cord working mainly as the communication pathway between the brain and the rest of the body [2].

Nervous tissue contains two main types of cells: **neurons** (nerve cells) and **glial/neuroglial cells**. While neurons constitute the **functional units of the CNS**, being unique in their ability to transmit and store information, glial cells play a vital role in supporting neuronal development and signaling. In fact, in the CNS, neurons are outnumbered by glial cells, that include **oligodendrocytes**, **astrocytes**, **microglial cells** and other specialized cells. Although they present anatomic and physiological differences, both the brain and spinal cord are composed of **grey matter** (neuronal cell bodies) and **white matter** (myelinated axons), therefore sharing many regulatory processes [1, 2].

Besides the cellular components comprising the CNS, the surrounding extracellular matrix (ECM) produced by neurons and glia – approximately 10-20 % of the total CNS volume [3] – forms a three-dimensional (3D) network that not only contributes as a biological scaffold for the structure of the nervous tissue, but also controls the diffusion and availability of molecules for biochemical signaling and communication; thus, it is extremely relevant in regulating both

biomechanical and physiological properties of the CNS [4] as further detailed in the section regarding the neurogenic niche (see 1.3.2).

In order to maintain the appropriate homeostatic conditions favoring neuronal functioning and signaling, including the highly controlled and stable microenvironment, the entire CNS is separated from the surrounding blood milieu by the **blood-brain barrier** (BBB), located at the level of endothelial cells - as illustrated in figure 1.1. Under normal conditions, the BBB prevents the entry of circulating immune cells and controls the paracellular diffusion of hydrophilic molecules into the brain by an elaborate network of complex tight junctions that interconnect the endothelial cells. Even though dissolved gases such as O_2 and CO_2 can freely diffuse across the BBB, the transport of larger molecules (such as nutrients) is dependent on active transport mechanisms, mediated by brain capillary endothelial cells [5, 6].

Besides the protection provided by the BBB, the CNS parenchyma is surrounded by a series of overlapping membranes that are collectively referred to as the **meninges** (figure 1.1). This protective triple-layered membrane consisting of fibrous connective tissue provides an additional barrier and interface between the CNS and the periphery, and encloses the cerebral spinal fluid (CSF), which serves as both a shock absorber and a nutrient/chemicals source and waste removal medium [7]. The meninges consist of three distinct cellular layers: (1) the *dura mater*, which is adjacent to the skull and consists of a dense highly innervated and vascularized collagenous membrane; (2) the *arachnoid mater*, which corresponds to a network of loose connective tissue lacking blood vessels and placed above the subarachnoid space through which CSF flows; (3) the *pia mater*, the innermost membrane covering the brain and spinal cord parenchyma [8]. Although the meninges have traditionally been considered structures that provide physical protection for the brain and spinal cord, recent studies have recognized these tissues as sites of active immunity. In fact, the meninges have been shown to play a role in both the normal immunosurveillance of the CNS (homeostasis), as well as in inflammatory conditions (pathology) [9].

1.2 CNS damage

All the different elements of the nervous tissue work together to maintain and regulate the microenvironment surrounding the neurons, thus ensuring proper functioning and coordination of the CNS. Nonetheless, upon damage, the organization of this complex system is challenged and its correct functioning might be compromised, possibly leading to severe consequences that may include long-term patient disability and impaired quality of life [11].

Different conditions leading to CNS injury range from infection, malignancy, trauma, ischemia to idiopathic degeneration, and include events of **traumatic brain and spinal cord injury** (usually induced by external physical insults), **stroke**, **neurodegenerative diseases** (*e.g.*, Alzheimer's disease, Parkinson's disease, multiple sclerosis, among others), **neurodevelopmental diseases** or even **cancer** [11]. These conditions affect millions of people worldwide and cover the entire age spectrum. Solely in the United States, every year, around 2.6 million people have some type of brain injury – whether as a result of trauma,

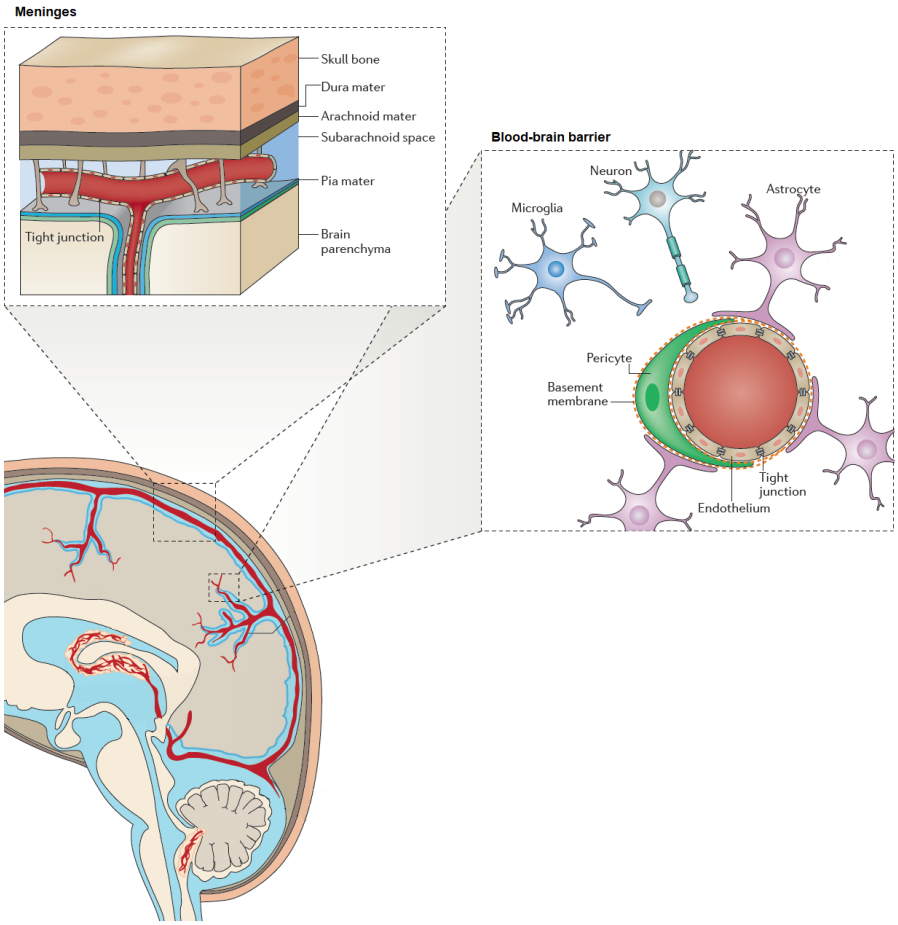

Figure 1.1: **Schematic representation of the meningeal and blood-brain barriers crucial for protecting the CNS and maintaining homeostasis.** Adapted with permission from [10]. Copyright © 2017, Springer Nature.

stroke, tumor or other illnesses –, and there are approximately 17,000 new spinal cord injury cases, which denotates the social and economic burden of this problem [12].

The common pathophysiological changes resulting from damage often lead to neurodegeneration, which includes progressive neuron atrophy/loss, demyelination, loss of glial support, and the subsequent alteration of the environment at the injured site [11]. For instance, **physical insults to the brain or spinal cord tissue** initially cause direct damage to neural cells and the vasculature, following a cascade of secondary events that lead to additional cell death, demyelination, axonal degeneration, formation of a glial scar, and an inhibitory environment for regeneration [13]. Particularly relevant after traumatic injury is the increased permeability of the BBB and the blood-spinal cord barrier – a hallmark of CNS injury/disease –, that results in the infiltration of inflammatory cells into the CNS; this activates astrocytes, favoring the inhibitory environment of the reactive glial scar, which in turn severely limits neuronal regeneration [14]. Additionally, after penetrating injuries that open the dura mater (outermost meningeal layer), fibroblast-like stromal cells (derived from the meninges) or pericytes can interact with the astroglial component of the scar and form a fibrotic-like layer internal to the astroglial capsule, which helps to seal the lesion, but may also contribute to blocking regeneration [15, 16]. Ergo, the physical and chemical

barrier formed at the lesion site hinders the reconstruction of the neural circuit and often culminates in devasting consequences including permanent loss of locomotor, sensory and cognitive functions [14].

On the other hand, in many cases of **cerebral ischemia**, the core region of necrotic brain tissue is usually surrounded by a penumbra area containing partially injured brain tissue [17]. In this condition, glial scarring and inhibitory/repulsive molecules at and around the lesion site are responsible for limiting regeneration and plasticity [14]. Moreover, in the case of **neurodegenerative disorders**, progressive CNS atrophy and neural cell death are commonly noticed [6]. Given this, it is evident that most neurologic disorders share common characteristics regarding the response to damage, including injury to neural cells, BBB permeabilization, immune cell infiltration, formation of a glial scar and consequential neurodegeneration.

It is currently accepted that unlike the peripheral nervous system (PNS), which has intrinsic repair and regeneration abilities, the CNS has a limited capacity to spontaneously self-repair and regenerate, meaning it is unable to replace injury-induced lost cells [18]. Although the reasons for this poor regeneration potential are not fully understood, it is thought to be related to the fact that **most mature neurons are post-mitotic cells incapable of cell division** and to an overall **absence of axon-growth promoting factors and presence of axonal growth inhibitory/repulsive molecules** (*e.g.*, Neurite outgrowth inhibitor (NOGO) proteins, myelin-associated glycoproteins and chondroitin sulphate proteoglycans [19, 20]). Hence, the hostile, non-permissive native extracellular environment developed after injury, characterized by the delayed removal of inhibitory myelin (compared to the PNS) and the rapid formation of glial scarring, counteracts remyelination and axon repair/regeneration [21]. A schematic representation of the main molecular and cellular changes occurred in the brain upon damage is shown in figure 1.2.

1.3 CNS regeneration and repair

For many years, the human adult CNS was thought to be a tissue lacking regenerative and self-repair potential. According to Ramón y Cajal (1852-1934), a pioneer of modern neuroscience, "in the adult CNS, the neural circuits were thought to be fixed in some degree, terminated and unchangeable; each neuron would die, but not regenerate". Nonetheless, in 1965, this dogma was shattered by Joseph Altman who first detected the constant neuronal mitosis in the adult brain using thymidine as a sensitive marker for mitosis [23]. Indeed, in his studies, endogenous neurogenesis could be observed both in the brain hippocampus [24] and olfactory bulb [25], thus showing that the brain has intrinsic regenerative capacity, although it may be limited.

Further seminal studies by David and Aguayo showed that adult rat CNS neurons could regenerate when presented with the appropriate environment. In those studies, axons from spinal cord neurons were able to regenerate for long distances within PNS grafts. This proved that mature neurons still retain some regenerative capacity and that the adult non-permissive CNS environment can be manipulated to induce regeneration [26]. Later, several other studies suggested that, under normal conditions, neurogenesis is observed in the subventricular

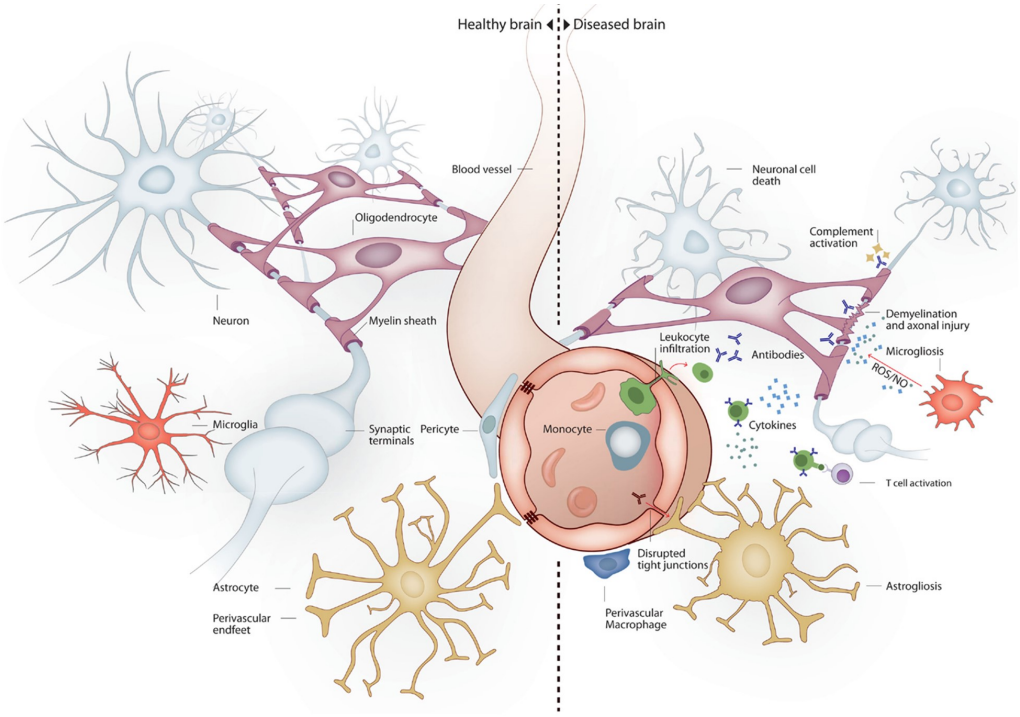

Figure 1.2: **Schematic representation of the typical architectural and environmental changes occurred in the brain upon damage/disease**. Upon damage, several alterations in cellular signaling and ECM environment are induced. Reproduced with permission from [22]. Copyright © 2015 Sankowski, Mader and Valdés-Ferrer.

zone (SVZ) of the lateral ventricules, the subgranular zone (SGZ) of the dentate gyrus in the hippocampus, and the central canal of the spinal cord of adult mammalians [27–31].

After traumatic brain or spinal cord injury (TBI and SCI, respectively), neurogenesis is sometimes observed within the first few months following injury [32]. In TBI, this can be interpreted as the injured brain attempting to repair through the recapitulation of developmental processes [33–35]. On the other hand, in SCI, the massive migration of neural progenitor cells capable of converting into mature functional neurons demonstrates that adult spinal cord neurogenesis is greatly amplified compared to normal conditions [36, 37]. Additionally, in the case of stroke, there is plenty experimental evidence supporting the idea that the stroke-damaged brain attempts to self-repair by producing new neurons, even in non-neurogenic areas (*e.g.*, the striatum and the cerebral cortex) [38].

These significant findings, coupled with others that have characterized the inhibitory environment within the damaged CNS tissue, have revealed that both physiological and reparative regeneration occurs within the CNS to sustain tissue homeostasis and repair. Importantly, the proliferation and differentiation of endogenous NSC residing within the healthy CNS, or surviving injury, are considered crucial in sustaining these events [39]. However, endogenous mechanisms of repair and regeneration are insufficient to result in significant functional restoration on their own. In fact, upon migration to injured/damaged regions, few neuroblasts survive to reach full neuronal differentiation; those that do often remain confined to the lesion border and are thus incapable of replacing extensive neuronal tissue loss, with only 0.2% of lost neurons being replaced, as shown by Martino et al. [40].

This knowledge has prompted the development of innovative regenerative strategies directed to replace lost neural cells and to induce neural growth, especially axonal regeneration and its subsequent myelination by oligodendrocytes. Ultimately, these strategies will contribute to rebuild the neural network connections, thus restoring the CNS tissue architecture and function [11]. Moreover, it is important to highlight that these novel therapies are also encouraged by the few effective pharmacological-based treatments available for acute neurological trauma or chronic neurodegenerative diseases. This is mostly related to the limited diffusion of drugs and other bioactive molecules across the BBB, which further restricts the utility of common administration methods (*e.g.*, oral and intravenous) and hinders the development of improved therapies [14].

1.3.1 CNS regenerative strategies

Several innovative therapeutical strategies are currently being pursued to overcome the CNS limited regenerative potential, from which two stand out: the **delivery of bioactive molecules** (such as small molecules, growth factors, and antibodies) which aims at promoting plasticity, axonal regeneration, neuroprotection and neurogenesis [32, 41], and **cell-based therapies** designed to promote neural cell replacement or neural survival through paracrine effects [42]. For both types of therapeutic approach, tailoring to the tissue target and pathological state needs to be made according to the differences found in anatomy, physiology and induced damaged.

1.3.1.1 Delivery of bioactive molecules

The delivery of bioactive biomolecules after CNS damage/injury has led to promising results both in pre-clinical studies and in clinical trials [14, 43]. It mainly concerns the use of neuroprotective molecules, which act on a variety of cellular targets, such as antiapoptotic pathways to prevent cell death and neuronal degeneration, anti-inflammatory pathways to inhibit microglial activation, or even particular genes/gene families known to be related to the glial scar formation or contributing to the establishment of an hostile environment at the lesion site [1, 44].

Several growth factors have been explored for their regenerative and neuroprotective potential. Particularly, nerve growth factor (NGF), brain-derived neurotrophic factor (BDNF), neurotrophin-3 (NT-3), ciliary neurotrophic factor (CNTF), glial cell-line-derived neurotrophic factor (GDNF) and fibroblast growth factor (FGF-1 and FGF-2) all are known to promote axonal outgrowth and enhance the survival of sensory and/or motor neurons [45–47].

Even though promising in limiting degeneration and promoting neuroregeneration, these strategies still present several restrictions. First, the CNS is an immunologically privileged site, with the BBB preventing the brain uptake of most pharmaceutical molecules. This means that systemic delivery is only suitable for molecules that can cross the BBB or the blood spinal cord barrier. Even for those bioactive molecules, the administration of high doses is necessary to ascertain a therapeutic effect, which might result in undesirable side effects. In the case of molecules incapable of crossing the BBB, local delivery is required.

Local injections can be performed into the epidural or intrathecal spaces of the spinal cord, into the ventricles in the brain, or directly into the tissue; however, these are often invasive and present their own disadvantages [48].

1.3.1.2 Cell-based therapies

Cell-based therapies for the treatment of CNS injury and disease include the **transplantation of exogenous/donor cells** and the **stimulation of endogenous neurogenesis**. Both these strategies aim to replace lost cells, provide trophic/neuroprotective support to the spared tissue and promote host tissue neural repair mechanisms, including neurogenesis, gliogenesis and angiogenesis [49].

There are several possible choices regarding the type and source of cells to use in transplantation (as reviewed in [49, 50]), but neural stem or progenitor cells (NSC/NPC) stand out as the most promising ones, owing largely to their proliferative and multipotent nature, which allows its application for a wide range of conditions demanding regenerative/repair [51, 52]. Besides being capable of self-renewal, these cells have the ability to differentiate into committed neural sub-types (including neurons, astrocytes and oligodendrocytes) and, as such, can contribute to the replacement of injury-induced lost cells. Moreover, NSC transplantation is thought to support the regeneration of the damaged CNS not only by re-establishing the cytoarchitecture and neuronal circuitry of the CNS (direct cell replacement), but also through *bystander effects* (namely immunomodulation and enhancement of endogenous repair mechanisms), both aiming at restoring lost neurological function [53] - as schematically illustrated in figure 1.3.

Human NSC (hNSC) derived from pluripotent cells (including embryonic stem (ES) or induced pluripotent stem (iPS) cells) or isolated from fetal CNS tissue can be used as undifferentiated cells, relying on the host signals to stimulate their proliferation and differentiation, or their differentiated progeny can be utilized. Additionally, they can also be directly converted from somatic cells, such as skin fibroblasts, urine cells and blood cells, easily harvested in a clinical context, giving rise to the so-called induced NSC (iNSC) [56]. The most important NSC sources are illustrated in figure 1.3.

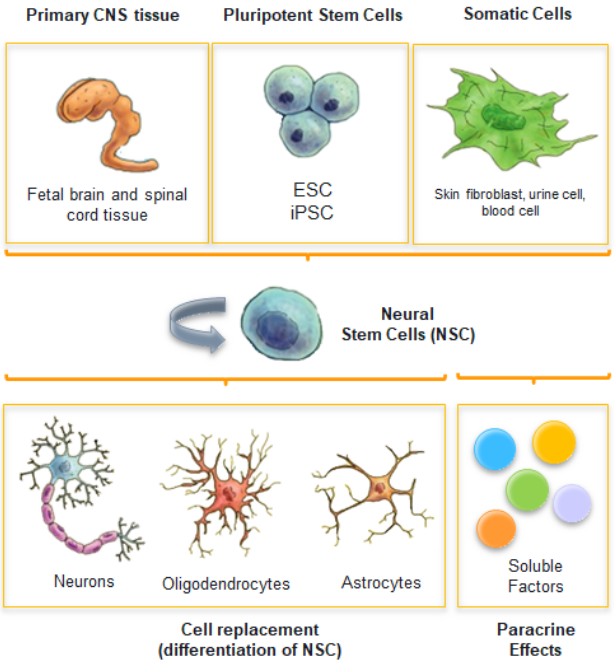

Figure 1.3: **Common NSC sources and therapeutic applicability of NSC after cell transplantation.** There are three main sources to generate NSC: isolation from primary CNS tissue; differentiation of pluripotent stem cells, and lineage reprogramming of somatic cells. Once on the injury site, NSC can be differentiated and secrete paracrine factors that support neurological repair and regeneration. Adapted with permission from [54] (Copyright © 2019 Pereira et al.) and [55] (Copyright © 2012 Olynik and Rastegar).

NSC expansion and differentiation

NSC, either isolated from *in vivo* sources or *in vitro* derived from pluripotent stem cells, can be expanded *in vitro* according to a neurosphere or a monolayer-based culture system (as schematically presented in figure 1.4). Both protocols have allowed the isolation and growth of developmental stage specific NSC populations, which can then be used for a variety of procedures, including transplantation [57].

First developed by Reynolds and Weiss, the neurosphere-based suspension assay demonstrates that NSC cultured as floating spherical aggregates (neurospheres) can be stimulated to proliferate when exposed to mitogens like epidermal growth factor (EGF) and FGF. These growth factors are crucial for maintaining the proliferative and self-renewal capacity of the NSC [27]. Although neurosphere-based neurodifferentiation protocols are commonly used to obtain neural progenitor cells (NPC), their tendency to clump in culture hinders the study and identification of neuronal cell types that can be derived after neurosphere transplantation [58]. Additionally, they usually give rise to considerably heterogeneous NSC populations, due to the exposure of cells to concentration gradients of nutrients, oxygen, endogenous/exogenous soluble factors and metabolic by-products, existing from the outer edge to the core of the aggregate [59, 60]. It is however worth noticing that depending on the protocol used, neurosphere-derived cells can exhibit promising neurogenic and gliogenic potentials [61].

Alternatively, the monolayer culture system allows the generation of pure NSC adherent cultures that can be stably maintained over several passages, while overcoming the limitations

of the neurosphere-based culture system. In this case, the expansion of progenitor cells occurs in a defined basal media supplemented with EGF and FGF. These conditions lead to the formation of a culture with homogeneous morphology and capacity to differentiate into neurons, astrocytes and oligodendrocytes [60].

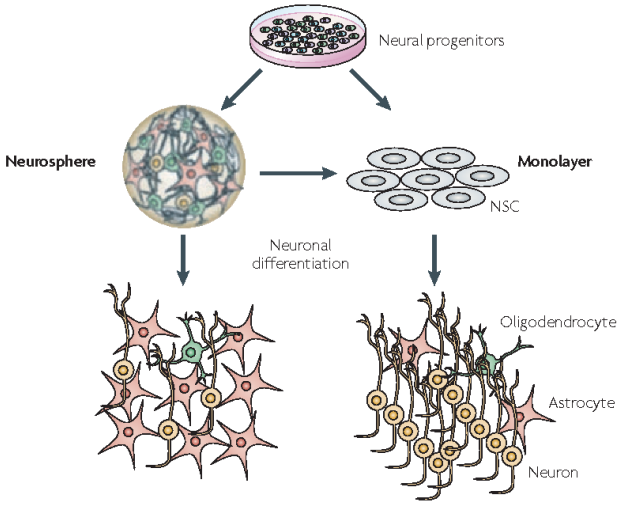

Figure 1.4: **Commonly applied neurosphere- and monolayer-based culture systems.** Adapted with permission from [60]. Copyright © 2010, Springer Nature.

Different CNS disorders resulting from damage have already shown promise as targets for NSC transplantation, both in pre-clinical and clinical trials (as comprehensively reviewed in [56, 62]). Studies using transplanted NSPC revealed the capacity of these cells to divide, differentiate and integrate into the injured tissue, partly overcoming functional deficits in animal models of SCI and ischemic stroke [56, 63]. Still regarding SCI, already in 2010, two trials were authorized for the use of hESC-derived oligodendrocyte progenitors (Geron Corporation) and fetal-derived NSC (StemCells, Inc.), which had previously demonstrated remyelinating and nerve-growth-stimulating properties leading to restoration of locomotor function in rat and mouse models of acute contusion SCI, respectively [64, 65]. Moreover, when transplanted after TBI, NSC have shown to promote motor and cognitive recovery [66]. This demonstrates the adapting ability of these cells to the surrounding environment, and its evolution according to the signals found *in vivo* (either in the brain or in the spinal cord).

Although the available clinical trials suggest the safety of NSC transplantation [56], the clinical implementation of NSC-based therapies still presents limited success, which owes to several ongoing challenges:

(a) **Cell distribution**: exogenously transplanted cells are usually delivered using saline solutions or culture media, which potentiates cellular aggregation, even before engraftment, as well as rapid clearance from the injection site [67].

(b) **Cell survival/viability**: cell suspension grafts reveal limited cell survival upon transplantation, particularly when compared to tissue grafts. This lower survival is thought to be linked to the absence of a 3D network and a reduced accessibility of extracellular adhesive proteins to which the donor cells can attach and use as scaffold for the establishment of

cell-cell and cell-substrate interactions. Moreover, the inhospitable environment formed at the injured site further limits cell viability and proliferation [68].

(c) **Host integration**: cell integration into the host tissue is often limited by physical and chemical barriers present at the lesion site, including oxidative stress, hypoxia and the host immune response; indeed, different studies have shown that less than 5% of transplanted cells remain at the site of injection within days of transplantation [69].

(d) **Cell differentiation**: the direct use of stem cells in its heterogeneous and undifferentiated state often culminates in an undefined/uncontrolled phenotypic distribution of the grafted cells upon transplantation [68].

Importantly, most experimental studies regarding the use of neural lineage-committed progenitors, have successfully promoted site-specific repair in focal CNS disorders, but have failed to foster substantial repair in disease models where the anatomical and functional damage is widespread [67]. This suggests that the clinical translation of NSC still demands a better understanding of the *in vivo* behavior of engrafted cells, so as to achieve broader and more substantial results regarding neuroregeneration and repair, but also to optimize the timing and route of transplantation, and anticipate potential side-effects.

1.3.2 Neurogenic niches

As previously mentioned, in order to achieve long-term functional integration of transplanted NSC into the host CNS and better support their survival and differentiation, a greater understanding of the surrounding microenvironment, as well as the underlying mechanisms controlling NSC fate is still needed. For that, it is important to focus on the contents and features typically found at the native NSC microenvironment – neurogenic niches. These are instrumental for getting insight into the complex interplay established between cells, ECM components and soluble factors, as well for trying to dismantle some of the individual cues leading neurogenesis during development and in the adult.

The neurogenic niche is a dynamic and complex microenvironment composed of several cell types and an intricate ECM. The most important cell players of the niche include quiescent NSC (type B cells), transit-amplifying cells (type C cells), migratory neuroblasts (type A cells) and oligodendrocyte precursors (both originated from type C cells), support cells (endothelial cells and astrocytes) and ependymal cells (absent in the SGZ) [70] - as illustrated in figure 1.5. The main function of the neurogenic niche is to support NSC and regulate their fate/behavior throughout development, in adulthood and also as a response to physiological and pathological stimuli [71]. Depending on intrinsic (cell specific) and extrinsic (environmental specific) cues, the niche determines whether the cells remain quiescent or divide and provides signals that guide early stages of differentiation (neuronal or glial) [72]. Furthermore, neurogenic niches are characterized by a high vascular density and a precise interaction with the cerebrospinal fluid (CSF). Both the vasculature and the CSF represent an important source of signaling molecules, which are mainly modulated by external factors [73].

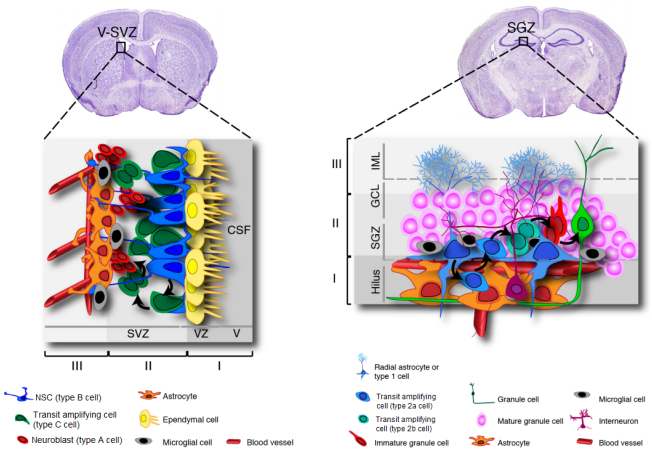

Figure 1.5: **Schematic representation of the different elements composing the adult SVZ and SGZ niches present in the brain**. Adapted with permission from [39]. Copyright © 2013 Donegà, M., et al.

1.3.2.1 Extracellular Matrix: developing brain *vs.* adult brain

As mentioned earlier, the ECM is a major part of the neurogenic niche. Besides providing many of the features required to form intricate networks with precise control over the distribution and connectivity of millions of neuronal and non-neuronal cells (namely structural support for cells to adhere, proliferate and migrate), the ECM also acts as a source of molecular signaling during development and adulthood. Indeed, the ECM is vital for the continuous process of cell proliferation, migration and differentiation required during the formation of the CNS [74]. But what exactly are the ECM components contributing to this tight and complex regulation allowing the correct wiring of the nervous system?

The main and best described component of the niche are **laminins**, a family of heterotrimeric glycoproteins made from combinations of five alpha (α), three beta (β) and three gamma (γ) subunits, which assemble into cross-shaped molecules [75] (as illustrated in figure 1.6A). Laminins play a key role in the formation and maintenance of the basement membrane architecture and properties, as well as on the modulation of several biological functions, including cell adhesion, migration, differentiation and matrix-mediated signaling [76]. The presence of laminin in the niche is both abundant and diverse; in fact, multiple laminin isoforms have been described in the SVZ, suggesting significant laminin trimer heterogeneity within the niche [74, 77]. Interestingly, several studies have shown that distinct laminin isoforms will signal from different niche components at different times of development, thus playing a crucial role in coordinating developmental processes. In the embryonic niche, the α1 chain (part of the classic laminin-111) is only present at low levels, while α2 and α4 chains are much more highly expressed [78]. Contrarily, heterotrimers containing the α5 chain (*e.g.*, laminin-511 and -521) have been identified as the major neuronal laminins in adulthood [79, 80].

Regarding the structural composition of laminins, it is important to highlight that the α-chain includes a long arm consisting of a coiled-coil region which terminates in a large globular domain formed by five laminin globular (LG) domains (LG1-LG5) [81]. The coiled-coil is

thought to help to orientate the LG domains, so they can be available to interact with cells, via cell surface receptors, including integrins [82], syndecans and dystroglycan [83], and bind to growth factors [84] and other ECM proteins [81] (as schematically shown in figure 1.6B).

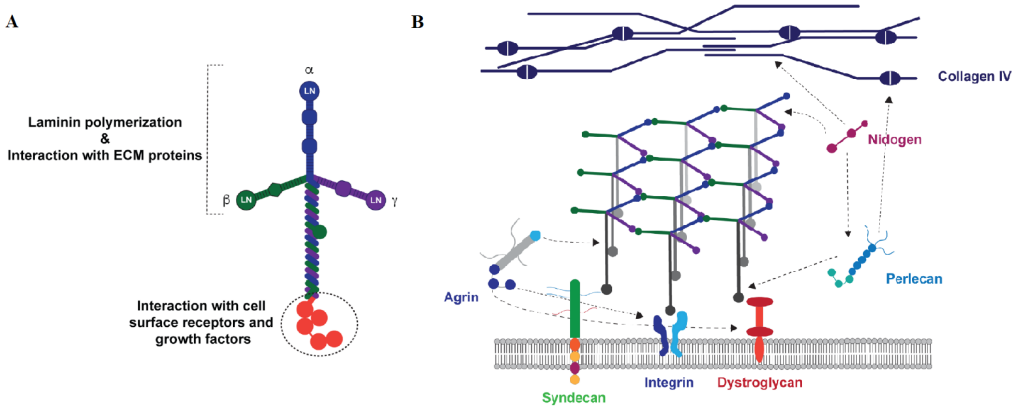

Figure 1.6: **Schematic representation of laminin's structure and main biological interactions.**(A) Representative model of laminin structure and domain architecture. The three α, β and γ polypeptidic domains composing laminin are presented in blue, green and purple, respectively. Adapted with permission from [80]. Copyright © 2013 Landes Bioscience. (B) Schematic representation of the supramolecular assembly of the basal membrane, in which laminin interacts with other ECM proteins and several cell receptors. Adapted with permission from [85]. Copyright © 2012 Landes Bioscience.

Other ECM proteins expressed in the neurogenic environment are **Tenascin C** (TnC) (abundant in both the embryonic and adult niche), **fibronectin**, **nidogen**, **perlecan** and **collagen IV** (expressed in lower levels), and also **chondroitin sulfate proteoglycans** (CSPG) and **heparan sulfate proteoglycans** (HSPG), expressed in higher levels [74]. NSC have cell adhesion molecules (CAMs) located on their surface through which they interact with other cells and the ECM components surrounding them. Integrins, immunoglobulins, selectins and cadherins are families of CAMs that interact with fibronectin, laminin, collagen IV, TnC, CSPG and HSPG. These cell receptors are involved on signaling transduction pathways that regulate cell survival, proliferation, differentiation and migration [86].

Even though the adult brain still presents defined germinal regions that support neurogenesis, there are differences that distinguish them from the embryonic proliferative environments, particularly regarding ECM composition and expression levels. Indeed, during neural development, NSC continuously divide symmetrically to increase in number; however, in the adult context, NSC are kept in a quiescent state [87].

Besides the highly abundant presence of interstitial laminin (common to the two stages of maturation), other complex ECM structures are found within the adult neurogenic niche, namely finger-like processes of basal lamina identified as **fractones** [88]. These structures consist mainly of laminin, collagen IV, nidogen and perlecan aggregates and are known to extend from the blood vessels, establishing connections with the cells present in the niche. Fractones are thought to present both a structural role in guiding cell migration, and a role in signal guidance, since they participate in activating and presenting several trophic factors to the cells within the niche [89]. Additionally, also CS and HS proteoglycans are highly expressed in the adult niches [74].

It is also relevant to highlight that besides ECM composition, ECM mechanical properties (*i.e.*, architecture and rigidity) play a pivotal role in regulating NSC behavior, tissue development and homeostasis [90]. The process through which cells sense and respond to the mechanical properties of their surrounding tissues is termed mechanotransduction and has been shown to have a major impact in cell behavior (both under physiological and pathological conditions) [91]. The mechanical properties sensed by cells are intrinsically related to the ECM composition and organization found in the tissues; particularly, in the case of the CNS, the soft mechanical properties are related to presence of glycosaminoglycans (GAGs), including hyaluronic acid (HA), proteoglycans such as lecticans and glycoproteins [77].

Taken together, it is clear that ECM has functions beyond passive provision of a supportive framework: it actively influences cell migration and axonal guidance during development and plays an important role in maintaining synaptic stability and controlling tissue remodeling in adulthood. This is achieved through an appropriate spatiotemporal dialog between the cells and the surrounding elements of the niche [77].

Although the intrinsic regulatory mechanisms controlling each process (particularly cell proliferation and renewal) are not yet fully understood, most of the elements present in the neurogenic niches (during both development and in the adult) are already known, which means there is some clue on how to mimic these complex microenvironments towards the recapitulation of *in vivo* developmental processes. Additionally, in the last few years, a lot of emphasis has been put on developing well-defined and tunable 3D platforms that better replicate the physical and chemical elements of the native neurogenic niches [14, 92]. These systems, comparatively to the traditional two-dimensional (2D) culture systems, are expected to provide more accurate insights into the *in vivo* cell physiology and interactions with the surrounding microenvironment, as well as contribute to the design of more effective NSC-based therapies in context of CNS tissue regeneration/repair.

This transition into biomimetic, pro-regenerative 3D constructs/scaffolds that aim to promote NSC survival, proliferation and differentiation, and ultimately try to augment functional neural tissue repair and regeneration will be throughout explored in the following section.

Chapter 2

Neural Tissue Engineering

This section will comprise the current state-of-the-art regarding the design of biomaterial-based vehicles for the culture/delivery of NSC in the context of neural tissue regeneration and repair. In accordance to the scope of this thesis, a great emphasis will be put on describing NSC vehicles based on synthetic hydrogels biofunctionalized with laminin-derived peptides and their biological performance.

2.1 Hydrogels: NSC delivery vehicles

One of the current approaches being investigated to surpass the limitations associated with NSC-based therapies comprises the engineering of biomaterial-based NSC vehicles, which closely mimic the microenvironment found in neurogenic niches and, therefore, promote the survival, proliferation and differentiation of NSC. These systems have revolutionized the field of neural regenerative engineering by providing the conducive conditions necessary for cells to communicate with the surrounding environment, as naturally promoted *in vivo* by cell-cell and cell-ECM interactions [93, 94]. As discussed in the previous section, this is achieved by recapitulating the main features of the native ECM regarding biochemical composition, biomechanical properties, and structural/topographical features [95].

Although cell-instructive matrices obtained from different biomaterials have been investigated for neural applications, their design must satisfy several biological and physical criteria common to all. Besides being **biocompatible** (unable to cause toxic or undesirable effects) and **biodegradable**, these materials should be able to **mimic** the **mechanical properties** (*e.g.*, stiffness and viscoelasticity), **permeability** and **porosity** of the target tissue (either brain or spinal cord). Particularly, being able to control the rate and mechanism of **matrix degradation** constitutes a vital feature when designing biomaterial constructs that aim to promote tissue regeneration and repair; the cell-induced remodeling of the matrix allows a better integration of the surrounding tissue (*e.g.*, cell infiltration), which in the long term can lead to the development of functional tissues capable of recovering lost neurological functions [96, 97]. However, it is important to highlight that even though slow degrading materials would be preferred to ensure physical support to the transplanted cells, and allow them to develop their own ECM, extend processes, and integrate into neural networks, these can lead

to an increased inflammatory response *in vivo*. Therefore, there needs to be a compromise between the cell supportive nature and the rate of degradation of the materials chosen to avoid any additional immune response [98].

Over the last few years, a wide range of biomaterials have been explored to assist NSC transplantation [99]. Hydrogels constitute one of the most attractive options for this purpose, mainly due to their biocompatibility, highly hydrated nature (which retains protein biological activity), good permeability and elasticity, which can be easily tuned to mimic the CNS-specific ECM microenvironment, in particular, its soft mechanical properties [92, 100, 101]. Based on these features, hydrogels can be used to produce bioengineered scaffolds that provide physical support to cells (including cell transplantation, by reducing the exposure of cells to shear stress during the injection process), as well as relevant trophic cues to transplanted and host cells with spatial and temporal control [102]. Hence, hydrogels can work as biomimetics of the neural ECM, thereby providing a permissive microenvironment for NSC engraftment and neuronal regeneration [103]. Evidently, the treatment of specific CNS pathological conditions involving neurodegeneration might require the introduction of additional factors (such as proteins, small molecules or even drugs) other than NSC/NSPC – as schematically illustrated in figure 2.1.

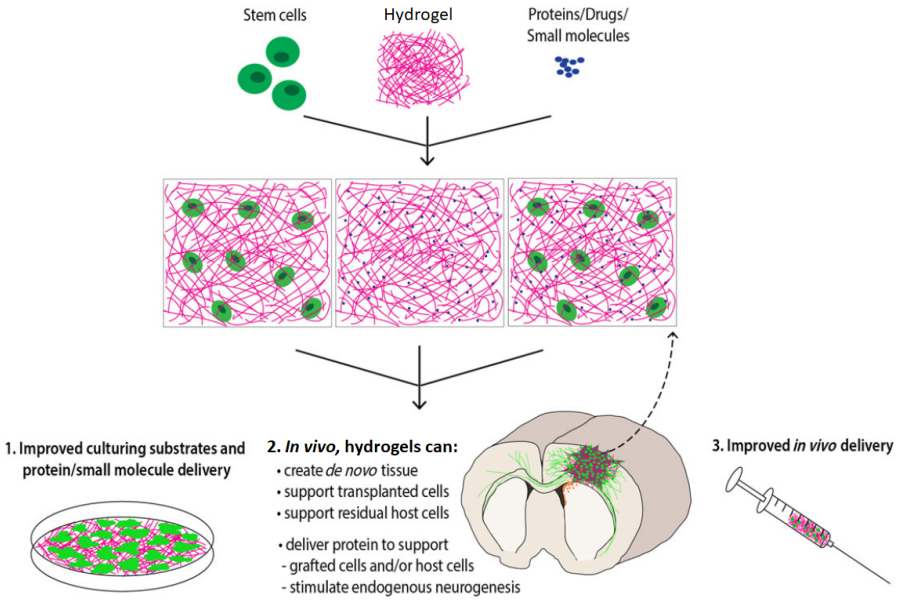

Figure 2.1: **Hydrogel applications in the context of neuroregeneration and repair.** Adapted with permission from [102]. Copyright © 2018, British Journal of Pharmacology.

Numerous studies using hydrogel-based biomaterials targeted at modelling the native 3D neural environment have demonstrated that neural progenitors cultured on these scaffolds adopt more in *vivo-like* morphologies and survive longer than those cultured on conventionally coated culture-ware. Moreover, many of these biocompatible scaffolds have also been shown to enhance survival and integration of transplanted neural progenitors, thus indicating that hydrogels are indeed capable of appropriately mimicking the CNS tissue [104, 105].

2.1.1 Hydrogel's Properties

Hydrogels are 3D cross-linked polymeric networks made from hydrophilic polymer chains. Their hydrophilic structure allows them to retain considerable amounts of water or biological fluids [106], which together with their porous structure and soft consistency makes them ideal candidates for filling irregular voids and interfacing with the surrounding tissue, while providing an aqueous environment in which cells can interact (as represented in figure 2.2) [107].

When compared to other biomaterials, hydrogels present highly tunable properties, thus allowing the control of different important parameters (e.g., porosity, mechanical strength, degradability) for the recapitulation of the physical and chemical environment found *in vivo*. Particularly, hydrogels' 3D structure and porosity can be controlled to allow for cellular infiltration and neurite outgrowth. Moreover, hydrogel's mechanical properties can also be manipulated to mimic those of the native CNS tissue to ensure that the cells within the hydrogel receive the appropriate mechanical growth cues. This is usually achieved by controlling the density or molecular weight of the polymer or the degree of cross-linking in the gel matrix [108, 109].

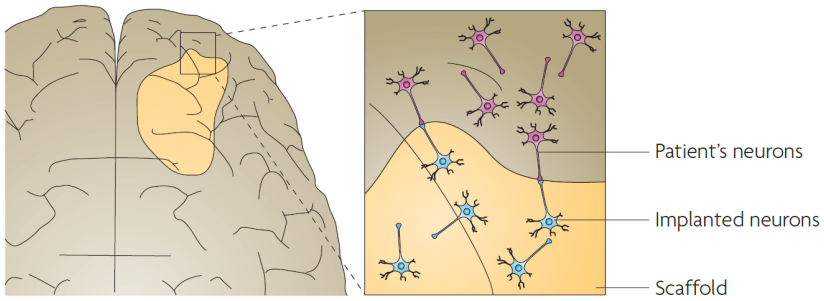

Figure 2.2: **Hydrogel-assisted integration with the host tissue.** Schematic representation of cell-cell interactions established between exogenous transplated cells and endogenous neurons in the presence of an injectable scaffold placed onto damaged brain tissue; the scaffold adapts to the lesion shape, protecting the damaged area and allowing mutual cellular infiltration, potentially promoting local tissue regeneration. Adapted with permission from [110]. Copyright © 2009, Springer Nature.

As previously discussed, NSC fate and lineage commitment are strongly influenced by the mechanical properties of the surrounding environment. As shown by different studies testing the effect of niche mechanics on hNSC behavior, softer substrates (with stiffness similar to the brain tissue) tend to guide NSC differentiation along the neuronal lineage, while substrates of increased stiffness foster glial differentiation [111–114] – as presented in figure 2.3.

Accordingly, when designing hydrogels to guide neuronal/glial NSC differentiation, it is important to consider the range of stiffness suitable for the desired application. In the case of the CNS tissue, significant differences in stiffness between the spinal cord and the brain are observed, with the brain constituting one of the softest tissues of the human body (Young's modulus, E $\approx$ 500 Pa) [115] – as shown in figure 2.4.

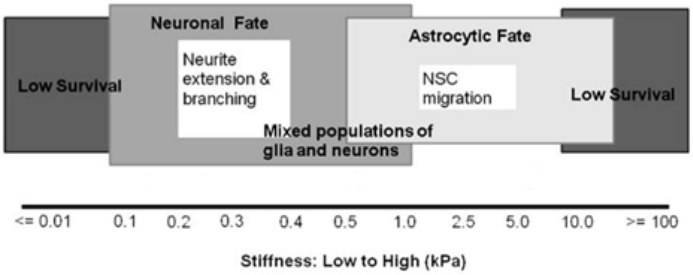

Figure 2.3: **Influence of substrate stiffness on NSC survival and fate.** Adapted with permission from [109]. Copyright © 2012, Elsevier.

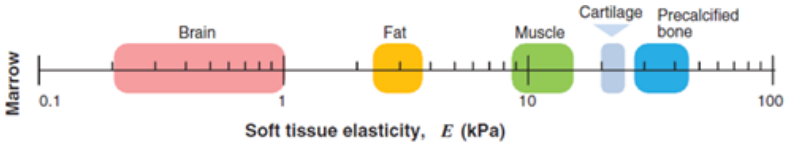

Figure 2.4: **Range of stiffness, as measured by Young's/elastic modulus (E), of different tissues in the body.** Adapted with permission from [115]. Copyright © 2009, American Association for the Advancement of Science.

The main criteria for the classification of hydrogels are related to the **polymer's nature** (natural or synthetic), and the **cross-linking method** (physical or chemical) [106]. The cross-linking method is crucial for both the mechanical properties and stability of hydrogels. Physically cross-linked hydrogels have transient junctions that arise either from polymer chain entanglements or physical interactions such as ionic interactions, hydrogen bonds, hydrophobic interactions or crystal formation. In chemically cross-linked hydrogels, the junctions are permanent as a result of various chemical reactions, such as radical polymerization, Michael addition, Schiff-base reaction, or photo-polymerization, which usually results in structures with higher stability and mechanical strength [106, 116].

Another relevant criterion is hydrogel **injectability**. Contrarily to non-injectable hydrogels, injectable hydrogels can be precisely injected into the CNS through the use of small gauge needles (minimally invasive procedures), preserving the remaining healthy neural tissue. Importantly, the use of injectable hydrogels also contributes to a great reduction in the number of cells required for transplantation, which is particularly appealing for clinical use [117, 118].

Given the context of this work, emphasis will be put on describing the most relevant differences between natural and synthetic polymers used to produce hydrogel scaffolds for NSC culture/delivery.

2.1.2 Natural vs. Synthetic Polymers

Natural polymers constitute a well-established choice for the development of injectable hydrogels for cell delivery into the CNS [119]. Hydrogels based on natural polymers present inherent bioactivity and mechanical properties similar to those of the CNS, which makes them

great candidates for recapitulating the native properties of the CNS tissue. Additionally, natural polymers present intrinsic cues conducive for cell adhesion and infiltration, which not only improves cell response upon contact with the biomaterial, but also allows the possibility to modulate cell behavior [97].

In the context of neural tissue engineering, the most commonly applied natural polymers are ECM-derived polymers (e.g., collagen, hyaluronic acid, fibronectin, fibrin, elastin), or polymers from other natural sources, such as alginate, agarose, chitosan and methylcellulose [108] – as shown in table 2.1.

Although a myriad of applications has already been developed from natural polymers for neural regeneration and neuroprotection (see [97] and [108] for a more detailed review), these materials present several drawbacks. First, their complex chemical structure not only hinders their manipulation, but also provides them with weak mechanical properties and high thermal sensitivity. Moreover, in order to minimize the risks of immunogenic reaction upon implantation in the body, most of these biomaterials have to be purified after isolation from their natural source, which coupled with the heterogeneity found between batches hampers their further use [101, 120].

On the other hand, **synthetic polymers** are human-made polymers that can be engineered to more accurately mimic the physical and mechanical characteristics of the ECM. Contrarily to their natural counterparts, synthetic polymers present highly tunable and reproducible properties, making possible to tightly control their chemical composition and molecular weight, and, as a result, the hydrogel's bulk mechanical properties [120, 121]. Synthetic polymers are also cheaper and easier to obtain, and present a lower risk of immunogenicity. Importantly, their well-defined structure allows their modification with reactive functional groups for subsequent biofunctionalization with cell adhesive, ECM-binding, and/or protease sensitive sequences, allowing a more precise control of the hydrogel bioactivity [122]. Hence, these polymers can be used to produce substrates with properties similar to those of the native neural tissue. In this context, the most commonly applied synthetic materials are polyesters of lactic and glycolic acid (PLA and PLGA, respectively) and polyethylene glycol (PEG) [108] – as shown in table 2.1, together with other synthetic-based polymers used in the field.

Table 2.1: Polymers of natural and synthetic origin commonly used for neural tissue engineering applications, including NSC culture/delivery.

Natural origin	Synthetic origin
Agarose	Poly (ethylene glycol) (PEG)
Alginate	
Chitosan	Poly (D, L-lactic acid) (PLA)
Collagen	
Elastin	Poly (lactic-co-glycolic acid) (PLGA)
Fibrin	
Fibronectin	Poly(lactide-co-glycolide) (PLG)
Hyaluronic Acid	Poly (2-hydroxyethyl methacrylate) (PHEMA)
Methylcellulose	Poly (hydroxypropyl methacrylate) (PHPMA)

2.1.2.1 Poly(ethylene) glycol-based hydrogels

Non-ionic, hydrophilic PEG hydrogels stand out as one of the most widely used synthetic polymers for biomedical applications, mostly due to the well-established *in vivo* tolerance and FDA-approval of PEG [123]. In fact, when compared to other synthetic platforms, PEG-based hydrogels exhibit substantial advantages, including intrinsic low-protein adsorption properties, minimal inflammatory profile, highly tunable features (in terms of mechanical/structural properties, degradability and bioactivity) and also the independent control over biochemical and biophysical properties [124, 125]. PEG-based hydrogel systems have been explored for neural tissue engineering, and the cytocompatibility of PEG hydrogel platforms towards NSC is already well established [126–129]. Additionally, PEG hydrogels can be cross-linked *in vitro* or delivered as an injectable formulation that can gel *in situ* at the site of implantation, which favors their application in the context of CNS regeneration and repair [130].

PEG is a relatively inexpensive, water-soluble, linear or branched (multi-arm or star) polymer that is synthesized by suspension polymerization from ethylene oxide with molecular weights ranging from 0.4 to 100 kDa. End-group modification with different reactive moieties makes it possible for PEG to participate in covalent bonding through several chemistries [124]. Figure 2.5 shows the chemical structure of PEG.

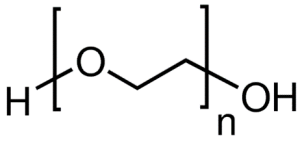

Figure 2.5: **Chemical structure of PEG.** Copyright © 2019 Merck KGaA, Darmstadt, Germany.

PEG hydrogels can be synthesized through a variety of gelation methods (physical/photopolymerization, ionic interaction and chemical/covalent cross-linking). Among these methods, photopolymerization is one of the most widely used techniques, mostly due to its simplicity and speed; nonetheless, it often requires the addition of toxic photoinitiators and the use of UV light, which reduces its clinical potential. Ergo, attentions have been focused on hydrogel chemical cross-linking techniques (*e.g.*, Michael-type addition, click chemistry, enzymatic reaction, among others), which are known to result in more stable hydrogel structures with tunable physicochemical properties such as permeability, molecular diffusivity, equilibrium water content, elasticity, modulus, and degradation rate [131]. Particularly, the biorthogonal thiol-ene Michael-type addition cross-linking system allows the easy and fast incorporation of thiol-containing peptides within appropriately functionalized PEG macromers. Besides occurring in the absence of cytotoxic free-radicals and other toxic reactants, it displays a rapid reaction rate in benign reaction conditions (no heat or light needed) and does not produce side-products [132]. Nevertheless, it requires the use of a nucleophilic buffering reagent, such as triethanolamine or HEPES to facilitate the addition reaction, which can have cytotoxic effects when used in high concentrations [125].

Maleimide-terminated poly(ethylene) glycol-based (PEG-MAL) hydrogels

Due to its versatile chemical structure, PEG macromers based on a 4- or 8-arm structure can be easily modified with different functional groups, including acrylate/methacrylate, maleimide, vinyl sulfone, among others, to allow hydrogel formation or conjugation with biomolecules [124]. Particularly interesting are degradable hydrogels formed via Michael-type addition reaction between maleimide-terminated PEG polymer and dithiol-terminated cross-linkers (whose reaction is schematically represented in figure 2.6).

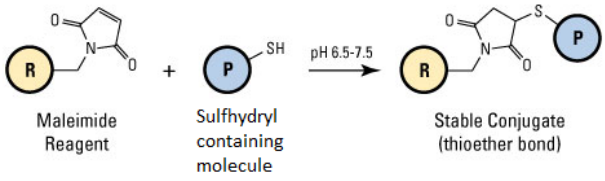

Figure 2.6: **Schematic representation of the thiol-maleimide (SH-MAL) Michael-type addition reaction used to prepare PEG-MAL hydrogels.** Copyright © Life Technologies

Compared to the remaining functional moieties, the maleimide group presents faster reaction kinetics, high specificity for thiols at physiological pH and requires a low concentration of nucleophilic buffering reagent. Moreover, PEG-4MAL hydrogels outperform other synthetic chemistries in generating structurally defined hydrogels with stoichiometric incorporation of bioligands, improved cross-linking efficiency and reaction time scales appropriate for *in vivo* applications with *in situ* gelation [128, 133]. Therefore, a great focus has been given to 4-arm maleimide-terminated PEG macromer (whose chemical structure is shown in figure 2.7).

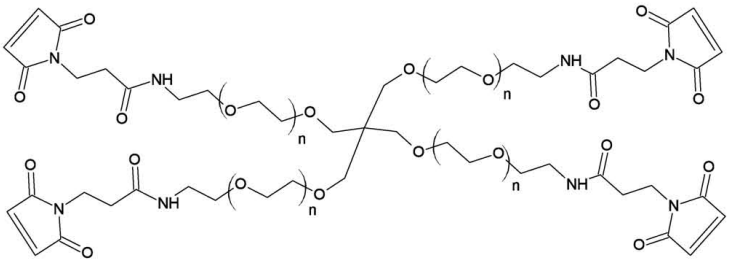

Figure 2.7: **Chemical structure of 4-arm PEG Maleimide-terminated (PEG-4MAL).** Reproduced with permission from [125]. Copyright © 2012 WILEY-VCH Verlag GmbH & Co. KGaA, Weinheim

The tunability of PEG-4MAL hydrogel properties enables the systematic and rigorous study of the independent contributions of ECM biophysical and biochemical properties, thus providing a robust platform for the *in vitro* culture of hNSC. The macromer size and polymer density can be modified to tune the density of cross-links within the hydrogel, which translates to changes in its biophysical properties; therefore, PEG-4MAL hydrogel properties can be modified to tune the matrix stiffness that provides the physical support and promotes the essential mechanosignals for the culture of hNSC. In this context, it is important to highlight

that elastic modulus of the gels increases, whereas equilibrium swelling (which is related to hydrogel structure) decreases as a function of polymer density [134] (figure 2.8).

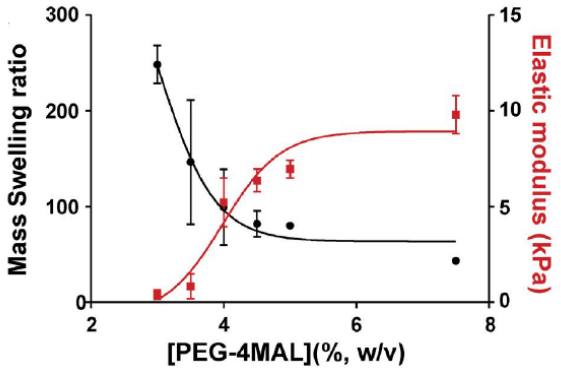

Figure 2.8: **Relationship between hydrogel mass swelling ratio and elastic modulus as a function of PEG-4MAL polymer density (% w/v).** Reproduced with permission from [134]. Copyright © 2016 Enemchukwu et al.

PEG-MAL hydrogels as cell-instructive microenvironments

As previously mentioned, the chemical and mechanical properties of PEG hydrogels can be tailored to produce favorable cell microenvironments that not only maximize survival and function of encapsulated cells, but also promote interaction with the host microenvironment. This can be achieved by controlling, among many others features, matrix adhesiveness and degradability; indeed, these are two critical factors to consider when designing cell-instructive microenvironments, as they will be key for the modulation of NSC function (*i.e.*, viability, proliferation, outgrowth and differentiation) and matrix remodeling [93, 134].

Considering this, PEG polymers can be synthesized to include reactive functional groups enabling the tethering of bioactive cues, such as protease-sensitive sequences, which often constitute enzymatically degradable bis-cysteine peptides. Importantly, the proteolytic cleavability allows for enzyme-mediated cell migration and degradation of the hydrogel, which serves as a provisional matrix for tissue repair. The level of hydrogel degradability by proteases can be modulated by varying the ratio between a relatively fast-degrading and a slow- or nondegrading cross-linking agent. Therefore, when designing a PEG-4MAL hydrogel matrix, it is important to consider the use of a cross-linking peptide that is sensitive to the proteases expressed by the cells to be embedded in the gel [135].

The structural and viscoelastic properties of these hydrogels can also be tuned by varying the polymer concentration, chain length, chain configuration (*e.g.*, linear, multi-arm, etc.) and cross-linking density [133, 136]. The modulation of these properties will ultimately impact different cellular functions. In addition, the fine control over hydrogel mechanical and structural properties will be crucial to direct neural stem cell fate [101, 114].

However, besides being better chemically defined, synthetic polymers (including PEG) are in most cases biologically inert, which contributes to their low immunogenicity, but hardens cellular integration into the material [124]. In this regard, several strategies have been implemented to improve the interaction between adherent cells and its surrounding environment,

thus promoting host tissue integration of neural biomaterials (as represented in figure 2.9). One of the most relevant approaches corresponds to the modification with tethered bioactive molecules, such as cell adhesion motifs [124].

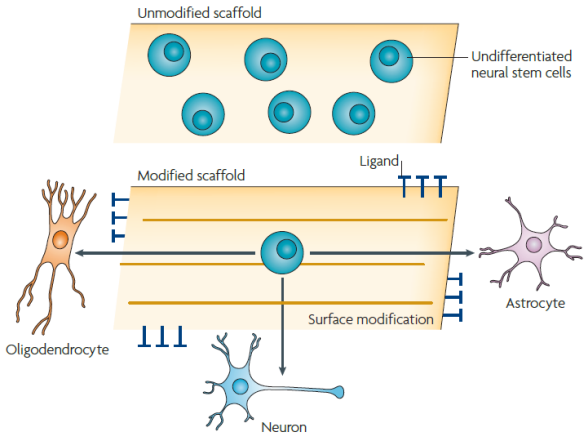

Figure 2.9: **Schematic illustration of the inducive properties arising from the modification of hydrogel scaffolds with cell-adhesive motifs.** Upon functionalization, hydrogel scaffolds can modulate cell fate. Adapted with permission from [110]. Copyright © 2009, Springer Nature.

Commonly used adhesive ligands include full-length ECM adhesive proteins such as laminin, collagen type I and fibronectin, or alternatively, ECM protein-derived peptides. Despite the fact that full-length adhesive proteins provide hydrogels with multiple bioactive ligands for cell adhesion and short peptidomimetics retain only 10% to 30% of their biological activity as compared to the whole protein [137], the tethering of short peptides has several advantages. First, shorter peptides present higher stability against conformational changes and allow the incorporation of a higher density of bioactive domains along with a higher control over their exposure; in fact, they are less likely to exhibit steric hindrance after biomaterial modification. Additionally, shorter synthetic peptides typically show higher resistance to denaturation and enzymatic degradation, lower immunogenicity and are easy to synthesize on a large scale (thus presenting lower production costs), as well as easier to store and characterize [137, 138].

2.1.3 Hydrogel's functionalization: mimicking the neural ECM

Given the abundance and key role of laminin in neurogenic niches, a number of laminin-derived sequences have been explored to render hydrogel matrices adhesive to NSC or NPC. These include **IKVAV** (Ile-lys-Val-Ala-Val), **YIGSR** (Tyr-Ile-Gly-Ser-Arg), RNIAEIIKDI (Arg-Asn-Ile-Ala-Glu-Ile-Ile-Lys-Asp-Ile) or RYVVLPR (Arg-Tyr-Val-Val-Leu-Pro-Arg) peptides [139]. The YIGSR peptide (from mouse β1 laminin chain) supports NPC survival, proliferation, and neurite outgrowth [140], while IKVAV (found on the C-terminal end of mouse α1 laminin chain) is stated to support differentiation, migration and neurite extension of neural cells [141]. These peptides are recognized by the β1 integrin receptor subunit, which was shown to be highly expressed in ESC-derived neural stem/progenitors [142]. On the other hand, RNIAEIIKDI is a sequence present on mouse γ1 laminin chain [143] found to

promote neurite outgrowth of dorsal root ganglia cells, whereas RYVVLPR is derived from β1 chain [144]. In addition to these laminin-derived peptide sequences, also the tripeptide RGD (Arg-Gly-Asp) binding site, found in fibronectin and as a cryptic domain in laminin α1 chain, is used for purposes of hydrogel functionalization [94, 145, 146].

These small bioactive sequences have in fact been widely explored for the design of biomimetic 3D matrices (of both natural and synthetic origin) for cell culture and NSC transplantation – as reviewed in Table 2.2 [147–154] and Table 2.3 [155–160]. Interestingly, in the last few years, studies have been exploring the additive or synergistic effect of the combined incorporation of different cell adhesive peptides (e.g., IKVAV, YIGSR, RGD, AG73, RNIAEIIKDI). Examples of such work can also be found in Table 2.2 [150].

Whereas most of the referred peptides mediate cell interaction via integrin receptors [161], the use of cell binding ligands interacting with HSPG cell receptors has become highly attractive, as a result of their key role in the regulation of NSC stemness [162]. For instance, syndecans are known to participate in the modulation of stem cell maintenance and neurogenesis (*e.g.*, proliferation, self-renewal, differentiation, migration and maturation), either through independent signaling or by working alongside with other receptors, such as integrins [163–165].

2.1.3.1 Syndecan receptors

Syndecans are transmembrane HSPGs, with a key role on the modulation of different biological processes, including neural patterning, angiogenesis, inflammation and wound healing [166]. These cell adhesion receptors are composed by an extracellular domain, comprising GAG chains, including HS and CS ones, which mediate the interaction with growth factors, ECM proteins, as well as with other receptors (figure 2.10). This extracellular domain varies between the four members of the syndecan family identified in mammals (Syndecan-1, -2, -3 and -4) [166, 167].

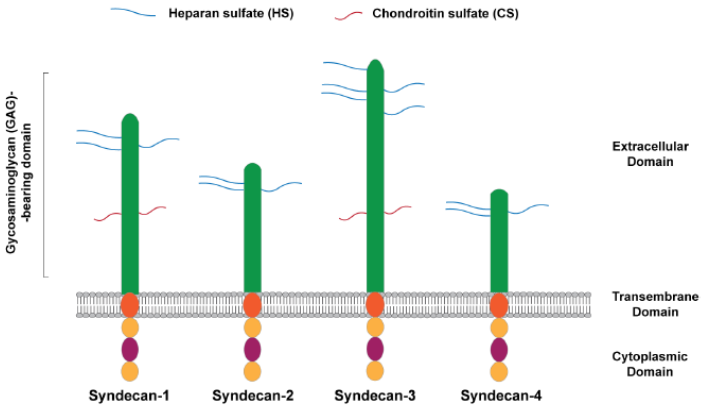

Figure 2.10: **Schematic representation of mammalian syndecan receptors.** As found in [168].

The four members of the syndecan family present distinct cell and tissue-specific expression patterns [169]. Syndecan-1 is highly expressed during neurogenesis and is key to support

NSC proliferation and progenitor cell maintenance [170, 171], while syndecan-4 constitutes a key marker of NSC differentiation [162]. These evidences are in agreement with previous studies from [151], showing that hNSC derived from the H9-ESC line, cultured under basal conditions, express high levels of syndecan-1 (98.6%), whereas syndecan-4 levels were found in much lower amounts (2.62%). Syndecan-3 is key for the modulation of axon guidance [172] and neurite outgrowth [173], and together with syndecan-4 controls neuronal migration. Lastly, syndecan-2 exerts a remarkable effect in dendritic spine morphogenesis [174].

2.1.3.2 AG73 peptide sequence

AG73 (RKRLQVQLSIRT) is a synthetic peptide derived from the laminin globular 4 (LG4) domain of mouse laminin α1 chain, which interacts with syndecan-1 [175, 176] and syndecan-4 [177]. This peptide was reported to promote cell adhesion, migration, neurite outgrowth and angiogenesis in cellular models such as HT-1080 cells, B16-F10 cells, the HSG cell line, the GT1-7 mouse neuronal cell line and human dermal fibroblasts [178–180]. In addition, this cell-adhesive peptide has been shown to enhance neurite outgrowth of PC12 cells when in combination with several natural-based hydrogel (*e.g.*, alginate [181], hyaluronic acid [182], agarose [183], collagen [184] and chitosan membranes [185, 186]). Recent studies by Bento et al. [151], have revealed that the functionalization of fibrin hydrogels with AG73 improves cell outgrowth of hNSC. Despite the promising results, the intrinsic bioactivity presented by natural-based polymers makes it difficult to deconvolute the contribution of the syndecan-binding peptide to the final biological outcome. Synthetic-based polymers, in turn, constitute an attractive alternative in this regard, as they are chemically defined materials that allow a precise and independent control over the biochemical and biophysical properties of the matrix [121].

Table 2.2: Laminin-derived peptides explored for the biofunctionalization of hydrogels based on natural polymers envisaged for use in NSC culture/delivery. For more details see [147], [148], [149], [150], [151], [152], [153] and [154], respectively.

Adhesive Peptide	Peptide Sequence	Source	Hydrogel Backbone	Cells	Biological Performance		Concentration	Reference
					In Vitro	*In Vivo*		
IKVAV	VVAAEEEEG-IKVAV-COOH	Laminin (α1 chain)	Peptide amphiphile (PA)	Mouse NPC	IKVAV modification enhanced neurite outgrowth, while the alignment guided these neurites along the direction of the nanofibers; after 2 weeks of culture, differentiated neurons displayed spontaneous electrical activity and ability to establish synaptic connections	The transplantation of the NPC-laden IKVAV-PA gels into a rat model of SCI promoted both the neuronal differentiation and neurite outgrowth of NPC in aligned gels.	Mixed solutions of the base and epitope-presenting PAs (4:1 by weight) were thermally annealed to induce the formation of aligned nanofiber domains	[147]
	-		Silk fibroin	human NSC	IKVAV-modified silk fibroin hydrogels showed increased cell viability and enhanced neuronal differentiation capability of hNSC (demonstrated by higher β3 tubulin and MAP 2 expression, after 7 days of differentiation)	-	2 mg per g of dry silk fibroin	[148]
IKVAV + RGD	**RADA16-RGD**: Ac-(RADA)4-DGDRGDS; **RADA16-IKVAV**: Ac-(RADA)4-RIKVAV	Laminin (α1 chain), Fibronectin	RADA-16	NPC, NSC	RADA 16-I hydrogels modified with IKVAV and RGD peptides promoted a higher survival of NPC/NSC, as well as a more permissive environment to assist with neuron and glial differentiation, when compared to the plain RADA 16-I gels	IKVAV-/RGD-functionalized nanofiber gels provided a more permissive environment for Schwann cell recruitment and nerve regeneration when implanted into different nerve injury models	-	[149]
IKVAV + YIGSR + RGD	**RGD**: Ac-GCGYGRGDSPG-NH2; **IKVAV**: Ac-IKVAVGYGCG-NH2; **YIGSR**: Ac-GCGYGYIGSR-NH2	Laminin (α1 chain), Laminin (β1 chain) Fibronectin	Hyaluronic acid	iPS-NPC	Maximum survival and differentiation of iPS-NPC was observed at the third round of optimization, which considered the highest IKVAV concentration.	-	Optimal combined concentration: 100 μM RGD, 48 μM YIGSR, 300 μM IKVAV, 2 μM RDG	[150]
AG73	RKRLQVQQLSIRT	Laminin (LG4 module of the α1 chain)	Fibrin	human NSC	AG73-functionalized hydrogels efficiently promoted neurite outgrowth of hNSC	-	60 μM	[151]
G3P	PPFLMLLKGSTR	Laminin (LG3 domain of the α3 chain of laminin-332)	Collagen	Rat fetal NSC	Modification of the collagen scaffolds with the G3P laminin-derived peptide increased cell adhesion and survival and stimulated maturation.	-	300 μg/mg collagen	[152]
CLG3/CLP	FNTPSIEKP	Heterodimer consisting of the LG3 domain of the laminin α1 chain (CLG3) and the C-terminal peptide from laminin γ1 chain (CLP)	Collagen	Rat NSC	NSC survival was promoted in collagen hydrogels incorporating the laminin-derived heterodimer	Improved viability of NSCs in the early stage after transplantation into the striatum when incorporated in collagen-modified gels	3 μM	[153, 154]

Table 2.3: Laminin-derived peptides explored for the biofunctionalization of hydrogels based on synthetic polymers or synthetically-derived biopolymers envisaged for use in NSC culture/transplantation. For more details see [155], [156], [157], [158], [159] and [160], respectively.

Adhesive Peptide	Peptide Sequence	Source Protein	Hydrogel Backbone	Cells	Biological Performance *In Vitro*	Adhesive peptide concentration	Reference
IKVAV	CGGAS**IKVAV**S	Laminin (α1 chain)	Porous p[HEMA-AEMA]	human fetal NSC	Ac-CGGASIKVAVS-OH-modified P(HEMA-AEMA) hydrogels supported the attachment, proliferation, differentiation and process spreading of fetal NSC during the first 2 weeks of expansion and contributed to the formation of a high percentage of more mature neural cells after 4 weeks of expansion.	1.3 mM	[155]
	CCRR**IKVAV**WLC		PEG	human fetal NSPC	Short-IKVAV-modified PEG hydrogels improved hNSC attachment, proliferation, migration and spreading compared to plain hydrogels and hydrogels modified with the full laminin	Optimal concentration: 0.01 mM	[156]
	CSRARKQAAS**IKV**AVSADR		PAM + PLL	Embryonic and Adult Cortical Progenitor cells	IKVAV was found to synergize with PLL to promote differentiation and neurite outgrowth of embryonic cortical neurons with the formation of focal adhesions containing β1-integrin. Furthermore, in adult NSC-culture, bifunctionalized gels promoted neurogenesis via the expansion of neurogenic clones	100 μg/mL (0.05 mM)	[157]
IK(HANBP)VAV	IK(HANBP)VAV		PAAm-AA	eNPCs isolated from mouse embryonic cortex (E 14.5)	Photoactivated modified gels supported neurite outgrowth of eNPCs and allowed site-selective guidance of neurites extension	Optimal concentration: 0.2 mM	[158]
YIGSR	CGKG**YIGSR**	Laminin (β1 chain)	PEG	IPSC	YIGSR-modified hydrogels resulted in the highest iPSC viability and formed the most permissive environment for iPSC differentiation into NPC	2 mM	[159]
IKVAV + YIGSR	**IKVAV**: NH2-CGIKVAVEGC-CONH2; **YIGSR**: NH2-CGEYIGSRGC-CONH2	Laminin (α1 and β1 chains, respectively)	PEG	Mouse adult NPSC	3D encapsulation of NPSC in PEG hydrogels functionalized with both IKVAV and YIGSR promoted the highest cell viability and metabolic activity, after 8 days	DTT/IKVAV/YIGSR (85/7.5/7.5 mol/mol/mol); equivalent moles of thiol groups to acrylate in the polymer were used	[160]

2.2 Summary and Motivation

As clarified throughout the previous sections, CNS damage, whether caused by traumatic injury, neurodegenerative diseases, ischemia or cancer, constitutes a highly prevalent condition with high socioeconomic burden. To improve the CNS limited capacity to spontaneously regenerate, cell-based therapies are being explored, with emphasis on the transplantation of NSC; however, the limited cell survival, uncontrolled differentiation, and poor integration into the host tissue have hampered the efficacy of this therapeutic approach.

To surpass these hurdles, hydrogels mimicking the microenvironment of NSC niches have been explored as cell-delivery vehicles, to favor NSC survival, proliferation and differentiation. Synthetic-based engineered hydrogels constitute an attractive option for this purpose, by allowing an independent control over biochemical and biophysical properties. As such, efforts to produce synthetic hydrogels capable of recapitulating important features of the native neural *in vivo* environment have been made, with promising results. Nevertheless, most of the biochemical and mechanical effects induced by these systems on entrapped NSC are not yet fully understood, which hinders the establishment of the optimal hydrogel features (*i.e.*, in terms of cell adhesive cues, cross-linking density/degradability, mechanical and viscoelastic properties, etc.) for a given application. Moreover, although there are plenty suitable candidates for use as cell-binding ligand, the selection of the ideal cell adhesive molecule (or molecule combination) is still a question with no definite answer.

Considering the current scenario, it is evident that further studies exploring the biologic effect of cell adhesive ligands interacting with syndecan receptors on NSC behavior in a modular synthetic hydrogel platform is of much interest. These studies can provide insights for the improvement of neural tissue engineering, particularly with respect to the use of biofunctionalized hydrogel systems as cell-instructive 3D platforms for the culture and transplantation of NSC, which can ultimately bring us closer to a clinical solution for neural damage. Additionally, such information can also contribute to the development of improved platforms for *in vitro* drug screening and disease modeling that better mimic the complex CNS environment typical of neurological disorders.

2.3 Research goals & Strategy

This thesis focuses on the development of a synthetic hydrogel platform for the culture of hNSC based on a four-arm maleimide terminated poly(ethylene glycol) (PEG-4MAL) backbone, and the exploration of the bioactive effect of the laminin-derived AG73 syndecan-binding peptide sequence with reported neurite promoting ability. Hence, we propose to prepare AG73-functionalized PEG-4MAL hydrogel matrices that recapitulate the native microenvironment of NSC niches. Importantly, in order to allow the cell-induced matrix remodeling, protease-sensitive peptides were used to cross-link the matrices via a Michael-type addition reaction.

With this work, we excepted to understand the concentration-dependent effect induced by the matrix functionalization with bioactive domains recognized by hNSC in terms of mechanical/viscoelastic and structural properties, as well as biological response from hNSC.

Overall, this study aimed to provide valuable insight into the potential of this syndecan-binding adhesive motif for the biofunctionalization of 3D synthetic hydrogel platforms designed for the culture of hNSC, or for use as vehicles of NSC in the context of regenerative therapies for CNS disorders.

Specific objectives included:

- **Preparation of AG73-functionalized PEG-4MAL hydrogels** and their characterization in terms of: macroscopic morphology, peptide binding efficiency and viscoelastic and structural properties, to get insight into the impact of AG73 tethering on hydrogel stiffness and average mesh size.
- **3D culture of hNSC within AG73-functionalized PEG-4MAL hydrogels** under neuronal differentiation conditions, to unravel the ability of grafted AG73 to support cell viability and neuronal differentiation, as well as matrix remodeling.

Chapter 3

Materials and Methods

3.1 Preparation of AG73-functionalized PEG-4MAL hydrogels

Four-arm maleimide-end functionalized poly (ethylene glycol) (PEG) macromer (PEG-4MAL, 40 kDa, 97.8-99.3% purity, 92.9-100% end-group substitution, polydispersity of 1.02, Jenkem USA) was used as the hydrogel backbone. Macromer solutions were prepared by dissolving PEG-4MAL in 10 mM 4-(2-hydroxyethyl) piperazine-1-ethanesulfonic acid (HEPES) buffer in 1× phosphate-buffered saline (PBS, pH 6.5), to obtain a final polymer density of 10% (w/v).

The syndecan-binding AG73 peptide (Acetyl (Ac)-*C*GGRKRLQVQLSIRT-Amide (NH_2)), with a single cysteine for coupling to PEG-4MAL, was custom synthetized at GenScript (1.7 kDa, 97.3% purity). AG73 peptide was dissolved in ultrapure water at 5-fold the final ligand density (0.01, 0.10, 0.50, 1.00 and 2.00 mM) and added to the PEG-4MAL macromer solution at a 2:1 PEG-4MAL/AG73 volume ratio to generate PEG-AG73 conjugates. The different molar ratios of PEG-4MAL to AG73 peptide used in the formulation of AG73-functionalized PEG-4MAL hydrogels are presented in Table 3.1. The resultant solution was vigorously mixed prior to the reaction to reduce the polydispersity of the conjugates, and the pH adjusted to 7.4 (by addition of 0.1 M NaOH) to favor Michael-type addition reaction between the reactive thiol and the maleimide group [187]. The reaction proceeded for 15 min at room temperature (RT), under N_2 atmosphere.

AG73-functionalized PEG-4MAL was then cross-linked with a cysteine-flanked matrix metalloproteinase 2 (MMP2)-sensitive peptide (Ac-GD*C*DDSGESPAY↓YTADD*C*DG-NH2[1]), custom synthetized at GenScript (2.1 kDa, 87.3% purity), and PEG-dithiol (3.5 kDa; 99.8% purity, Jenkem USA), both dissolved in HEPES buffer (10 mM in 1× PBS, pH 6.5). Different molar ratios of degradable (MMP2-sensitive peptide) to non-degradable (PEG-dithiol) cross-linkers were explored, namely 100:0, 80:20, 60:40, 40:60, 20:80 and 0:100 [2]. The cross-linkers were added at a stoichiometrically balanced 1:1 maleimide/cysteine molar ratio after

[1] ↓ denotes the enzymatic cleavage site.

[2] The purity of all hydrogel components, as well as maleimide substitution efficiency of PEG-4MAL macromer was considered when calculating the corresponding masses.

accounting for maleimide groups reacted with AG73 to ensure the theoretically complete cross-linking of the gels.

PEG-4MAL hydrogels (total volume of 10 μL) were obtained by transferring the cross-linkers solution (20% of the final hydrogel volume) to the wells of an uncoated 8-well chamber μ-Slide (IBIDI®) plate, prior to the addition of the precursor solution containing AG73-functionalized PEG-4MAL (remaining 80% of the final hydrogel volume). Given the rapid kinetics of the cross-linking reaction, the two solutions were throughout mixed using a wide orifice pipette tip to ensure a homogeneous cross-linking of the gel. Cell-laden gels were prepared similarly by adding the cell suspension to the AG73-functionalized PEG-4MAL precursor solution before cross-linking. Table 3.2 shows the final volume fraction and respective concentration factor considered for each hydrogel component (2:1:1:1 PEG-4MAL: adhesive peptide: cells: cross-linkers). Lastly, hydrogels were incubated at 37 °C, 5% CO_2 for 15 min before the addition of 1× PBS (pH 7.4) or culture medium, in the case of acellular or cell-laden gels, respectively.

Unmodified (0.00 mM AG73) and PEG-4MAL gels functionalized with a scrambled sequence of AG73 peptide (Ac-CGGLQQRRSVLRTKI-NH_2, 1.7 kDa, 97.5% purity, GenScript) were also prepared and used as controls. For a better understanding of the described process, a schematic representation of AG73-functionalized PEG-4MAL hydrogels' preparation is presented in figure 3.1.

Table 3.1: Molar ratios of PEG-4MAL to AG73 peptide used in the formulation of AG73-functionalized PEG-4MAL hydrogels.

AG73 peptide concentration (mM)	**PEG-4MAL:AG73 molar ratio**
0.00	1:0
0.01	1:0.004
0.10	1:0.04
0.50	1:0.2
1.00	1:0.4
2.00	1:0.8

Table 3.2: Volume fraction and corresponding concentration factor of each component of AG73-functionalized PEG-4MAL hydrogels.

Hydrogel Component	**Volume Fraction**	**Concentration Factor (×)**
PEG-4MAL	0.4	2.5
Adhesive ligand (AG73 peptide)	0.2	5
Cross-linkers	0.2	5
Cells	0.2	5

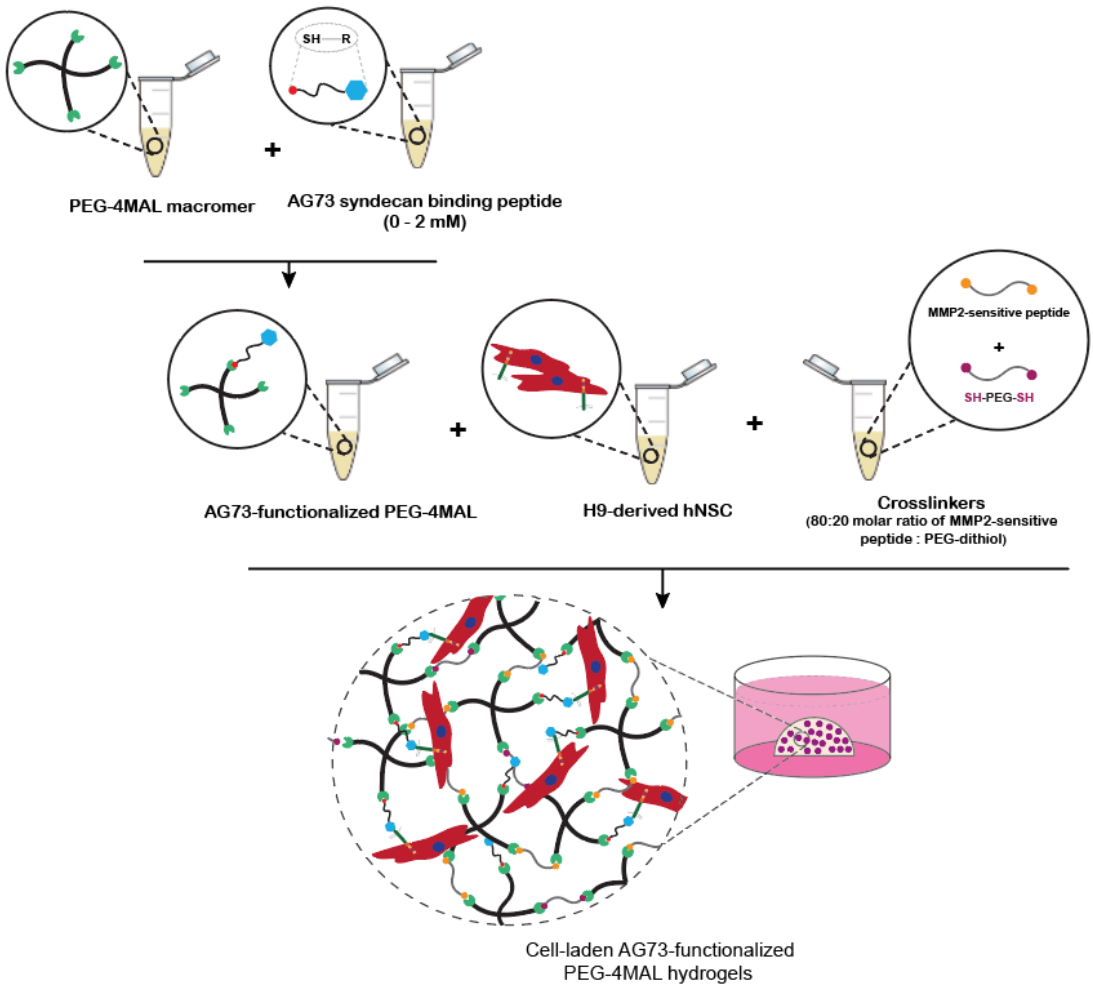

Figure 3.1: **Schematic representation of the preparation of cell-laden AG73-functionalized PEG-4MAL hydrogels** (not to scale). Hydrogel precursor solutions are prepared in separate tubes. AG73-functionalized PEG-4MAL is obtained by mixing the PEG-4MAL macromer solution with the AG73 peptide solution. AG73-functionalized PEG-4MAL is then reacted with a mixture of protease degradable (MMP2-sensitive peptide) and non-degradable (PEG-dithiol) cross-linkers in the presence of cells.

3.2 Physical and chemical characterization of AG73-functionalized PEG-4MAL hydrogels

3.2.1 Morphological analysis

The macroscopic morphology of cell-free AG73-functionalized PEG-4MAL hydrogels was examined using a stereo microscope (Olympus SZX10). For that, hydrogels with different AG73 input concentrations (0.00, 0.01, 0.10, 0.50, 1.00 and 2.00 mM) were prepared as described above and representative images were taken pre-sweeling (before the addition of any hydration medium).

3.2.2 Peptide tethering efficiency

3.2.2.1 Measure-iT^{TM}Thiol Assay

Peptide tethering efficiency was first determined by measuring unreacted/free thiols in the reaction buffer using a fluorometric assay: *Measure-iT^{TM} Thiol Assay Kit* (M30550, Invitrogen), according to the manufacturer's instructions. Briefly, precursor solutions of AG73-functionalized PEG-4MAL were prepared as described above and used as unknown samples (with undefined free thiol concentration). Unmodified PEG-4MAL macromer solution prepared in HEPES buffer (10 mM in 1× PBS, pH 6.5) was used as blank (and its background fluorescence value subtracted). The samples – AG73-functionalized PEG-4MAL/ unmodified PEG-4MAL or standard solutions – were then mixed with the thiol-quantitation reagent in wells of a black-walled 96-well fluorescence plate (Greiner) and the fluorescence read using a microplate plate reader (BioTek^{TM}Synergy^{TM}Mx; $\lambda_{excitation}$/ $\lambda_{emission}$ maxima of 494/517 nm). Serial dilutions of the thiol quantitation standard (reduced glutathione; 0 – 44 μM) were used as standards to generate a calibration curve.

Controls and unknown samples were analyzed in duplicate and triplicate, respectively (n = 1). The concentration of free thiols in AG73-functionalized PEG-4MAL solutions was inferred from the calibration curve and the peptide immobilization efficiency (%) calculated based on the input AG73 peptide concentration used.

3.2.2.2 Analytical high-performance liquid chromatography (HPLC)

The efficiency of the covalent immobilization of AG73 peptide to the PEG-4MAL macromer was also determined by analytical high-performance liquid chromatography (HPLC; Merck-Hitachi). Hydrogels with different AG73 concentrations (0.00, 0.01, 0.10, 0.50, 1.00 and 2.00 mM) were prepared as described above, and incubated in 0.5 mL 1× PBS buffer (pH 7.4) at 37 ^{o}C, for 24h. The chromatographic separation and subsequent quantification of the amount of peptide in the supernatant was performed by HPLC using a detection wavelength of 220 nm. Samples were run at 0.5 mL/min over 55 min (at 25^{o}C) on a LiChroCART 250-4 C18 column (Merck). A linear gradient of water and acetonitrile containing 0.065 and 0.05% (v/v) trifluoroacetic, respectively, was used as the mobile phase (starting composition (%): 95/5 dH_2O/acetonitrile). The calibration curve for peptide quantification was obtained using the peptide diluted in PBS at different concentrations (0 – 5 mM).

3.2.3 Viscoelastic properties and mesh size

The viscoelastic/mechanical properties of cell-free AG73-functionalized PEG-4MAL hydrogels were examined by dynamic shear rheology. For that, hydrogels with different AG73 input concentrations (0.00, 0.01, 0.10, 0.50, 1.00 and 2.00 mM) were prepared as described above, and incubated in 1× PBS buffer (pH 7.4) at RT for 24h. Specifically, for these studies, hydrogels were casted onto an embedding Parafilm ® to ensure the formation of reproducible spherical hydrogel drops. Unmodified and scrambled AG73 peptide-presenting gels were used as controls.

A Kinexus Pro rotational rheometer (Malvern Instruments Ltd, Malvern, United Kingdom) with a standard steel parallel-plate geometry (4 mm in diameter), was used for the oscillatory shear measurements. The temperature was controlled at 37 °C and a humidified atmosphere was maintained. The samples were carefully placed onto the surface of the lower plate, and a 30% compression was applied to the gel to avoid slippage. Before testing, samples were allowed to equilibrate for five minutes.

The linear viscoelastic region (LVR) of PEG-4MAL hydrogels was first determined for plain gels by oscillatory amplitude strain sweeps (constant frequency of 0.1 Hz, strain 1–100%) and then extrapolated for the remaining conditions. Ensuing frequency sweeps were performed in controlled deformation within the LVR (frequency 0.01– 10 Hz, constant strain 1%). The storage modulus (G'), a measure of the elastic energy stored during stress-induced deformation, was determined and used as a measure of PEG-4MAL hydrogels' stiffness. The loss modulus (G''), which reflects the energy dissipated by the gels during deformation, the complex modulus (G^*), as well as the phase angle (δ) were also recorded. The relative mesh size (ξ) value was estimated using the following equation [188]:

$$\xi = \left(\frac{G'A}{RT}\right)^{\frac{1}{3}},$$

where G' = storage modulus in Pa, A = Avogadro's constant ($6.022140857 \times 10^{23}$ mol^{-1}), R = gas constant (8.314 m^3.Pa.mol^{-1}.K^{-1}), T = temperature (37 °C = 310.15 K).

3.3 Adherent culture of human Neural Stem Cells (hNSC)

3.3.1 Cell expansion

Human neural stem cells (hNSC) derived from the NIH approved H9 (WA09) human embryonic stem cell line were purchased from Life Technologies (N7800-200). Cells were expanded according to the manufacturer's protocol on poly-L-Ornithine/laminin-coated six-well tissue culture polystyrene (TCPS) plates (Corning). TCPS plates-coating included an incubation with poly-L-Ornithine (20 μg/mL, Sigma-Aldrich) for 1h, 37 °C and 5% CO_2 humidified environment, following a washing step with cell-culture grade water (ddH_2O), and a 2h-incubation with laminin from mouse Engelbreth-Holm-Swarm sarcoma (10 μg/mL, Sigma-Aldrich). Cells were initially plated at a high seeding density (1×10^5 cells/ cm^2), to promote their recovery and efficient proliferation after thawing, and cultured in complete StemPro® NSC serum-free medium (SFM) (Life Technologies) supplemented with 1% (v/v) penicillin/streptomycin (Pen/Strep). This medium is a low glucose medium containing 20 ng/mL basic fibroblast growth factor (bFGF) and 20 ng/mL epidermal growth factor (EGF) to sustain NSC proliferation.

The medium was refreshed every other day until cells reached an 80-90% confluence. At this point, cells were passaged using StemPro® Accutase® (Life Technologies) by incubation at 37 °C and 5% CO_2-humidified atmosphere for 3-5 min, following inactivation of Accutase® in Glasgow Minimum Essential Medium (GMEM) supplemented with 10% (v/v)

heat-inactivated Fetal Bovine Serum (FBS) and 1% (v/v) Pen/Strep. After centrifugation (200×g, 4 min), the pellet was resuspended in expansion medium and the number of viable cells was determined through Trypan Blue exclusion method using a hemocytometer under an optical microscope. Cells were plated at 5×10^4 viable cells/ cm^2 for subculture or used in cellular assays (passage 2 after thawing). hNSC were used between passages 6 and 16.

3.3.2 Neuronal differentiation

hNSC were plated on poly-L-ornithine/laminin-coated 13-mm diameter TCPS coverslips (SARSTEDT) at 2.5×10^4 viable cells/ cm^2 and cultured in complete StemPro® NSC SFM containing 20 ng/mL bFGF and 20 ng/m EGF for 2 days. Spontaneous neuronal differentiation was induced by growth factors withdrawal and by switching the culture medium to a 1:1 mixture of StemPro® NSC SFM and Neurobasal™ medium (Life Technologies) supplemented with 2% (v/v) B27 (Gibco), 2 mM L-glutamine (Gibco) and 1% (v/v) Pen/Strep – hereinafter referred as Neurobasal/B27. At day 8, half of the medium was replaced by a 1:3 mixture of StemPro® NSC SFM and Neurobasal/B27 supplemented with 10 ng/mL of brain-derived neurotrophic factor (BDNF, PeproTech) and 500 μM of N6, 2'-O-Dibutyryladenosine 3', 5'-cyclic monophosphate sodium salt (dibutyryl cAMP, Sigma-Aldrich). Half of the medium was refreshed every other day, up to 21 days.

3.4 Culture of hNSC within AG73-functionalized PEG-4MAL hydrogels

hNSC were embedded in AG73-functionalized PEG-4MAL hydrogels as described in section 3.1 (and illustrated in Figure 3.1). Briefly, hNSC were dissociated into single cells, resuspended in expansion medium at 4×10^6 viable cells/mL (5× the final cell density), and added to the solution containing AG73-functionalized PEG-4MAL. Cell-laden hydrogels were prepared in the wells of uncoated 8-well chamber μ-Slide (IBIDI®) plates, by adding the precursor solution containing AG73-functionalized PEG-4MAL and cells to the solution containing the cross-linkers. After thoroughly mixed, the polymerizing solutions were incubated at 37 °C, 5% CO_2 for 15 minutes. After this period, 400 μL of culture medium was added to each well and the cell-laden hydrogels were transferred to the CO_2 incubator. Cell-laden hydrogels were cultured under proliferation or neuronal differentiation conditions for periods up to 7 or 14 days, respectively, following the protocol described above for the adherent culture of hNSC.

hNSC cultured within unmodified and scrambled AG73 peptide-presenting gels were used as controls. Figure 3.2 provides a schematic overview of the steps undertaken during the culture of H9-derived hNSC within PEG-4MAL hydrogels from the time of encapsulation until day 21 of cell culture.

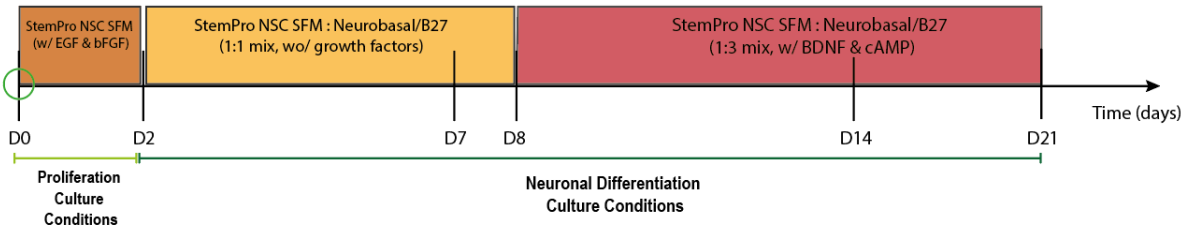

Figure 3.2: **Timeline of H9-derived hNSC culture under neuronal differentiation conditions** after encapsulation within AG73-functionalized PEG-4MAL hydrogels. For proliferation conditions, hNSC were kept in expansion medium for 7 days.

3.5 Biological Activity Assessment

3.5.1 Cell Viability

3.5.1.1 Qualitative analysis

Qualitative analysis of the viability of hNSC entrapped within AG73-functionalized PEG-4MAL hydrogels was assessed using a live/dead assay. Cell-hydrogel matrices were rinsed with warm 1× PBS (pH 7.4) and incubated with 2 μM calcein-acetoxymethyl ester (Calcein AM, Molecular Probes) and 3 μM propidium iodide (PI; Sigma-Aldrich), for detection of viable and dead cells via green and red fluorescence, respectively. Briefly, Calcein AM is a cell permeant non-fluorescent dye that is hydrolyzed by nonspecific esterases into fluorescent products that are retained by cells with intact plasma membranes, thus staining viable cells. In turn, PI only crosses compromised cell membranes and stains the nuclei of compromised/dead cells. After 30 min of incubation at 37 °C, the samples were rinsed twice with 1× PBS (pH 7.4), transferred to culture medium, and immediately observed under confocal laser scanning microscopy (CLSM, Leica TCS SP5; Leica Microsystems). Samples were scanned using a 488 nm and a 561 nm laser for the excitation of the green and red dye, respectively. Z-sections, covering a thickness of 200-400 μm, were acquired using an HC Plan APO CS 10× / 0.40 NA objective and processed with Fiji software.

3.5.1.2 Quantitative analysis

Quantitative analysis of hNSC viability was conducted by flow cytometry performed in nine-pooled hydrogels, after cell isolation from the AG73-functionalized PEG-4MAL gels. Briefly, the cell-containing hydrogels were washed with 1× PBS and sequentially incubated with 1.25 mg/mL of collagenase type II (Gibco; 1h at 37 °C) and StemPro® Accutase® (20 min at 37 °C) under stirring (70 rpm). After Accutase® inactivation with serum-containing medium (GMEM containing 10% (v/v) heat-inactivated FBS), cells were mechanically dissociated by pipetting, centrifuged (300×g, 5 min) and suspended in 1× PBS (pH 7.4). The single cells suspensions were then transferred to the wells of a round-bottomed 96-well plate (9,6 × 10^4 cells/ well) and incubated with calcein AM (67 nM, 20 min at 37 °C) or PI (6 μM, 10 min at 37 °C), for detection of viable and dead cells, respectively. Cells were finally washed trice

and suspended in FACS buffer (1× PBS containing with 2% (v/v) FBS, pH 7.4) for flow cytometry analysis (BD FACS Canto® II, BD Biosciences).

Cells were gated based on forward scatter (size) and side scatter (cell complexity) criteria and unlabeled cells were used to set the fluorescence gates. FITC (fluorescein isothiocyanate) channel photomultiplier (PMT) (wavelength of detection of 520 nm), was used for fluorescence signal detection of calcein, while for PI both PE (R-Phycoerythrin) and PerCP channel PTMs (wavelengths of detection of 575 and 675 nm, respectively) were used. For each flow cytometry analysis, 10,000 events were acquired within the gate. Resulting data was analyzed using FlowJo software (Tree Star).

3.5.2 Total cell number

The total cell number of hNSC cultured within PEG-4MAL hydrogels was estimated from total DNA amount using the CyQUANT® cell proliferation assay kit (Life Technologies), according to manufacturer's instructions. Briefly, cells were isolated from the cell-laden hydrogels as described above and the cell pellets stored at -80°C. For the analysis, the cell pellets were thawed at RT and incubated with CyQUANT® GR dye/cell lysis buffer. Each sample was added per well of a black-walled 96-well fluorescence plate (Greiner) and the fluorescence read using a microplate plate reader (BioTek™Synergy™Mx; λ_{ex} = 480 nm; λ_{em} = 520 nm). The total number of cells was estimated from a standard curve generated with a known amount of hNSC over a range of 50 to 250,000 cells. For each condition, cell-free hydrogels cultured in parallel and processed similarly to those with cells were used as blanks and their background fluorescence values subtracted.

3.6 Characterization of hNSC phenotype and ECM deposition: Immunohistochemistry

Immunohistochemistry was used to characterize the phenotype of H9-derived hNSC cultured on poly-L-ornithine/laminin-coated 2D substrates (under neuronal differentiation conditions), as well as to assess the biologic effect of AG73 peptide on hNSC phenotype cultured within functionalized PEG-4MAL hydrogels (under both proliferation and neuronal differentiation conditions). To that end, characteristic phenotypic markers were considered, namely nestin (NSC marker), Ki67 (proliferative marker), βIII-tubulin (early/immature neuronal marker) and the microtubule-associated protein 2 (MAP2) (mature neuronal marker).

Moreover, the ECM deposition capacity of hNSC cultured on poly-L-ornithine/laminin-coated 2D substrates (for 14 and 21 days under neuronal differentiation conditions), as well as of hNSC cultured within AG73-functionalized PEG-4MAL hydrogels (for 7 days under proliferative conditions) was also assessed by immunohistochemical analysis of specific ECM components, namely laminin, collagen IV and fibronectin.

Immunofluorescence (IF) staining was performed in cell-containing hydrogels/ 2D samples fixed in cell culture media containing 2% (v/v) paraformaldehyde solution (30 min; 37 °C)

and subsequently washed trice with PBS (5 min; RT). When staining for intracellular markers, cell–PEG-4MAL constructs were permeabilized with 0.2% (v/v) Triton X-100 in 1× PBS (45 min; RT). Subsequently, to minimize non-specific adsorption of the antibodies, samples were blocked for 1h (RT) and incubated (overnight at 4°C) with the appropriate primary antibody. After the incubation with the primary antibody, samples were washed trice with PBS (30 min; RT). To detect primary antibodies, samples were incubated with the appropriate secondary antibody – 1h at RT, followed by 5h at 4 °C. Afterwards, samples were again washed in PBS (3 × 30 min; RT) and the nuclei counterstained with Hoechst 33342 (0.1 μg/mL; Life Technologies, H1399) for 20 min at RT. All incubation steps were performed under stirring (50 rpm) and protected from light. Finally, samples were mounted in Fluoromount^{TM}Aqueous Mounting Medium (Sigma-Aldrich) and observed under CLSM. IF analyses were performed after 7 and 14 or 21 days of culture under proliferation and neuronal differentiation conditions, respectively. All primary and secondary antibodies used, as well as corresponding dilutions and appropriate blocking buffer solutions are listed in Table 3.3.

z-sections were acquired with the CLSM using different objectives: HC Plan-Apochromat (Apo) CS 10× / 0.40 NA, HC Plan Apo Lbl. Blue 20× / 0.70 NA IMM and HC Plan APO CS 40× / 1.3 NA. The resulting image stack was then projected into 2D images.

Table 3.3: Primary and secondary antibodies used for immunohistochemistry studies.

Blocking Solution	Primary Antibody	Dilution	Product Source/ Reference	Secondary Antibody	Dilution	Product Source/ Reference
5% (v/v) NGS or NDS in PBS containing 0.05% (v/v) Tween-20	Mouse monoclonal anti-Nestin	1:200	Abcam, AB22035	Alexa Fluor 594 goat anti-mouse IgG (H+L) or Alexa Fluor 647 donkey anti-mouse IgG (H+L)	1:1000	Invitrogen, A11020 / Invitrogen, A31571
10% (v/v) NGS in 1% BSA containing 0.05% (v/v) Tween-20	Rabbit polyclonal anti-Ki67	1:500	Abcam, AB15580	Alexa Fluor 488 goat anti-rabbit IgG (H+L)		Invitrogen, A11070
5% (v/v) BSA in PBS	Mouse monoclonal anti-Tubulin β3 (TUBB3)	1:500	Biolegend, 801201	Alexa Fluor 488 donkey anti-mouse IgG (H+L)		Life Technologies, A21202
1% (v/v) BSA and 4% (v/v) FBS in PBS	Mouse monoclonal anti-MAP2	1:200	Invitrogen, 13-1500	Alexa Fluor 647 donkey anti-rabbit IgG (H+L)		Invitrogen, A31571
	Rabbit polyclonal anti-laminin	1:50	Sigma-Aldrich, L9393			
5% (v/v) BSA in PBS	Anti-collagen IV	1:50	Abcam, AB6586			
	Rabbit polyclonal anti-fibronectin	1:100	Sigma-Aldrich, F3648			

3.7 Measurement of hydrogels' gelation time

The hydrogel's gelation time was recorded as the time taken to complete the manual homogenization of the AG73-PEG-4MAL precursor and cross-linkers solutions with a pipette. This parameter was measured by an external operator using a stopwatch.

3.8 Metabolic activity of hNSC cultured within PEG-4MAL hydrogels

The metabolic activity of hNSC cultured within PEG-4MAL hydrogels was evaluated through a resazurin-based assay. Briefly, when reduced by metabolically active cells, the non-fluorescent

dark blue dye (resazurin) becomes fluorescent pink (resorufin) and can thus work as an indicator of cell viability and metabolic activity.

Cell-laden unmodified PEG-4MAL hydrogels were prepared as described previously and cultured for up to 3 days under proliferation conditions. After 24h and 72h of culture, cell-laden gels were incubated with 20% (v/v) of resazurin dye (Sigma-Aldrich) for two hours. Following the incubation, 100 μL of cell culture supernatant was transferred to the wells of a black-walled 96-well fluorescence plate (Greiner) and the fluorescence read using a microplate plate reader (BioTek™ Synergy™ Mx; $\lambda_{excitation}$/ $\lambda_{emission}$ maxima of 530/590 nm). The conditioning medium of cell-free PEG-4MAL gels was used as blank and its fluorescence subtracted. The percentage of resazurin, as well as the time of incubation considered, had already been optimized for NSC (NS-5 line) derived from a mouse embryonic stem cell line (ES-46 cell line) cultured within fibrin-based hydrogels by previous work in our group.

3.9 Image Analysis

Fiji Software [189, 190] was used for image analysis quantification processes.

3.9.1 Quantitative analysis of Nestin$^+$ and Ki67$^+$ hNSC

After projecting the 3D stack (Max Intensity method) into a 2D plane, a background subtraction (rolling ball algorithm [191] with radius of 50 pixels) was applied to all channels. The cellular reconstruction was performed with the marker-controlled-watershed function of the MorphoLibJ plugin [192, 193]. This function requires three images as input: (a) a marker image, (b) a mask and (c) the main Image. The marker image (a) was obtained by the nuclei/Hoechst channel. From each nucleus one seed point was identified (manual selection) to be used as seeds for cell reconstruction. Subsequently, the Nestin (or Ki67) channel was duplicated. One of the copies was used as a mask (b) after segmenting the cellular areas (manual threshold) and the other copy was used as the main image input (c). Finally, the resulting segmented regions (one per cell) were used to automatically access the location of each cell and extract relevant measurements (*i.e.*, number of cells expressing Nestin or Ki67).

A total of 5 images obtained with the HC Plan Apo Lbl. Blue 20× / 0.70 NA IMM objective were analyzed to quantify the average number/percentage of nestin-positive (Nestin$^+$) and Ki67-positive (Ki67$^+$) cells. The number of double-positive cells (Nestin$^+$/Ki67$^+$) was infered from the previous quantification.

3.9.2 Quantitative analysis of βIII-tubulin$^+$ hNSC

After subtracting the background (rolling ball algorithm [191] with radius of 300 pixels) a median filter with 1 pixel radius was applied to remove noise. The 3D stack was then projected (Max Intensity method) into a 2D plane and hNSC were segmented with the "MaxEntropy" thresholding algorithm [194]. The segmentation was then improved by filling the holes inside segmented particles and touching particles were then separated with the watershed algorithm. Finally, the segmented particles were used to automatically access

the location of each hNSC and extract relevant measurements (average area occupied by βIII-tubulin$^+$ hNSC; percentage of area occupied by βIII-tubulin$^+$ hNSC).

A total of 4-5 images per condition, obtained with the HC Plan-Apo CS 10× / 0.40 NA objective, were analyzed to quantify the average area occupied by βIII-tubulin$^+$ cells, as well as the corresponding percentage of the total area.

3.10 Statistical Analysis

Statistical analysis was performed using SPSS® Statistics 25 software (IBM) and GraphPad Prism 7 software. Sample distribution was initially tested for normality using the Shapiro-Wilk test (commonly used for datasets with less than 50 samples). For normally distributed data, comparisons between two groups were performed with the unpaired t-test, while comparisons between three or more groups were performed with the one-way analysis of variance (ANOVA) followed by the Bonferroni's or the Dunnett's T3 multiple comparison test, for samples with or without homogeneous variances, respectively. For categorical data, Kruskal-Wallis non-parametric test with Tukey's test for multiple comparisons was used. Two-tailed significance levels were considered, and results found statistically significant for p-values $<$ 0.05. Data is reported either as mean ± Standard Deviation (SD) or mean ± Standard Error of the Mean (SEM), as indicated in each figure.

Chapter 4

Results and Discussion

4.1 AG73-functionalized PEG-4MAL hydrogels: a fully defined, synthetic platform for hNSC culture

As stated in the research strategy 2.3, a synthetic hydrogel platform based on a PEG-4MAL macromer functionalized with the laminin-derived AG73 syndecan-binding peptide was prepared to explore the bioactive effect of AG73 on the modulation of hNSC behavior. Besides exhibiting excellent *in vitro* and *in vivo* biocompatibility with different cell types [195–198], the modular nature of PEG-4MAL hydrogels allows independent control over different biochemical and biophysical properties such as type and density of cell-adhesive ligands, mechanical and structural properties, and protease-dependent degradation [125, 134, 195]. These features make the use of PEG-4MAL-based matrices especially advantageous to assess the effect of a specific biochemical or biophysical cue on the modulation of cell behavior, as was the purpose of this work.

The ability of PEG-4MAL hydrogels to support hNSC culture was previously explored in our group by D. Barros in the framework of her PhD thesis [168]. In those studies, PEG-4MAL hydrogels functionalized with site-specific immobilized laminin were optimized in terms of cell seeding density, type of degradable cross-linker, and molar ratio of degradable and non-degradable cross-linkers. AG73-functionalized hydrogels were first prepared based on preliminary studies carried out by D. Barros [168], using a PEG-4MAL macromer with the same molecular weight and polymer density (40 kDa; 10% (w/v)), as well as cross-linkers molar ratio.

In this context, it is important to highlight that the molar ratio of protease degradable (cysteine-flanked matrix metalloproteinase (MMP)-sensitive peptide) and nondegradable (PEG-dithiol) cross-linkers was established to allow the culture of hNSC for 14 days, the time frame of 3D culture sufficient for hNSC differentiation along the neuronal lineage. Among the different protease degradable peptides available, a fast-degrading sequence shown to be relatively specific for MMP2 [199] was selected, as this MMP is expressed at high levels by NSC [200, 201]. Hydrogels prepared at an 80:20 molar ratio of MMP2-sensitive peptide to

PEG-dithiol were the ones supporting the highest cell viability after 14 days of cell culture under neuronal differentiation conditions [202].

Unmodified and PEG-4MAL gels functionalized with a scrambled sequence of AG73 peptide were used as controls. Although presenting the same aminoacidic composition as the bioactive AG73 peptide sequence, the scrambled sequence presents a random distribution of the aminoacidic residues; consequently, its use allows not only the evaluation of incorporating scrambled sequences on the mechanical properties of PEG-4MAL hydrogels, but also the validation of the biospecificity of the AG73 peptide in promoting survival, proliferation and neurite-outgrowth in hNSC.

4.2 Physical and chemical characterization of AG73-functionalized PEG-4MAL hydrogels

The AG73-functionalized PEG-4MAL hydrogels were first characterized in terms of macroscopic morphology, peptide binding efficiency and mechanical/viscoelastic properties. For these studies, cell-free gels were considered.

4.2.1 Morphological analysis of AG73-PEG-4MAL hydrogels

Both plain and AG73-functionalized PEG-4MAL hydrogels, incorporating hNSC protease-sensitive peptides, were successfully prepared, accordingly to the defined protocol. Nonetheless, regardless of the input peptide concentration, all gels revealed the presence of local network heterogeneities at the micrometer-scale (figure 4.1). This gel inhomogeneity is likely due to spatial variations of cross-link density caused by an insufficient mixing of the hydrogel components. In fact, the fast maleimide-thiol reaction is thought to be responsible for the extremely reduced time available for the manual homogenization of the hydrogel components and its subsequent fast gelation kinetics.

The formation of these heterogeneous regions with non-uniform ligand densities and cross-linking gradients (random in density and shape) is in accordance with results reported in the literature for the formation of PEG-4MAL-based hydrogels via Michael-type addition [203, 204]. Even though the thiol-maleimide modality achieves the highest macromer coupling efficiency of the reported Michael-type pairs, the resulting hydrogel networks are usually described to be heterogeneous due to the entrapment of gelation defects (polymer entanglements) created by insufficient mixing [203]. This matter has in fact been recently addressed by a few groups in attempts to control or slow the cross-linking speed of these networks to achieve more uniform PEG-based hydrogels functionalized with bioactive peptides such as RGD or YIGSR [136, 203, 204]. This will also be further addressed in following sections.

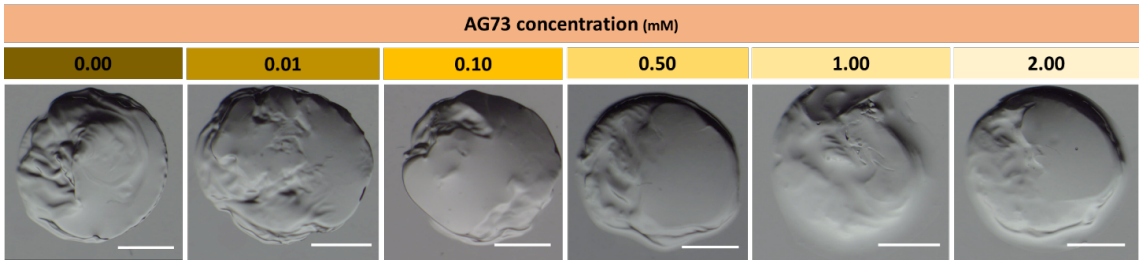

Figure 4.1: **Macroscopic view of acellular AG73-functionalized PEG-4MAL hydrogels** (10 μL) taken pre-swelling, showing several polymer inhomogeneities at the micrometer-scale, independently of the input peptide concentration. Representative images obtained using a stereo microscope (Olympus SZX10) are shown. Scale bar = 500 μm.

4.2.2 Peptide tethering efficiency

4.2.2.1 Measure-iT^{TM}Thiol Assay

Maleimide groups in PEG-4MAL macromers efficiently react with thiol-containing peptides through Michael-type addition, enabling a fine tuning of ligand incorporation, and thus the formation of structurally defined matrices [125]. To assess the effect of AG73 peptide density on hNSC biological response, PEG-4MAL macromers were covalently modified with different concentrations of this syndecan-binding peptide (0.00, 0.01, 0.10, 0.50, 1.00 and 2.00 mM) and the conjugation efficiency determined by a highly sensitive fluorometric assay based on the measurement of unreacted/free thiols in the reaction buffer (AG73-PEG-4MAL precursor solution).

For the various reaction buffers tested, the detected fluorescence was always lower than the limit fluorescence detected for the lowest concentration of the calibration curve (0.55 μM, the lower detection limit of the assay) – Appendix A. Hence, free thiols could not be detected, which indicates that AG73 was tethered onto the PEG-4MAL macromer with an immobilization efficiency higher than 96%, regardless of the input AG73 concentration – as presented in Table 4.1. These values were calculated according to the total concentration of AG73 present in the reaction buffer (for each input concentration considered) and the minimum concentration capable of being detected (0.55 μM).

Table 4.1: AG73 peptide immobilization efficiency onto PEG-4MAL macromer after tethering via a Michael-type addition reaction.

Input $\|AG73\|_{gel}$ (mM)	Immobilization Efficiency (%)
0.01	> 96.70
0.10	> 99.67
0.50	> 99.93
1.00	> 99.97
2.00	> 99.98

Altogether, we were able to effectively immobilize the AG73 bioactive peptide sequence onto the PEG-4MAL backbone, thus producing functionalized hydrogels with varying peptide densities and bioactivity. Importantly, the high yield achieved for AG73 tethering (Figure 4.2) demonstrates the precise control over adhesive ligand density provided by the functionalization methodology used, as previously reported in [151, 202].

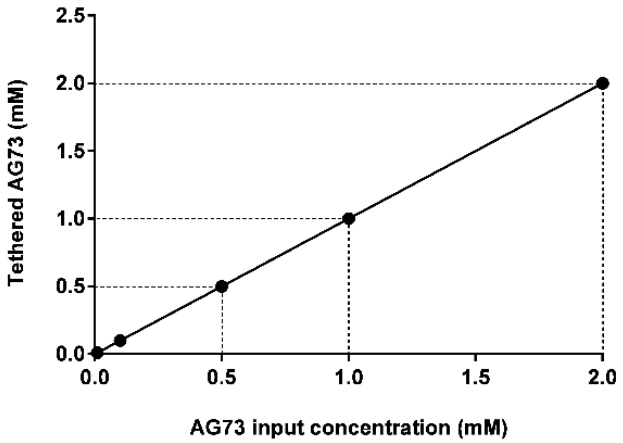

Figure 4.2: **Tethered AG73 density as a function of input AG73 concentration** (0.01 – 2.00 mM), determined by quantifying unreacted/free thiols in the reaction buffer. Results are the mean of three replicates ($n = 1$).

4.2.2.2 HPLC

HPLC was also used as a thiol quantifying method prior to the *Measure-iT*$^{\text{TM}}$ *Thiol kit*. In this case, the amount of AG73 peptide remaining in the supernatant after swelling for 24h was quantified using a detection wavelength of 220 nm. Nevertheless, this method was not sufficiently sensitive to detect the low thiol concentrations remaining in the supernatant (no peak could be detected for AG73 concentrations below 0.156 mM). In fact, the minimum volume needed to cover the gels (500 μL) led to a considerable dilution of the unreacted AG73 released to the supernatant. The multi-chromatographic data corresponding to the calibration curve can be found in Appendix B.

4.2.3 Viscoelastic and structural properties

It has become increasingly clear that biochemical cues/signals are not the only factors governing NSC fate; in fact, the mechanical and structural properties of the surrounding microenvironment are thought to play a key role in regulating NSC survival, proliferation and differentiation [91, 205]. Several studies have revealed the influence of the substrate's mechanical properties on the behavior of NSC, with most findings indicating that hydrogels with elastic modulus comparable to that of neural tissues ($G' = 100$-1000 Pa) are associated with higher NSC proliferation and enhanced expression of the neuronal marker βIII-tubulin [118, 206, 207].

Given this, it is evident that when developing hydrogel-based matrices for NSC culture it is crucial to not only ensure that hydrogels provide an adequate density of bioactive domains for integrin/growth factor/ECM binding, but also to evaluate hydrogel's mechanical/viscoelastic properties and assess whether or not these match those of native neural tissues [208]. In this regard, not only polymer concentration and cross-linking density regulate hydrogel's stiffness, also peptide density and affinity constitute important parameters influencing the biophysical properties of these materials [209]. Hence, evaluating the effect of adding increasing concentrations of AG73 peptide to the PEG-4MAL macromer is extremely relevant for the further deconvolution of biochemical and biophysical effects induced in NSC upon entrapment in the hydrogels.

In this work, the effect of peptide density on the mechanical/viscoelastic (stiffness) properties and structure (mesh size) of functionalized PEG-4MAL hydrogels was investigated by dynamic rheological studies. Briefly, acellular hydrogel samples were subjected to oscillatory shear experiments where a non-destructive sinusoidal signal was applied under rest conditions (before flow). An amplitude strain sweep was performed to confirm that subsequent measurements were conducted within the linear viscoelastic region (LVR) – data included in Appendix C. Storage/Elastic (G') and Loss/Viscous (G'') moduli, as well as phase angle (δ), were measured as a function of frequency (0.01 - 10 Hz) in a constant-strain (1%) mode to determine the hydrogels' mechanical spectra.

Figure 4.3 shows the results of the dynamic frequency sweep tests regarding both G' and G''. As shown in Figures 4.3A and 4.3B, all the prepared hydrogels exhibited $G' > G''$, which confirms the gel-like behavior of PEG-4MAL hydrogels and denotates the predominance of the elastic behavior when a constant load is applied. Hydrogels' elastic modulus exhibited a plateau in the range of 0.01 - 1 Hz, which is indicative of a stable, cross-linked network. At higher frequencies (1 - 10 Hz), however, all the hydrogels showed an increase in G'. The magnitude of viscoelastic response is related to the length of the polymer chains and the nature of the imposed mechanical motion. For long polymeric chains, such as those of the PEG-4MAL used, relaxation times are prolonged and so, when submitted to high frequencies, they fail to rearrange in the time scale of the imposed motion, giving rise to a sharp increase in G' [210, 211].

On the other hand, G'' decreased for low-frequency values and increased with increasing frequency at high frequency values (Figure 4.3B). These results show that at high frequencies, both G' and G'' increase considerably (*i.e.*, the material becomes more dissipative), which does not represent the mechanical properties of PEG-4MAL under stable conditions. Additionally, a great dispersion between samples was observed with respect to G''. This fluctuation might be related to the fact that, for both plain and functionalized PEG-4MAL hydrogels, the percentual uncertainties associated with G'' are considerably higher than the ones associated with G', which results from the prevalence of G' over G'', since the PEG-4MAL hydrogels considered are predominantly elastic.

Given the results of the dynamic frequency sweep, a range of frequencies (0.02 - 0.2 Hz) where G' and G'' reached a stable equilibrium was chosen. Considering this plateau range, all the prepared hydrogels presented $G' > G''$ (Table 4.2), showing that PEG-4MAL had transitioned from a viscous liquid to a gelled state. Moreover, all the formulations presented

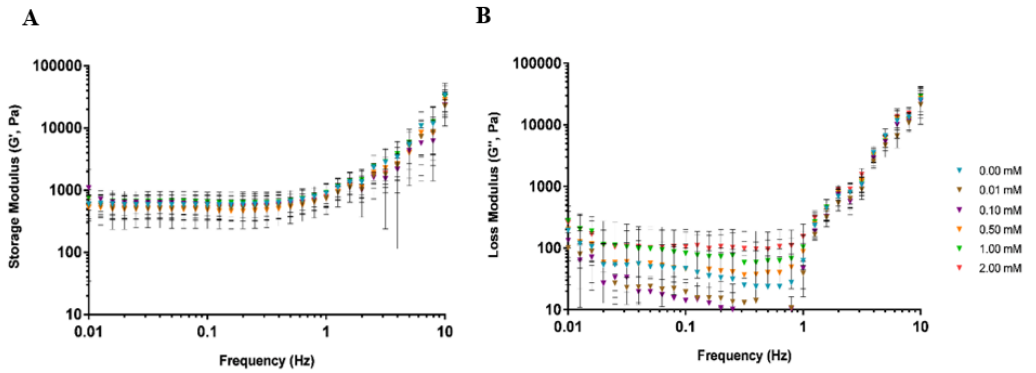

Figure 4.3: **Dynamic frequency sweeps** determined for AG73-functionalized PEG-4MAL hydrogels, at a fixed strain of 1%. (A) Storage Modulus (G') and (B) Loss Modulus (G'') as a function of frequency of oscillatory shear stress. Data represents mean ± SD ($n \geq 8$).

phase angle (δ) values below 10° (Table 4.2), meaning PEG-4MAL hydrogels have a predominance of elastic over viscous behavior[1] after swelling for 24h and that the viscoelastic properties of the hydrogels were stable for the conditions tested.

When compared to plain hydrogels, the tethering of AG73 peptide did not significantly impact the G' and G'' of PEG-4MAL hydrogels, independently of the input AG73 concentration (Figure 4.4). The dynamic complex modulus (G^*)[2] of these gels also did not change significantly for the different concentrations considered. This shows that the elastic and viscous components of the gels are not appreciably affected by the incorporation of this adhesive peptide for the range of concentrations tested, which indicates that both plain and functionalized PEG-4MAL swollen hydrogels present equivalent bulk mechanical/viscoelastic properties. Additionally, all biofunctionalized gels exhibited an average G' of $\approx$ 500 Pa, a stiffness lying in the range of those reported for human brain tissue (100 – 1000 Pa) [111–114].

Given a constant PEG-4MAL polymer density, when the adhesive peptide concentration is increased, the number of remaining MAL-terminated PEG chains available for cross-linking is reduced, which means a lower cross-linking density is required. This can be translated in terms of mechanical properties since a higher density of cross-links in the hydrogel network is associated with increased matrix stiffness and vice-versa [134]. Hence, as the concentration of AG73 peptide increases, gels with a lower G' value would be expected. However, since AG73-PEG-4MAL hydrogels only exhibit a maximum of 20% decrease in cross-linking density compared to plain hydrogels for PEG-4MAL functionalization with the highest AG73 concentration tested (2.00 mM), the different hydrogels prepared present cross-linking densities of similar magnitude order, and thus, show equivalent mechanical properties. This is also corroborated by the fact that polymer density (kept constant in this study) together with the cross-linking density strongly dictate hydrogel's mechanical properties [212], suggesting the range of AG73 peptide concentrations tested is possibly not sufficient to significantly affect the stiffness of PEG-4MAL hydrogels.

[1] The phase angle (δ) refers to the phase difference established between the applied sinusoidal compressive force and the resulting strain (deformation) of a viscoelastic material. $\delta = 0°$ indicates purely elastic materials, while $\delta = 90°$ refers to purely viscous materials.

[2] $G^* = \tau A$ / γA, where τA and γA represent the shear-stress amplitude (in Pa) and the strain amplitude (dimensionless, or expressed in %), respectively.

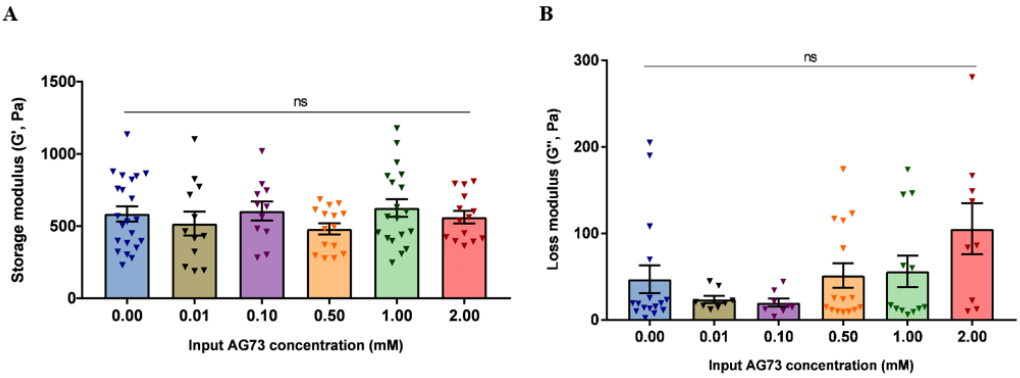

Figure 4.4: **Biophysical properties of functionalized PEG-4MAL hydrogels as a function of input AG73 concentration**, as assessed by dynamic rheometry. (A) Storage Modulus (G'); no significant differences (ns) were found between conditions ($p = 0.5115$, One-way ANOVA). (B) Loss Modulus (G''); no significant differences were found between conditions ($p = 0.429$, Kruskal-Wallis). Data represents mean ± SEM ($n \geq 8$).

It is however important to highlight that nanoscale heterogeneities observed in some hydrogels are often lost in bulk rheometric measurements [213], which means there might be critical differences in the PEG polymeric matrix at the cellular scale that influence the mechanical properties (*i.e.*, stiffness) sensed by hNSC and in turn affect their biological response. This is one of the reasons why the formation of uniform/homogenous networks is so relevant when developing hydrogel-based matrices for 3D cell culture.

Interestingly, the tethering of a scrambled sequence of AG73 (AG73T) resulted in PEG-4MAL gels with significantly reduced G', compared to plain gels and gels functionalized with equal amount of bioactive AG73 (Figure 4.5).

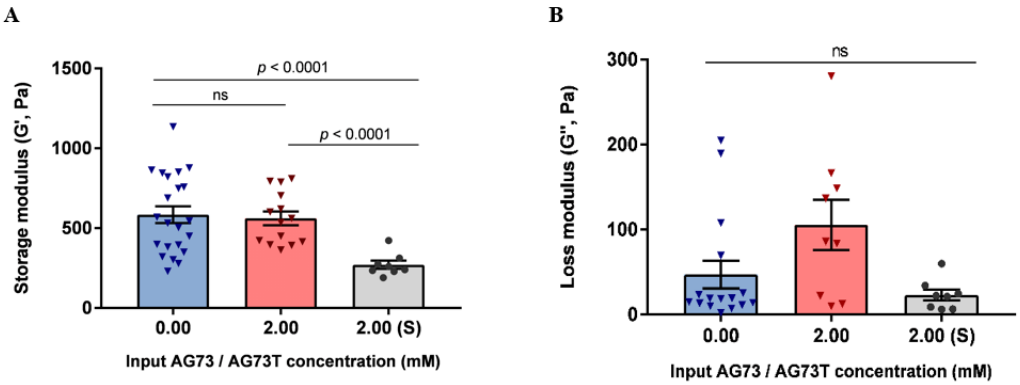

Figure 4.5: **Biophysical properties of functionalized PEG-4MAL hydrogels as a function of input AG73/AG73T concentration**, as assessed by dynamic rheometry. (A) Storage Modulus (G'); the tethering of a scrambled sequence of AG73 resulted in PEG-4MAL gels with significantly reduced G' (One-way ANOVA followed by Dunnett's T3 test). (B) Loss Modulus (G''); no significant differences (ns) were found between conditions (One-way ANOVA followed by Bonferroni's test). Data represents mean ± SEM ($n \geq 8$).

Scrambled inactive peptide sequences are typically used to achieve varying peptide functionalization densities while maintaining identical structures among hydrogel formulations, with the rationale that a constant cross-linking peptide density is kept [134]. However, the

results shown here demonstrate that this may not be true for all scrambled sequences. The data obtained suggests that the scrambled sequence may be interfering with the cross-linking process, leading to the formation of softer polymeric networks. This may result from electrostatic or hydrogen-bond interactions occurring between the scrambled peptide residues and the MMP2-sensitive peptide (degradable cross-linker). In fact, AG73T peptide exhibits a different hydropathic distribution of hydrophobic and hydrophilic amino acids compared to the bioactive AG73 peptide (as illustrated in Figure 4.6). Upon immobilization onto PEG-4MAL, the basic residues in the scrambled peptide (*i.e.*, arginine (Arg) and lysine (Lys)) are more exposed and available to interact with the MMP2-sensitive peptide when compared to AG73.

Considerations regarding peptides' net charge and isoelectric pH (identical for both scrambled and bioactive peptides), and even hydrogen-bonds/electrostatic interactions between the Arg/Lys side chains of the scrambled peptide and the aspartic acid side chain of the MMP2-sensitive sequence have been taken into thought, in agreement with studies evaluating the effect of ligand incorporation in the mechanical properties of PEG-based gels [137, 214]. Nevertheless, further characterization studies regarding the molecular interactions established between these two peptides would be required to understand the differential effect of AG73 and AG73T on the mechanical properties of PEG-4MAL hydrogels.

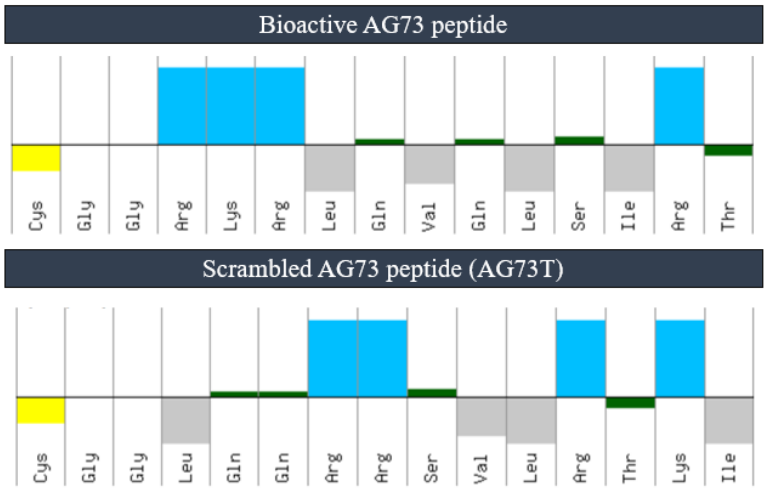

Figure 4.6: **Amino acid distribution of the bioactive** (top) **and scrambled** (bottom) **AG73 peptide sequences** used to functionalize PEG-4MAL hydrogels. For each scheme, amino acids denoted above and below the line represent amino acid residues with hydrophilic and hydrophobic properties at physiological pH, respectively. Blue represents amino acids with positively charged side chains (basic); green represents amino acids with polar uncharged side chains; grey represents amino acids with hydrophobic side chains (aliphatic).

Given the results obtained for the scrambled-presenting gels, the entire viscoelastic behavior of these materials, namely G^* and δ were also evaluated, as a measure of the material's stiffness and overall viscoelastic/mechanical properties. As shown in Figure 4.7A, the tethering of AG73T resulted in PEG-4MAL gels with significantly reduced G^* compared to both plain hydrogels and gels modified with the same concentration of bioactive peptide, even though no significant differences were found regarding δ (Figure 4.7B). This corroborates the previous

results that showed that functionalized gels are predominantly elastic, but it also indicates that scrambled-presenting gels exhibit softer mechanical properties (*i.e.*, lower resistance to deformation). As for δ, it is important to reckon that a high dispersion between samples was observed, which means a much higher number of replicates would be needed to detect significant differences between conditions.

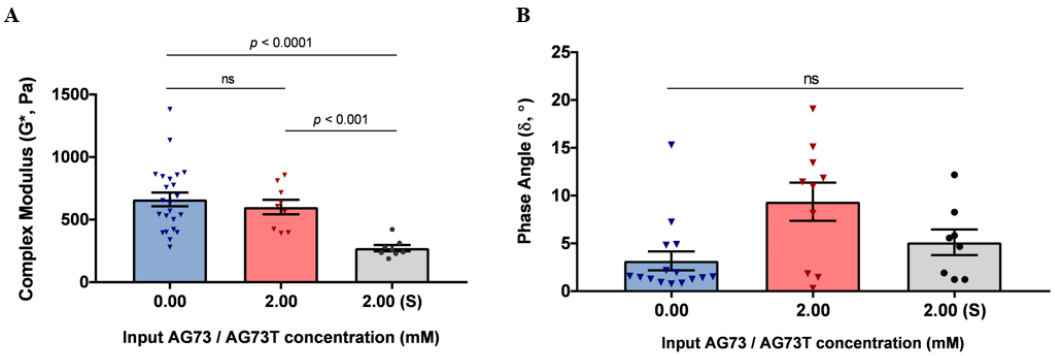

Figure 4.7: **Biophysical properties of functionalized PEG-4MAL hydrogels as a function of input AG73/AG73T concentration**, as assessed by dynamic rheometry. (A) Complex Modulus (G^*); the tethering of a scrambled sequence of AG73 resulted in PEG-4MAL gels with significantly reduced G^* (One-way ANOVA followed by Dunnett's T3 test). (B) Phase angle (δ); no significant differences (ns) were found between conditions ($p = 0.0598$, Kruskal-Wallis). 'S' stands for scrambled peptide sequence. Data represents mean $\pm$ SEM ($n \geq 8$).

As previously mentioned, the fine control over the hydrogels' viscoelastic properties is crucial to direct NSC fate, as well as to modulate the integrity of these hydrogel-based matrices (*in vitro* and *in vivo*) [109]. Hence, these results point to the importance of the characterization of the viscoelastic properties of hydrogels functionalized with scrambled sequences of bioadhesive peptides, to avoid misleading interpretation of cell experiments.

As a further indicator of the physical network structure of plain and AG73-PEG-4MAL hydrogels, the mesh size (ξ) was also estimated. This parameter quantifies the average distance between two-adjacent cross-linking points (as schematically shown in Figure 4.8A), thus giving an approximation of the molecular hydrogel porosity and diffusibility [215]. No significant differences were found regarding the mesh size of AG73-PEG-4MAL hydrogels, regardless of the input AG73 concentration considered (Figure 4.8B).

Contrarily, the functionalization with a scrambled peptide sequence led to the formation of a significantly looser polymer network, as evidenced by the greater average mesh size value of these gels when compared to plain hydrogels and gels modified with the same amount of the bioactive AG73 peptide (Figure 4.8C). As expected, this is in accordance with previous results regarding the lower G' of the hydrogels modified with the scrambled peptide sequence, since this estimation is based on the elastic modulus of the corresponding gels. In addition, these results also corroborate the hypothesis of scrambled peptide–degradable cross-linker interaction and subsequent reduced cross-linking of the polymer network, since the removal of cross-linking points typically results in the formation of looser networks with higher average mesh sizes [195], as evidenced by scrambled-presenting gels. When some of the cross-linking points are disrupted, as seems to be the case of these gels, there is the formation of local

"pockets" with larger mesh that are able to incorporate more water, thus increasing the soft nature of PEG-4MAL gels functionalized with scrambled AG73 peptide sequence (2.00 mM).

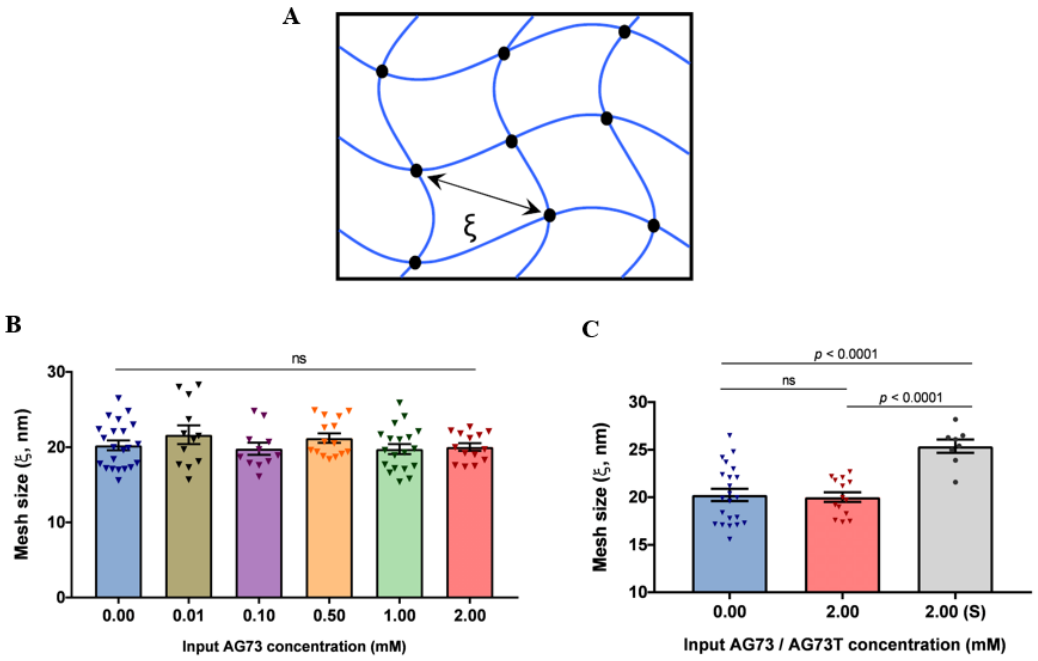

Figure 4.8: **Hydrogels' mesh size estimation.** (A) Simplified cross-linked hydrogel structure. Black dots represent cross-linking points; ξ represents the average mesh size of the gel. As found in [131]. (B) Mesh size as a function of input AG73 concentration; no significant differences (ξ) were found between conditions ($p = 0.4249$, One-way ANOVA). (C) Mesh size as a function of input AG73/AG73T concentration; the tethering of a scrambled sequence of AG73 significantly impacted the mesh size of PEG-4MAL gels (One-way ANOVA followed by Bonferroni's test).'S' stands for scrambled peptide sequence. Data represents mean ± SEM ($n \geq 8$).

It is important to notice that the mesh size estimation presumes the ideal cross-linking of the synthetic network, when, in reality, there are molecular defects (*e.g.*, unreacted groups leading to dangling chains or matrix inhomogeneities) that can substantially increase the effective mesh size, or even physical entanglements that instead contribute to its decrease [216]. Therefore, given the evident heterogeneities formed upon gelation in all prepared gels, it is possible that the space available among the polymer chains in the 3D hydrogel matrix (*i.e.*, the "real" mesh size) encountered by cells slightly differs from the estimation made based on the G' [216, 217].

Table 4.2: Summary of the different biophysical properties of AG73-functionalized PEG-4MAL hydrogels, assessed by dynamic rheology. δ values are highlighted since G', G'' and ξ plots have already been presented. Data represents mean ± SEM ($n \geq 8$).

Input AG73 concentration (mM)	Storage Modulus (G', Pa)	Loss Modulus (G'', Pa)	Complex Modulus (G*, Pa)	Phase angle (δ, °)	Mesh size (ξ, nm)
0.00	584.4 ± 52.9	47.0 ± 16.1	662.2 ± 55.3	3.2 ± 1.0	20.2 ± 0.6
0.01	517.5 ± 82.8	23.8 ± 4.2	693.2 ± 94.6	1.9 ± 0.5	21.7 ± 1.2
0.10	604.8 ± 65.8	19.78 ± 4.7	841.5 ± 79.0	1.2 ± 0.1	19.8 ± 0.8
0.50	481.0 ± 39.1	51.2 ± 14.3	642.6 ± 86.4	8.2 ± 2.6	21.2 ± 0.6
1.00	625.4 ± 61.2	56.0 ± 18.2	850.6 ± 80.1	6.0 ± 2.2	19.8 ± 0.7
2.00	561.6 ± 43.3	105.3 ± 30.0	601.2 ± 58.1	9.4 ± 2.0	20.0 ± 0.5
2.00 (S)	271.2 ± 25.2	23.1 ± 6.3	272.9 ± 25.1	5.1 ± 1.3	25.4± 0.7

Based on the evidence obtained from the characterization of AG73-functionalized PEG-4MAL hydrogels, one can argue that because the adhesive peptide-functionalized macromer building blocks are symmetric and form a regular mesh structure, the AG73 peptide should be uniformly distributed throughout the hydrogel network within the average δ (20-22 nm), apart from local network heterogeneities in which a random distribution of cross-links is found.

Overall, we showed that, regardless of the input AG73 concentration, stable cross-linked networks with a known level of functionalization and a stiffness comparable to that of brain tissue could be obtained. Additionally, since the incorporation of the bioactive peptide did not significantly affect the biophysical properties of PEG-4MAL hydrogels, the independence between mechanical/structural proprieties and matrix bioactivity was ensured.

4.3 Phenotypic characterization of the hNSC cell line

Since a high cell passage number (6-16) was being used (according to the H9-derived hNSC technical datasheet [218]), and it is reported that hNSC neuronal differentiation potential can be affected with increasing passages, both the stemness and neuronal differentiation capacity of hNSC was evaluated upon culture on 2D substrates. This study allowed us to investigate hNSC status and to understand if the results obtained for the 3D culture of hNSC within AG73-PEG-4MAL hydrogels would be compromised. To this end, hNSC were seeded at a low cell seeding density and cultured under neuronal differentiation conditions for 2, 7, 14 and 21 days of culture on poly-L-ornithine/laminin-coated coverslips. As depicted in Figure 3.2, neuronal commitment by growth factor withdrawal is only induced two days after cell platting, which means hNSC could still proliferate as progenitors during this period. Hence, the first selected time point should provide valuable insight regarding the stemness and proliferative potential of the hNSC used. The expression of stem/multipotency marker genes, as well as of differentiated lineage markers was examined through immunohistochemical analysis using specific lineage markers.

Nestin is a class VI intermediate filament protein that is commonly used as a neural stem/progenitor cell marker. Although it is predominantly expressed in undifferentiated

CNS cells during development, its expression is absent from nearly all mature CNS cells, which makes it a valuable candidate for the assessment of NSC stemness and multipotency [219]. The **Ki67** nuclear protein is a well-known endogenous cell proliferation marker that can be immunohistochemically detected during all active phases of the cell cycle [220]. Due to the highly proliferative nature of neurogenesis, Ki67 has also been used as a cellular maker for NSC proliferative status [221].

After two days of culture in complete serum-free medium and prior to growth factor withdrawal, hNSC thoroughly expressed nestin, and most were positive for the proliferation marker Ki67, as evidenced by the blue-green fluorescence resulting from the colocalization of the nuclei (blue) and Ki67 (green) (Figure 4.9). These results are indicative of the high stem and proliferation potential of the hNSC used. In addition, hNSC acquired a bipolar morphology (as illustrated by the cells marked with an arrow in Figure 4.9), typical of the NSC phenotype upon culture in serum-free conditions [222].

Following qualitative image analysis, the images acquired were processed using Fiji software to get information regarding the number of stem/multipotent and proliferating hNSC. The quantitative analysis revealed that on average 87 ± 2 % of the cells stained positive for the neural stem cell-type specific marker nestin (Nestin$^+$ cells), while 82 ± 5 % of the cells stained positive for the proliferation marker Ki67 (Ki67$^+$ cells), thus confirming that the hNSC used retain both their stemness and proliferative potential after several passages. These results are in agreement with the features enunciated for GIBCO® hNSC (H9-Derived) in their technical datasheet [218], as well as with studies that have comprehensively analyzed hNSC's features [223–225]. Of note, the quantification also showed that on average 75 ± 9 % of the cells stained positive for both Nestin and Ki67 (Nestin$^+$/ Ki67$^+$ cells), indicating that most stem/multipotent cells are indeed proliferating cells.

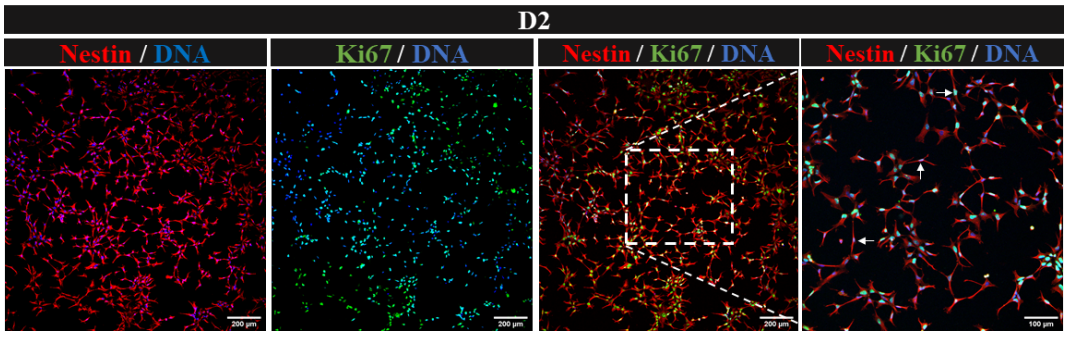

Figure 4.9: **Nestin (NSC marker) and Ki67 (proliferative marker) expression in hNSC at day 2 of neuronal differentiation** on poly-L-ornithine/laminin-coated 2D substrates (before EGF and bFGF withdrawal). Images show representative 2D projections of CLSM stack images of hNSC processed for immunofluorescence labelling of Nestin (red) and Ki67 (green); cell nuclei were counterstained with Hoechst (blue). Scale bar = 200 μm; 100 μm (amplification).

Regarding the differentiation potential and lineage commitment of differentiated hNSC, two neuronal specific markers were chosen: βIII-tubulin and MAP2. **βIII-tubulin** (TuJ1) is a microtubule protein, thought to be involved in the process of neuronal differentiation. It is usually found in the dendrites, axons and axonal terminations of immature neurons. On the other hand, **MAP2** is a neuron-specific cytoskeletal protein that is also frequently used as a

marker of a more mature neuronal phenotype. Its expression is weak in neuronal precursors but becomes pronounced right after βIII-tubulin expression [226]. MAP2 is thought to play a role in determining and stabilizing dendritic shape during neuronal development and is accordingly observed within the dendritic arbor [227].

At day 2, hNSC thoroughly expressed nestin (comparable to what is shown in Figure 4.9), but there was also a significant percentage of cells expressing βIII-tubulin (Figure 4.10A). By qualitative image analysis, a high percentage of Nestin$^+$/ βIII-tubulin$^+$ hNSC was found, which indicates the presence of hNSC already committed to the neuronal lineage. Comparing these results with the same immunofluorescent staining performed at day 7 of cell culture (Figure 4.10B), evident differences can be pointed out. First, the number of hNSC has reduced substantially, which can be related to the fact that cells are no longer actively proliferating (due to the absence of mitogenic factors) and a lot of cell death has occurred. Additionally, βIII-tubulin expression seems to have intensified, even though nestin expression is still present in most cells. This data shows that after 7 days in culture under neuronal differentiation conditions, the hNSC used still have some stemness potential, but have been greatly affected in number.

Further analysis at day 7 of cell culture revealed MAP2 expression in most of the cells (Figure 4.10B), thus confirming hNSC neuronal phenotype and maturation, as well as neuronal differentiation capacity *in vitro*. MAP2-stained neurons did not display long, branched processes, which indicates that hNSC are still in the beginning of the neuronal maturation process [228]. Additionally, after 14 and 21 days of culture, a population of differentiated neurons expressing βIII-tubulin and forming a dense neuronal network could be observed (Figures 4.10C and 4.10D, respectively). In fact, for both timepoints hNSC developed neural sphere-like structures from which βIII-tubulin-positive cells with long processes grew out, indicating that hNSC were able to differentiate into mature neurons and establish neuronal interconnections. These results are in accordance with the typical hNSC H9 phenotype upon adherent culture in serum-free medium conditions [229].

Given that the purpose of this work was to develop proteolytically degradable AG73-PEG-4MAL hydrogels allowing cell-induced remodeling and matrix deposition, the deposition of neurogenic ECM proteins (*i.e.*, laminin, collagen type IV and fibronectin) after 14 and 21 days of hNSC neuronal differentiation was also investigated. hNSC were found to secrete endogenous ECM proteins present in the embryonic neural stem cell niche, namely laminin, collagen IV and fibronectin. These were shown to be closely associated with the area surrounding the cellular aggregates formed at both 14 and 21 days of culture (Figure 4.11), which not only demonstrates the mature phenotype of hNSC, but also confirms their neuronal differentiation capacity. The presence of such ECM components has already been shown by previous studies using hNSC [200, 229]. On the other hand, laminin's expression was absent after 14 days of culture and still on day 21 a limited expression and distribution of this ECM protein could be observed, comparatively to collagen IV and fibronectin (Figure 4.11C). Given laminins' abundance and key role in the neurogenic niches, as regulators of both neural progenitor proliferation and neuronal differentiation, an early laminin expression by hNSC was expected. However, there are several arguments that may justify this absence: (1) the antibody used in immunohistochemical studies detects the human α1 laminin chain, which is thought to be present in low levels in the embryonic SVZ [74]; (2)

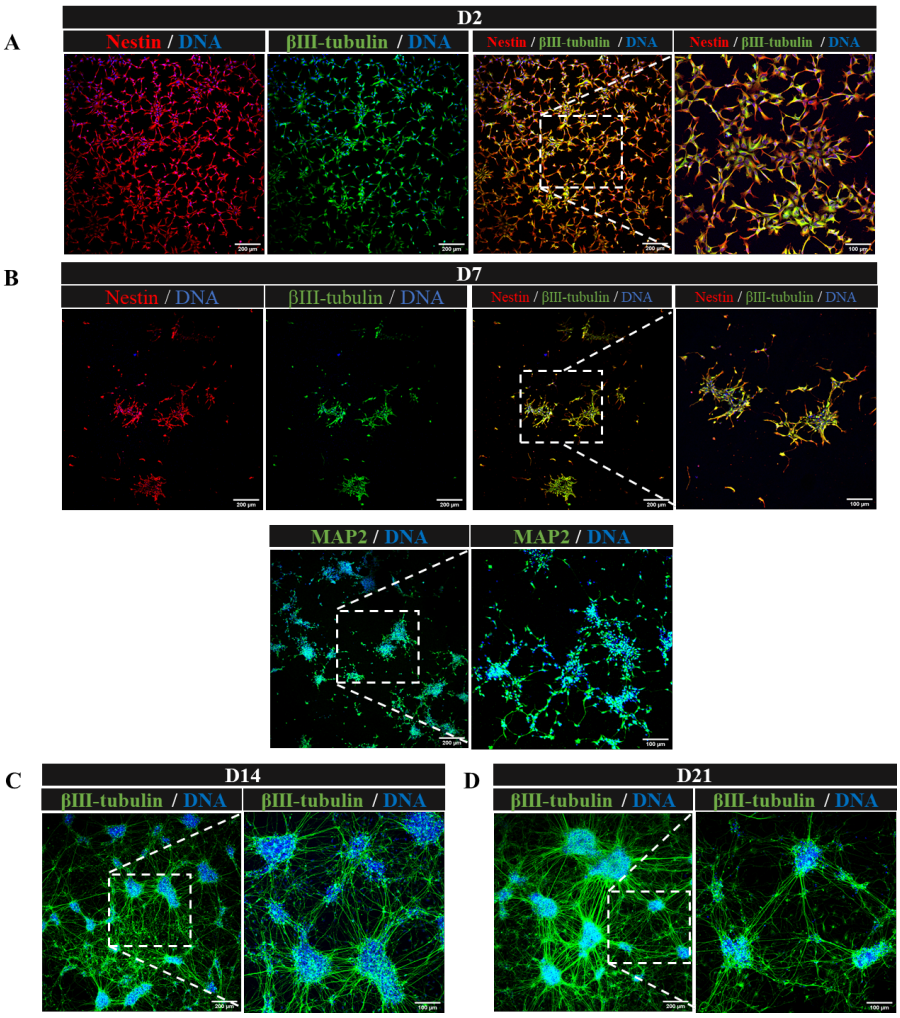

Figure 4.10: **Nestin (NSC marker), βIII-tubulin (early neuronal marker) and MAP2 (mature neuronal marker) expression in hNSC** cultured on poly-L-ornithine/laminin-coated 2D substrates under neuronal differentiation conditions. Images show representative 2D projections of CLSM stack images of hNSC processed for immunofluorescence labelling after (A) 2, (B) 7, (C) 14 and (D) 21 days of cell culture; cell nuclei were counterstained with Hoechst (blue). Scale bar = 200 μm (10×); 100 μm (20×).

laminins' polymerization process requires the exposure and interaction of laminin short arms (N-terminus) from α, β and γ chains [230, 231], so when it is not connected in a polygonal network, soluble laminin can be easily removed from the culture system, hindering detection [232]; (3) most laminin present in the neurogenic niches is produced by other important cells such as ependymal cells (in the case of laminin present in fractones) and endothelial cells [70, 74]. Given this scenario, it would be interesting to evaluate the presence of other laminin isoforms (such as α2, α3 or α5) in the 2D cultures, but also to investigate the expression of these isoforms by hNSC using reverse transcription quantitative polymerase chain reaction (RT-qPCR).

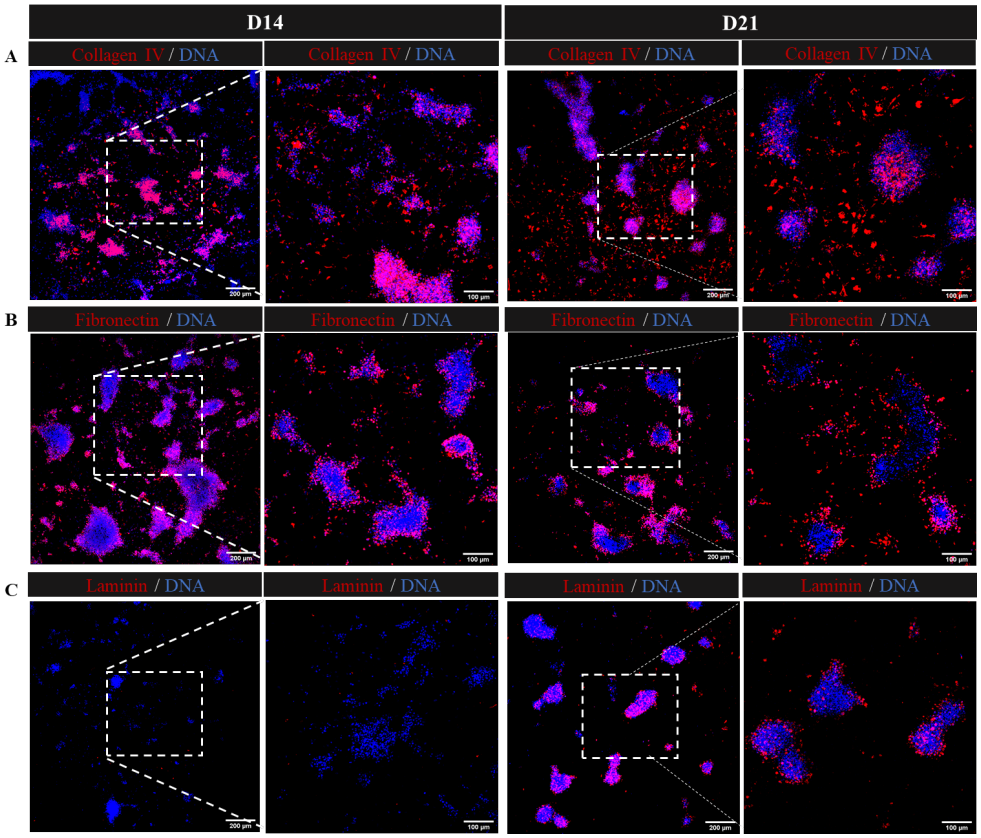

Figure 4.11: **ECM deposition by hNSC** cultured on poly-L-ornithine/laminin-coated 2D substrates under neuronal differentiation conditions. Images show representative 2D projections of CLSM stack images of hNSC cultured for 14 and 21 days, and processed for immunofluorescence labelling of (A) collagen IV (red), (B) fibronectin (red) and (C) laminin; cell nuclei were counterstained with Hoechst (blue). Scale bar = 200 μm (10×); 100 μm (20×).

4.4 Biological characterization of AG73-functionalized PEG-4MAL hydrogels

The potential of AG73-PEG-4MAL hydrogels to support hNSC viability, proliferation and neuronal differentiation was subsequently evaluated. For this purpose, H9-derived hNSC were cultured within AG73-functionalized hydrogels under neuronal differentiation conditions for up to 14 days, and the effect of AG73 peptide density on hNSC behavior assessed.

The viability of hNSC within AG73-PEG-4MAL hydrogels was first qualitatively assessed at day 2 and 7 of cell culture using a live/dead assay. Confocal microscopy analysis of cell-laden gels incubated with vital/dead dyes showed the presence of live cells widely distributed throughout all hydrogels, often growing as cellular spheroids (Figure 4.12A). However, when compared to plain gels (0.00 mM AG73), a higher density of viable cells was consistently found for PEG-4MAL hydrogels functionalized with $\geq$ 0.5 mM of AG73 peptide (Figure 4.12A). Although evident in both timepoints selected, images taken at day 7 of culture illustrate this difference more clearly, possibly because hNSC had already had time to recover from the encapsulation-induced stress and were thus more receptive to the surrounding environment. Altogether, these results confirm the good cytocompatibility of the proposed

matrices and suggest the importance of the AG73 syndecan binding peptide in supporting hNSC viability.

Contrarily, hydrogels functionalized with a scrambled sequence of AG73 failed to support hNSC viability right after two days of culture. As evidenced in Figure 4.12A, hNSC cultured in scrambled-modified gels aggregated into cellular spheroids of large dimensions that disintegrated overtime due to the lack of a supportive matrix. Adding these results to the fact that PEG-4MAL hydrogels functionalized with a scrambled sequence of AG73 exhibited significantly reduced G' values, it can be suggested that the weaker mechanical properties (lower stiffness) of the scrambled-modified gels were responsible for the lower hNSC viability observed. Moreover, when comparing hNSC behavior on these gels with unmodified ones, it is clear that the bioinertness of plain gels does not severely compromises cell viability, thus suggesting the lack of biospecificity of the scrambled sequence is not responsible for the lower hNSC viability, but rather the lower integrity of the polymeric network. In fact, of all hydrogels prepared, scrambled-modified gels were the ones presenting the fastest degradation rate, which is in accordance with their softer nature and looser polymer network (possibly responsible for a higher water content and easier disintegration of the synthetic matrix).

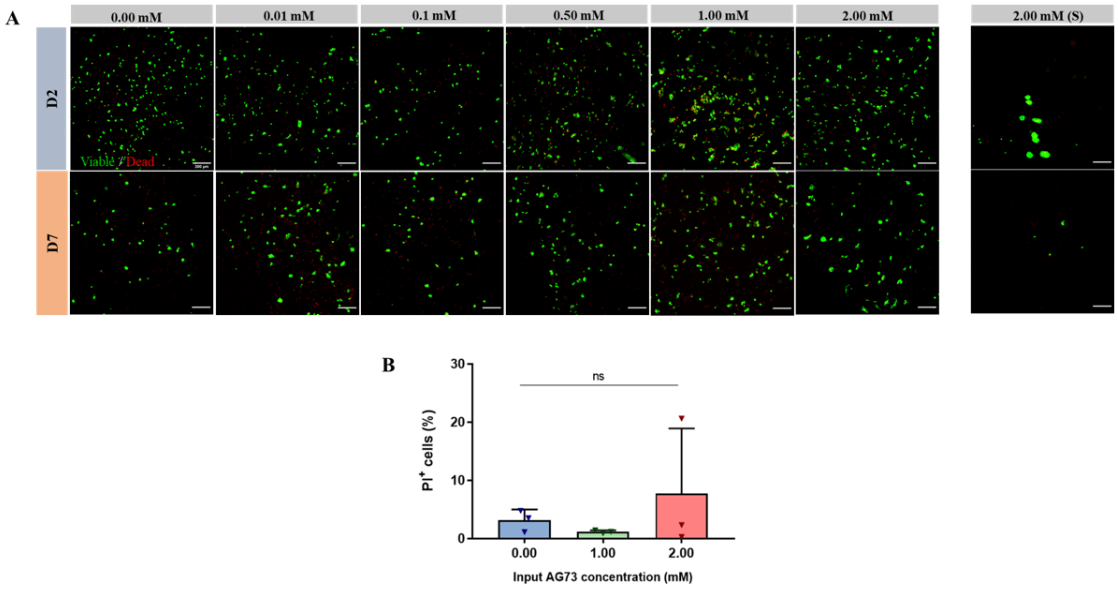

Figure 4.12: **Ability of AG73-functionalized PEG-4MAL hydrogels to support hNSC viability.** (A) Representative 2D projections of CLSM 3D stack images of cell-laden hydrogels incubated with calcein AM and PI, for detection of viable (in green) and dead (in red) cells, respectively; images taken at day 2 and 7 of culture under neuronal differentiation conditions, covering a thickness of 200-300 μm; Scale bar = 200 μm. Images are representative of three independent experiments. (B) Quantitative analysis of dead cells (PI^+ cells) at day 7 of culture, as determined by flow cytometry; no significant differences (*ns*) were found between conditions ($p = 0.5756$, One-way ANOVA); data represent mean ± SD of three independent experiments.

The viability of hNSC cultured within AG73-functionalized PEG-4MAL hydrogels was also assessed by flow cytometry at day 7 of culture, after cell isolation from the gels. The quantitative analysis of live and dead cells showed values of average cell dead lower than 10% for all the conditions tested, evidencing the cytocompatibility of PEG-4MAL hydrogels towards

hNSC (Figure 4.12B). Representative scatter dot-plots are shown in Appendix D. It is important to highlight that the percentage of live cells was not considered for the quantitative analysis of hNSC viability since a very reduced amount of cells was consistently reported as positive for calcein (in contrast to what was observed in live/dead assays). We hypothesize that the calcein AM concentration used was not sufficient to detect the effective number of live cells, possibly due to the lower cell metabolic activity induced by the distress of hydrogel dissociation or the hNSC's physiological state.

To get insight into the effect of peptide density on hNSC proliferation, cells were cultured for 7 days within degradable PEG-4MAL hydrogels and characterized in terms of total cell number (proliferative capacity) using the CyQuant® Cell Proliferation kit (based on the quantification of total DNA amount). Although no significant differences regarding hNSC growth were found between AG73-PEG-4MAL hydrogels and unmodified gels, a slight increase in cell number of 1.1-fold (vs. plain gels) was observed for gels modified with 1.00 mM of AG73 (Figure 4.13), which suggests that the use of this amount of AG73 improves the hNSC outcome comparing to gels without biospecificity. It is however worthy of note that the total number of hNSC after 7 days of culture was considerably low comparing to the initial number of entrapped cell (4×10^4 cells/hydrogel). In fact, after the process of cell isolation from cell-laden hydrogels and cell dissociation, on average, 15 ± 3 % of the initial cell amount was found for unmodified gels, while for gels functionalized with 1.00 mM of AG73, 17 ± 5 % of the initial cell number was detected. It is important to highlight that the process of gel dissociation could have also contributed to the early loss of hNSC due to the mechanical stress induced on cells during the isolation from the polymeric network. Additionally, the presence of polymer network inhomogeneities at the cellular scale may have provided locally different mechanical stimuli that negatively influenced the biological response of hNSC.

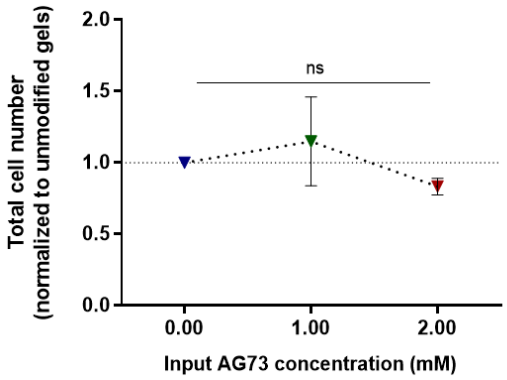

Figure 4.13: **Total number of cells present in AG73-functionalized PEG-4MAL hydrogels** after 7 days of culture under neuronal differentiation conditions, inferred from total DNA amount quantification. Results are presented as a fold increase comparatively to unmodified gels (adjusted to 1). No significant differences (*ns*) were found between conditions ($p = 0.2769$, One-way ANOVA). Data represents mean ± SD of three experiments performed in triplicate.

4.4.1 Ability of AG73-functionalized PEG-4MAL hydrogels to support hNSC neuronal differentiation

Besides assessing the effect of immobilized AG73 peptide on hNSC viability and proliferation, the influence of this syndecan-binding peptide on hNSC neuronal differentiation was also evaluated. This allowed us to examine the neuronal differentiation potential and maturation level of hNSC upon entrapment and culture within the synthetic matrices. For this purpose, hNSC cultured within AG73-functionalized PEG-4MAL hydrogels for 14 days were processed as whole-mounts for βIII-tubulin and DNA staining.

Qualitative analysis of CLSM images revealed a higher number of hNSC-derived neurons expressing βIII-tubulin for PEG-4MAL gels functionalized with the highest AG73 concentrations (1.00 and 2.00 mM) - Figure 4.14. These results indicate that the AG73 peptide improves hNSC neuronal differentiation, possibly by recapitulating some of the features present in neurogenic niches. Despite the inconclusive results, it would make sense that greater concentrations of AG73 peptide were required to effectively promote hNSC outgrowth upon culture within PEG-4MAL hydrogels, since these lack inherent biospecificity (*e.g.*, integrin or heparin-binding motifs), compared for instance to fibrin-based hydrogels, which have been shown to promote hNSC outgrowth when functionalized with lower concentrations of AG73 (60 μM) [151]. These natural-based gels contain fibrinogen, a glycoprotein that has heparin-binding domains at its N-terminus with high affinity to syndecans, thus potentiating the effect of AG73, even at low concentrations.

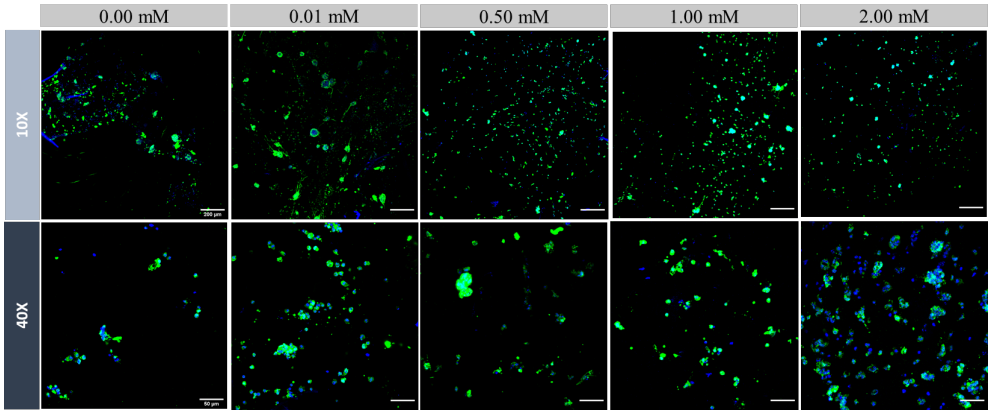

Figure 4.14: **Ability of AG73-functionalized PEG-4MAL hydrogels to support hNSC neuronal differentiation.** Images show representative 2D projections of CLSM 3D stacks of hNSC cultured within unmodified (0.00 mM) and AG73-functionalized (0.01, 0.50, 1.00 and 2.00 mM) PEG-4MAL hydrogels for 14 days under neuronal differentiation conditions, and processed for immunofluorescence labeling of βIII-tubulin (early neuronal marker, in green); cell nuclei were counterstained with Hoechst (blue). Scale Bar = 200 μm (10×); 50 μm (40×). Images are representative of three independent experiments.

Even though the culture of hNSC for 14 days in AG73-functionalized gels promoted the formation of βIII-tubulin$^+$ cells capable of some neurite extension – without following any clear pattern (as illustrated in Appendix E) –, all the conditions tested failed to support significant neurite outgrowth.

Taken together, we can hypothesize that the process of hNSC neuronal differentiation will be delayed upon embedment in the gels, not only because cells undergo a reduction in number, but also due to accumulation of some mitogenic factors (such as EGF and bFGF) in the hydrogel polymeric structure during the first two days of culture. Even though crucial for maintaining proliferation of hNSC, the removal of EGF and bFGF is known to significantly increase neuronal differentiation and neurite extension. The presence of residual amounts of these factors might be contributing to the delayed differentiation of hNSC [233]. Therefore, given the culture conditions presented, the assessment of βIII-tubulin expression after longer periods of culture (*e.g.*, after 21 days) becomes relevant for better understanding the effect of AG73 peptide on NSC behavior.

Although the hydrogel's mechanical and structural properties are known to have a key role on the modulation of different cellular functions, including survival, proliferation and neurite outgrowth, we have confirmed that the incorporation of AG73 peptide does not significantly impact the bulk mechanical properties of PEG-4MAL hydrogels. This suggests that the results observed regarding hNSC behavior are not related to possible bulk stiffness variations induced by the tethering of an adhesive peptide, but rather associated to the bioactivity of the AG73 syndecan-binding peptide. It is however important to recall that the rheological characterization of functionalized PEG-4MAL hydrogels does not account for local heterogeneities at the nanoscale, and these can be relevant at the cellular level. In fact, hydrogel inhomogeneities are thought to promote different cell behavior within the polymer matrix and from gel to gel (given the reduced reproducibility between drops), making it difficult to recognize the culture conditions favoring neurite extension.

4.5 Optimization of AG73-functionalized PEG-4MAL hydrogels' biophysical properties for a better support of hNSC culture

Gathering all the information regarding hNSC viability, proliferation and neuronal differentiation upon culture within AG73-functionalized PEG-4MAL hydrogels (for a maximum of 14 days), it becomes evident that changes in the hydrogel's biophysical properties have to be made so as to create a more favorable environment to the proliferation and differentiation of hNSC. From previous results we have seen that the several polymer network inhomogeneities present in the PEG-4MAL matrices might have contributed to a less uniform cell behavior or even to the worsening of hNSC's biological response, as at the cellular scale the environment sensed by cells might have not been the most suitable to proliferation and neuronal differentiation.

Additionally, both unmodified and AG73-functionalized gels exhibited a high degradation rate, which means at a certain point hNSC stop having the 3D environmental support necessary for establishing cell-cell and cell-ECM interactions. More importantly, this does not give cells enough time to completely remodel the surrounding matrix and establish interconnections that culminate in complex neuronal networks.

In fact, since our end-goal is to improve cell-based therapies by developing artificial niches that mimic the native neural environment, it is crucial that the hydrogel-based hNSC delivery vehicles be not only homogenous in structure and mechanical properties, but also stable over the time frame required for hNSC differentiation. Hence, in order to achieve the best biological response (in terms of cellular behavior and biomaterial overall integrity), both the **gelation kinetics** and **degradability** of the hydrogels should be tuned to improve the overall polymer network homogeneity and time available for culture, respectively. In the context of this thesis, both these parameters have been addressed in parallel and will be further discussed in the following sections.

4.5.1 Optimization of the gelation kinetics of PEG-4MAL hydrogels

Although PEG-4MAL hydrogels present many advantages comparing to other engineered synthetic-based systems, mainly because of their biocompatibility, high cross-linking efficiency and easiness of functionalization with bioactive ligands, they exhibit a very fast gelation/polymerization speed that often results in the formation of heterogeneous networks [125, 234]. The high reaction efficiency of the maleimide functional group causes the polymer network to assemble faster than individual components can be evenly mixed, which results in non-uniform ligand densities and cross-linking gradients, randomly placed across the matrices [136, 204]. Hence, even though PEG-4MAL hydrogels can be easy and rapidly prepared *in situ*, while under physiological conditions [235], they usually present several matrix inhomogeneities visible at the macroscopic scale [236, 237]. As previously showed, the AG73-functionaled PEG-4MAL hydrogels prepared also encountered this heterogeneity issue due to their rapid gelation kinetics, which is thought to have influenced the behavior of hNSC cultured within the gels.

Several studies examining the kinetics of these Michael-type addition reactions and assessing the biophysical properties of the resulting gels have been developed [125, 134, 238]; however, few have actually addressed the tuning of the gelation kinetics with the goal of slowing the cross-linking speed of these networks to achieve more uniform gels [136, 203, 204]. In this regard, changing the pKa of the thiol (Michael-type donor) or altering the buffer conditions (*e.g.*, by lowering the pH) are the most common strategies used to interfere with the thiolate formation and slow the polymerization rate of PEG-4MAL hydrogels [204, 239].

Attempts to increase the pKa of the thiol group and thereby reduce the availability of the reactive thiolate upon mixing of the precursor solution (containing PEG-4MAL macromers) and the cross-linkers solution had already been made by previous work in our group [168]. The di-thiol-containing MMP2-sensitive cross-linker peptide used in this work was designed to include negatively charged amino acids (*i.e.*, aspartates, D) flanking the thiol-bearing cysteine residue (DCDD). Although this strategy considerably improved the mixing of the hydrogel solutions before gelation comparatively to the MMP2-sensitive peptide without negatively charged amino acids (by allowing more time for the manual homogenization of the solutions) – data not shown –, it was not enough to greatly reduce the inhomogeneities formed upon hydrogel polymerization. Therefore, we tried an additional strategy which included lowering the pH of the buffer solution.

Since the thiol-maleimide reaction depends on the thiol pKa, because the thiol/thiolate equilibrium is modulated by buffer pH (as described by the Henderson-Hasselbalch relationship) [203, 204], our hypothesis was that leaving the pH of the precursor solution at 6.5 (instead of adjusting it to 7.4) would lower the pH of the final hydrogel solution, thus slowing the gelation speed and allowing the formation of more uniform gels. When using this kind of approach, it is important to recall that cells tolerate a rather restricted pH range, meaning cell viability can be affected if cells are put at non-physiological pH. Although a pH of 6.5 is still within the physiological range of many biochemical reactions, it was unknown how sensitive hNSC were to external buffer changes and what would be the impact of a lower pH in their viability; hence, a high glucose supplement was added to the reaction buffer (*i.e.*, the PEG-4MAL macromer solution). This was done in accordance with a recent study that used high glucose concentrations to preserve the cell viability of MDA-MB-231 and SkBr3 breast cancer cell lines upon entrapment in hydrogel-based matrices [203].

With this rationale in mind, hNSC-laden functionalized PEG-4MAL hydrogels were prepared according to the different reaction conditions; variables under study included the pH of the hydrogel precursor solution (7.4 *vs.* 6.5) and the presence/absence of a high glucose supplement (used at a final concentration of 25 mM in the gels [3]).

The time allowed for the manual mixing of the different hydrogel components, herein described as the gelation time, was first determined. This parameter was recorded as the time taken to complete the manual homogenization of the precursor and cross-linkers solutions with a pipette. As shown in Figure 4.15, hydrogels prepared from precursor solutions which pH was left at 6.5 exhibited significantly slower gelation kinetics when compared to hydrogels where the pH of the precursor solution had been adjusted to 7.4. Hence, by increasing the pH of the precursor solution to a physiological value (7.4), we are reducing the time allowed for the homogenization of the hydrogel's individual components, which contributes to a poorer mixing process. These results are in accordance with previous data showing that more basic pHs increase the kinetics of the thiol-maleimide reaction and are thus associated with faster gelation rates, while acidic pHs decrease the speed of the reaction which correlates to slower gelation rates [203].

Additionally, the hydrogels prepared at a lower pH also presented a more uniform polymer network, with a lower number of visible heterogeneities (as illustrated in Figure 4.16), as compared to the corresponding hydrogels prepared at a physiological pH (Figure 4.1). This confirms the correlation between slower polymerization processes (favored at lower pHs) and the formation of more homogenous hydrogel structures. Importantly, the impact of slower gelation kinetics was not examined at the microscale structure level, which indicates that the polymer networks prepared might still exhibited smaller and non-visible inhomogeneities. However, the effect of these irregularities on the biological response of hNSC is expected to be considerably reduced.

Subsequently, the viability and metabolic activity of hNSC entrapped in the gels resulting from the different reaction conditions were assessed by a live/dead assay and a resazurin-based assay, respectively. These studies were performed using unmodified (0.00 mM AG73)

[3] In cell culture medium, 5.5 mM is considered a low glucose media, while 30 mM is considered high glucose media.

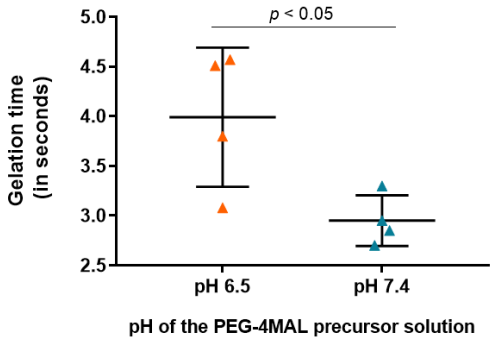

Figure 4.15: **Effect of the pH of the PEG-4MAL precursor solution on PEG-4MAL hydrogel gelation time.** Lowering the pH of the precursor solution from 7.4 to 6.5 significantly increased the time available for the manual mixing of the different hydrogel components (Unpaired t-test). Data represents mean ± SD of four replicate samples. (n = 1)

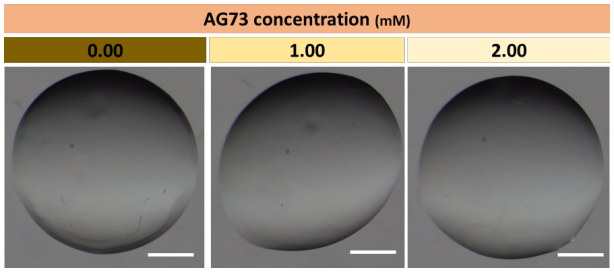

Figure 4.16: **Macroscopic view of acellular AG73-functionalized PEG-4MAL hydrogels** (10 μL) **prepared at a pH of 6.5**, taken pre-swelling. Representative images obtained using a stereo microscope (Olympus SZX10) are shown. Scale bar = 500 μm.

PEG-4MAL hydrogels so that the functionalization with an adhesive peptide would not influence cell behavior.

Qualitative image analysis of cell-laden gels incubated with vital/dead dyes at day 3 of culture revealed a higher number of viable cells, as well as the formation of spheroids of higher dimensions for cells cultured within gels prepared at lower pH (Figure 4.17A). This evident different between the distinct reaction conditions (pH 6.5 vs. pH 7.4) confirms our theory that a greater network uniformity contributes to an improved biological response from hNSC, in terms of viability. In addition, the absence of such marked inhomogeneities in the polymer network also favored a more uniform cell aggregation across the matrix compared to what is seen for hNSC cultured within PEG-4MAL gels prepared at pH 7.4. On the other hand, when examining the effect of supplementation with high glucose, we can see that for both hydrogel types (prepared at a lower and higher pH), the presence of high glucose contributes to an increase in the number of viable cells. We hypothesize that glucose might be providing an additional proliferative/growth stimulus to hNSC, thereby compensating for encapsulation-induced stress and promoting a higher cell viability under both conditions.

Taken together, when cultured on more uniform gels, hNSC exhibit high cell viability and proliferate as cellular spheroids in a widely distributed manner. Even though high glucose is known to suppress NSC differentiation by decreasing the number of βIII-tubulin$^+$ cells

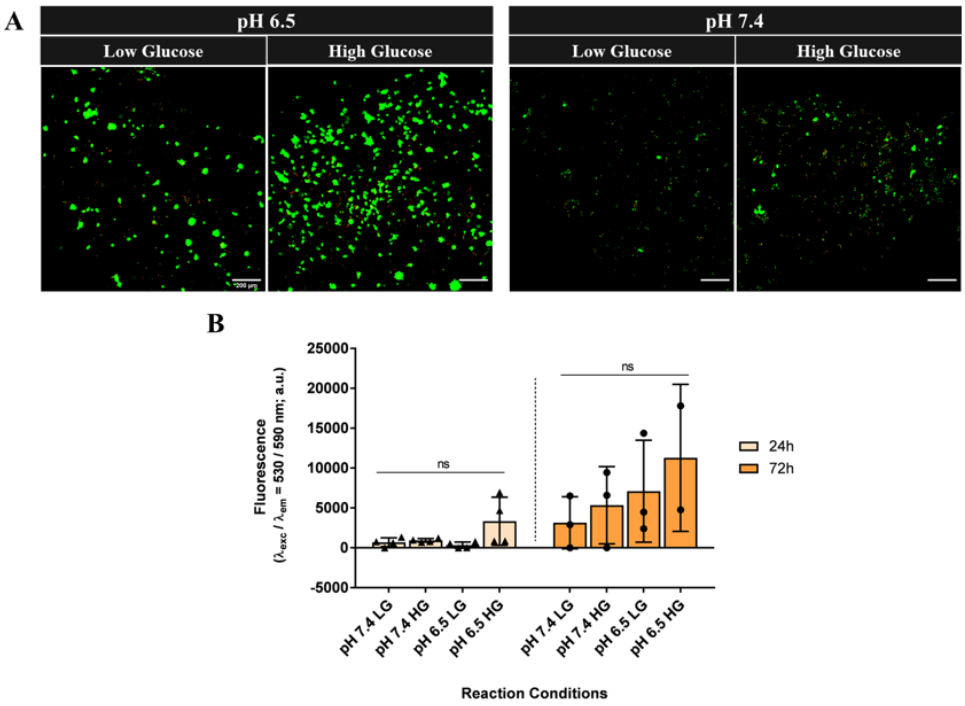

Figure 4.17: **Effect of the pH of the PEG-4MAL precursor solution and the addition of a high glucose supplement to the gel on hNSC viability and metabolic activity.** (A) Representative 2D projections of CLSM 3D stack images of cell-laden hydrogels incubated with calcein AM and PI, for detection of viable (in green) and dead (in red) cells, respectively; images correspond to day 3 of culture, and cover a thickness of 200-300 μm; the pH of the PEG-4MAL precursor solution and the absence/presence of a high glucose supplement is indicated on the top of each image; Scale bar = 200 μm. (B) Cell metabolic activity assessed at 24 and 72 h of cell culture using a resazurin-based assay; no significant (*ns*) differences were detected (two-way ANOVA followed by Tukey's multiple comparisons test); data represents mean ± SD ($n \geq 2$). For both the analysis, hNSC were cultured in unmodified (0.00 mM AG73) PEG-4MAL hydrogels under proliferative conditions.

(possibly by mechanisms of oxidative stress) [240], its presence seemed to contribute to a higher hNSC viability compared to when no additional glucose was added. In fact, hNSC were only left for 20 min in the hydrogel network before adding complete serum-free medium (suitable for hNSC expansion), which means high glucose should not have had time to influence the directed differentiation process (starting only at day 2 of culture).

In order to quantitatively assess the metabolic activity of hNSC cultured within PEG-4MAL hydrogels, prepared under differing reaction conditions, a resazurin-based assay was performed at 24 and 72 hours post-encapsulation. hNSC were kept under proliferative conditions for the total time of the assay, so that no extra variable was introduced from 24 to 72 hours[4].

The results show that, at both 24 and 72 hours of cell culture, the fluorescence detected tends to increase from gels prepared at a higher pH (7.4) to gels prepared at lower pH (6.5), even though no significant differences were obtained when comparing the variable pH (Figure

[4]Directed neuronal differentiation, mediated by withdrawal of growth factors and addition of Neurobasal/B27 medium, starts at day 2 of cell culture.

4.17B). Also, gels prepared without a glucose supplement showed lower fluorescence values compared to gels in which glucose was added, although no statistically relevant differences were identified. Translating these results in terms of hNSC' metabolic activity, it appears that PEG-4MAL hydrogels in which the pH of the precursor solution was adjusted to 7.4, and no high glucose was added, lead to the lowest cell metabolic activities, while gels prepared at a lower pH (6.5) and containing a high glucose supplement promote the highest metabolic activity. Both trends seem more evident 72-hours after cell encapsulation, which suggests hNSC undergo an increase in metabolic activity from day 1 to day 3 of cell culture.

These results are in accordance with the data obtained from the live/dead assay, which indicates that hNSC cultured within PEG-4MAL hydrogels prepared at a lower pH present not only increased viability, but also higher metabolic activity. Again, we hypothesize this is closely related to the formation of more uniform polymer networks when the pH is kept at 6.5, since there is appreciably more time for the homogenization of the different hydrogel components. Importantly, given the rather unknown effect of high glucose concentrations on hNSC behavior (especially regarding longer timepoints of the neuronal differentiation process), and the fact that no significant differences were found for both assays, the effect of high glucose concentrations on hNSC behavior was not further assessed. It would however be very interesting to further evaluate and quantify the effect of this variable on hNSC viability, proliferation and neuronal differentiation potential.

Additionally, the effect of the PEG-4MAL precursor solution pH on hNSC neuronal differentiation was also assessed and compared with previously obtained results (Figure 4.14). For this purpose, hNSC were culture within AG73-PEG-4MAL hydrogels for 14 days under neuronal differentiation conditions and then processed as whole-mounts for βIII-tubulin/DNA staining. As shown in Figure 4.18, reducing the pH of the precursor solution substantially improves the biological response of hNSC upon culture within PEG-4MAL gels. In fact, a higher number of βIII-tubulin$^+$ cellular spheroids extending neurites can be observed for PEG-4MAL hydrogels functionalized with 1.00 mM of AG73 and prepared at a pH of 6.5. These results suggest the importance of tuning the gelation kinetics of PEG-4MAL gels to the application of interest.

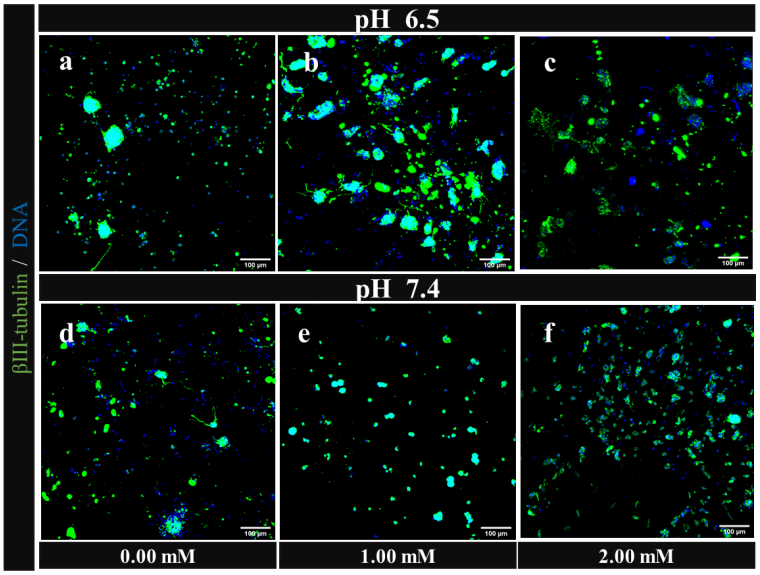

Figure 4.18: **Effect of the pH of the PEG-4MAL precursor solution on hNSC neuronal differentiation.** Images show representative 2D projections of CLSM stack images of cell-laden AG73-functionalized PEG-4MAL hydrogels (0.00, 1.00, and 2.00 mM AG73) cultured for 14 days under neuronal differentiation conditions, and processed for immunofluorescence labelling of βIII-tubulin (early neuronal marker, in green); cell nuclei were counterstained with Hoechst (blue). Scale bar = 100 μm.

4.5.2 Optimization of PEG-4MAL hydrogels' degradability

As previously mentioned, after 14 days of culture under neuronal differentiation conditions, either plain or AG73-functionalized PEG-4MAL hydrogels were extremely degraded. This fast degradation not only made it difficult to compare results across samples and affected sample processing for immunohistochemical analysis, but also prevented the assessment of hNSC behavior over longer periods of culture (for instance until day 21 so that matrix deposition and remodeling could be properly evaluated). Therefore, a screening assay was conducted to establish a degradable (MMP2-sensitive peptide) to non-degradable (PEG-dithiol) cross-linkers molar ratio allowing hNSC infiltration and neuronal differentiation, while assuring the overall integrity of AG73-PEG-4MAL hydrogels during the 14-day period necessary for hNSC neuronal differentiation assessment. In this screening assay the concentration of AG73 was fixed at 2.00 mM.

Representative images of cell-laden AG73-functionalized hydrogels taken after 14 days of culture under neuronal differentiation conditions are shown in Figure 4.19A. Results revealed that completely degradable PEG-4MAL hydrogels (100:0 molar ratio) lose their drop-like shape and almost entirely disintegrate after 2-weeks of culture, resulting into an irregular and almost undetectable form. Hydrogels prepared with a 80:20 molar ratio – the one used in all the previous experiments - also seem to undergo an intense process of degradation: besides losing their initial shape, they attach to the walls of the IBIDI® plate during the handling process of culture medium refreshment, which may impact the mechanical stimuli sensed by encapsulated cells. For the remaining gels, even though differences are not as evident, there is also a pattern for increased retention of the initial spherical shape and

overall hydrogel integrity with increasing molar percentage of non-degradable cross-linker, as expected due to the inability of hNSC to degrade PEG-dithiol. These results suggest that cell-laden AG73-PEG-MAL hydrogels formulated with a 60:40 degradable to non-degradable cross-linkers molar ratio preserve an overall matrix integrity at least for a culture period of 14 days under neuronal differentiation conditions.

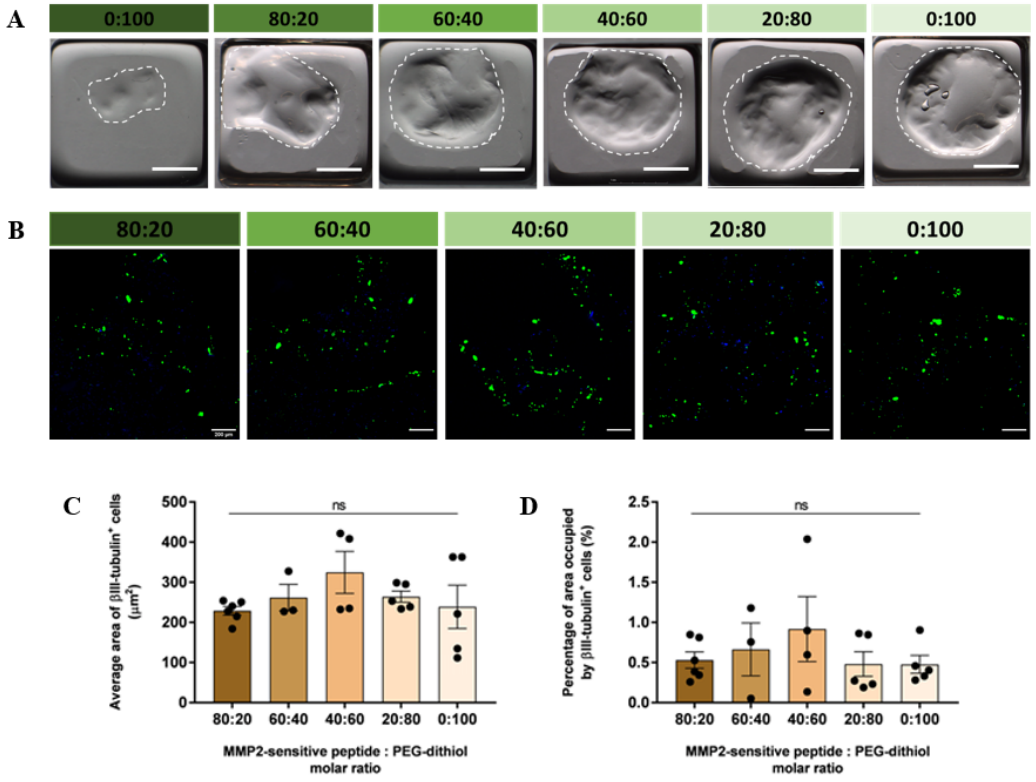

Figure 4.19: **Effect of varying the molar ratio of MMP2-sensitive peptide to PEG-dithiol on hNSC neuronal differentiation.**(A) Macroscopic view of cell-laden hydrogels. Images were obtained using a stereo microscope (Olympus SZX10). Scale bar = 500 μm. (B) Images show representative 2D projections of CLSM 3D stack images of cell-laden gels processed for immunofluorescence labeling of βIII-tubulin (early neuronal marker, in green); cell nuclei were counterstained with Hoechst (blue). Scale Bar = 200 μm. (C) Average area occupied by βIII-tubulin$^+$ cells (mean $\pm$ SEM, n $\geq$ 3); no significant differences (*ns*) were found between conditions ($p = 0.4019$, One-Way ANOVA). (D) Percentage of area occupied by βIII-tubulin$^+$ cells (mean $\pm$ SEM, n $\geq$ 3); *ns* differences were found between conditions ($p = 0.5844$, One-Way ANOVA). All cell-laden AG73-PEG-4MAL hydrogels (2.00mM) were cultured for 14 days under neuronal differentiation conditions

The effect of the degradable to non-degradable cross-linkers ratio on hNSC neuronal differentiation was assessed by IF staining of βIII-tubulin. Qualitative analysis of CLSM images showed the presence of a population of differentiated neurons, expressing βIII-tubulin for all hydrogel formulations prepared (Figure 4.19B). Except for the fully degradable hydrogels (which were lost during immunostaining due to their high degradation state), all the different molar ratios tested exhibited similar number of βIII-tubulin$^+$ cellular aggregates, which suggests hNSC neuronal differentiation capacity was not affected by the decrease in hydrogel degradability. However, neurite extension was not detected, independently of the cross-linkers molar ratio considered.

The images obtained were further quantitatively analyzed for detection of significant differences between the distinct conditions tested. In this regard, the average area occupied by βIII-tubulin$^+$ cells (early neuronal marker), as well as the percentage of area occupied by these cells were quantified from the 2D projections using ImageJ/Fiji. In line with the qualitative analysis, no significant differences were found regarding both the average area occupied by βIII-tubulin$^+$ cells and the corresponding percentage of the total analyzed area (Figures 4.19C and 4.19D). These results indicate that varying the molar ratio of degradable to non-degradable cross-linkers does not impact hNSC neuronal differentiation within AG73-PEG-MAL hydrogels.

Given the fact that RGD is the most commonly employed peptide sequence to confer cell adhesiveness to hydrogel matrices , namely due to its recognized ability to mimic protein adhesion domains and bind to cell-surface receptors [138, 241], the effect of varying the degradable to non-degradable cross-linkers molar ratio on the capacity of PEG-4MAL hydrogels to support hNSC neuronal differentiation was investigated using RGD as cell adhesive sequence (2.00 mM). Results are depicted in Appendix F. In RGD-functionalized hydrogels the average area occupied by neuronal cells was similar to that found in AG73-PEG-MAL gels and no significant impact of the degradable to non-degradable cross-linkers molar ratio on hNSC neuronal differentiation was found. Also, for these gels, no neurite outgrowth/extension was observed, regardless of the cross-linkers molar ratio tested. These results suggest that the heterogeneity of the PEG-4MAL hydrogels prepared (at pH 7.4) prevents the straightforward comparison between the different hydrogel formulations.

Although hydrogel degradability constitutes a critical factor for cell-induced matrix remodeling in 3D microenvironments and has been shown to be essential for *in vitro* cell survival and proliferation within synthetic niches [134, 195, 242], these results show that the use of PEG-4MAL matrices with a higher non-degradable component (comparatively to the 80:20 molar ratio of MMP2-sensitive peptide to PEG-dithiol considered so far) does not compromise the neuronal differentiation of hNSC cultured within the gels for a period of 14 days. Therefore, the 60% MMP2-sensitive peptide to 40% PEG-dithiol cross-linker ratio was chosen as the optimal compromise between hydrogel degradability, pivotal for cell migration and remodeling of the surrounding environment, and long-term stability. In fact, the latter is extremely important for the assessment of the hNSC biological response at longer culture periods, in which cells have possible developed more complex neuronal networks and produced their own ECM components, as shown in the 2D cultures of hNSC on poly-L-ornithine/laminin-coated TCPS coverslips.

Moreover, these AG73-PEG-4MAL hydrogels, prepared with a lower degradable component (60:40 molar ratio of degradable to non-degradable cross-linkers) were characterized in terms of their ability to support hNSC stemness and ECM-deposition. For this purpose, hNSC were cultured under proliferative conditions for 7 days.

Qualitative analysis of CLSM images revealed the presence of a small number of nestin$^+$ cells for unmodified PEG-4MAL hydrogels (Figure 4.20a), while for AG73-functionalized gels the formation of a higher number of nestin$^+$ cells was observed (Figure 4.20b-c). On the other hand, both plain and AG73-PEG-4MAL gels (1.00 mM) showed a wide distribution of βIII-tubulin$^+$, contrarily to PEG-4MAL gels functionalized with the highest concentration of

AG73 (2.00 mM), where a relatively low number of βIII-tubulin$^+$ cells was observed (Figure 4.20d-f). These results indicate that AG73 peptide provides cell adhesive cues that contribute to enhance PEG-MAL ability to support hNSC stemness while maintaining neuronal differentiation capacity (when used at an intermediate concentration - 1.00 mM). This study also revealed that hNSC cultured under proliferative conditions in plain or AG73-functionalized PEG-MAL hydrogels are capable of matrix remodeling, since the expression of both laminin (Figure 4.20g-i) and collagen IV (Figure 4.20j-l) is observed in all the conditions tested.

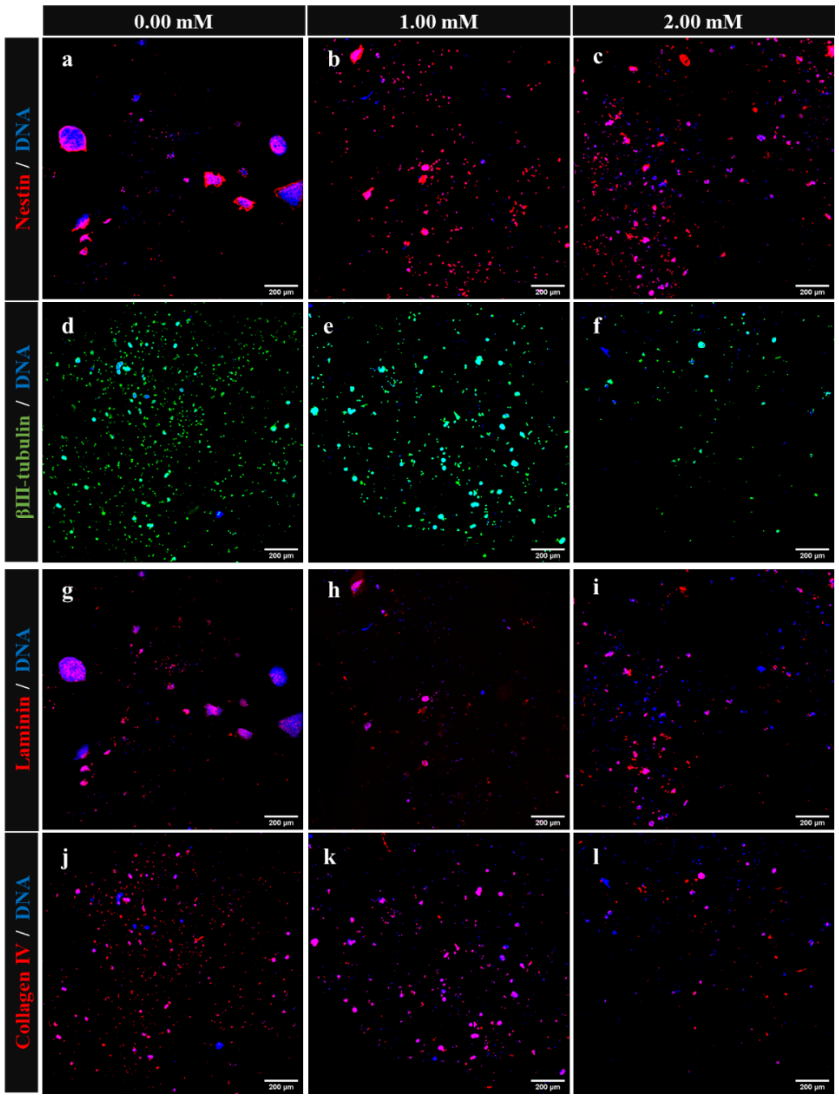

Figure 4.20: **Ability of AG73-functionalized PEG-4MAL hydrogels (60:40 molar ratio of MMP2-sensitive peptide to PEG-dithiol) to support hNSC stemness and ECM deposition.** Images show representative 2D projections of CLSM stack images of cell-laden AG73-functionalized PEG-4MAL hydrogels (0.00, 1.00, and 2.00 mM of AG73) cultured for 7 days under proliferative conditions and processed for immunofluorescence labelling of (a-c) Nestin (NSC marker, in red), (d-f) βIII-tubulin (early neuronal marker, in green), (g-i) laminin (red) and (j-l) collagen IV (red). Cell nuclei were counterstained with Hoechst (blue). Scale bar = 200 μm.

4.5.3 Biological characterization of PEG-4MAL hydrogel with optimized gelation kinetics and degradability

From all the optimization processes, a new formulation of AG73-functionalized PEG-4MAL hydrogels could be established. First, we verified that lowering the pH of the PEG-4MAL precursor solution led to the formation of more uniform and homogenous polymeric networks that resulted in a trend to higher hNSC viability, metabolic activity, and neuronal differentiation. Secondly, the use of a lower percentage of MMP2-sensitive peptide allowed us to prolong the integrity of the cell-laden while not compromising the hydrogel ability to support hNSC neuronal differentiation. Therefore, we hypothesize the combination of these strategies should provide a more favorable environment for the culture of hNSC within AG73-PEG-4MAL gels. In turn, these matrices should allow a more straightforward assessment of AG73 input concentration on the biological performance of the functionalized degradable PEG-4MAL gels.

In this regard, the ability of these gels to support neuronal differentiation was first assessed after 14 days of culture under neuronal differentiation conditions. hNSC were cultured within AG73-PEG-4MAL hydrogels prepared with a 60:40 molar ratio of MMP2-sensitive peptide to PEG-dithiol and which precursor solution was left at a pH of 6.5. Cell-laden hydrogels with the same degradability (formulated with the same molar ratio of MMP2-sensitive peptide to PEG-dithiol) but prepared with precursor solutions at a pH 7.4 were cultured in parallel to get insight into the effect of the pH on neuronal differentiation on less degradable gels.

The qualitative analysis of CLSM images showed that hydrogels prepared at lower pH (6.5) exhibited not only a higher number of βIII-tubulin$^+$ cells, but also a wider distribution of cells across the polymer matrices, compared to hydrogels prepared at a higher pH (7.4), and regardless of the input AG73 peptide concentration (Figures 4.21a-c). In fact, there is an evident reduction in the number of βIII-tubulin$^+$ cells when the pH of the PEG-4MAL precursor solution is adjusted to 7.4 (Figures 4.21d-f), which suggests the preponderant effect of matrix homogeneity in regards to the biological response of hNSC. Importantly, these results also show that PEG-4MAL gels functionalized with 1.00 mM of AG73 are the only ones permissive to neurite outgrowth/extension, as evidenced in Figure 4.21b. This is in agreement with the results obtained so far, which indicate this input AG73 concentration as the optimal density of adhesive bioligand for hNSC differentiation in degradable PEG-4MAL gels.

Altogether, the lowering of the pH and subsequent increase in gelation time revealed to be crucial for improving the culture of hNSC, both in terms of viability and neuronal differentiation capacity, when comparing to gels prepared at a pH of 7.4 (faster gelation speed and poorer homogenization).

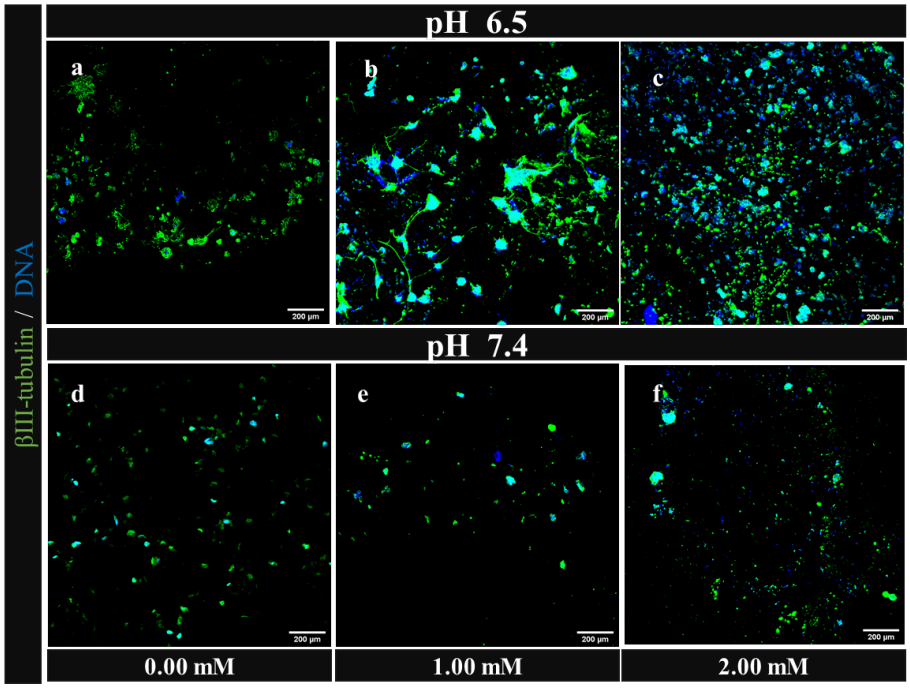

Figure 4.21: **Ability of the optimized formulation of AG73-PEG-4MAL hydrogels to support hNSC neuronal differentiation, as a function of input AG73 concentration.** Images show representative 2D projections of CLSM stack images of cell-laden hydrogels cultured for 14 days under neuronal differentiation conditions and processed for immunofluorescence labelling of βIII-tubulin (early neuronal marker, in green). Images corresponding to hydrogels with the same molar ratio of MMP2-sensitive peptide to PEG-dithiol (60:40) but prepared at pH 7.4 are also shown for comparison purposes. Cell nuclei were counterstained with Hoechst (blue). Scale bar = 200 μm.

Chapter 5

Conclusions and Future Perspectives

The main aim of the work presented was to develop a synthetic hydrogel platform for the culture/delivery of hNSC based on a PEG-4MAL backbone exploring the bioactive effect of the laminin-derived AG73 peptide sequence, a syndecan-binding ligand with reported neurite promoting ability. Given the initially established goals, conclusions can be outlined according to three major sections: (a) characterization of AG73-functionalized PEG-4MAL hydrogels in terms of peptide binding efficiency and viscoelastic and structural properties, (b) biological assessment of AG73-PEG-4MAL hydrogels' ability to support hNSC viability, proliferation and neuronal differentiation, and (c) optimization of AG73-functionalized PEG-4MAL hydrogels' biophysical properties for a better support of hNSC culture.

AG73-functionalized PEG-4MAL hydrogels, incorporating hNSC protease-sensitive peptides and different AG73 peptide densities could be prepared with a high peptide tethering efficiency ($> 96\%$), regardless of the input AG73 concentration. These results demonstrate the precise control over adhesive ligand density provided by Michael-type addition functionalization, which allowed the fine tuning of hydrogel bioactivity. Nonetheless, the macroscopic analysis of these gels revealed the presence of local network heterogeneities at the micrometer-scale, likely owing to spatial variations of cross-link density caused by an insufficient mixing of the hydrogel components. In fact, the fast gelation kinetics of these gels was the main hurdle limiting the preparation of AG73-functionalized PEG-4MAL hydrogels.

Regarding mechanical and viscoelastic properties, we have shown that the tethering of AG73 peptide did not significantly impact the storage and loss moduli, as well as mesh size of PEG-4MAL hydrogels, independently of the input AG73 concentration. Additionally, all the prepared hydrogels exhibited $G' > G''$, while maintaining low δ values, which confirms their predominant elastic behavior. Interestingly, the tethering of a scrambled sequence of AG73 resulted in PEG-4MAL gels with significantly lower G', compared to plain gels and gels functionalized with equal amount of bioactive AG73. This may result from electrostatic interactions occurring between the scrambled peptide residues and the MMP2-sensitive peptide (degradable cross-linker), which may compromise the cross-linking process and lead to

the formation of softer polymeric networks. Nevertheless, further characterization studies regarding the molecular interactions established between these two peptides would be required to elucidate their differential effect on the mechanical properties of PEG-4MAL hydrogels. Overall, stable MMP2-sensitive cross-linked networks with a controlled level of AG73 functionalization and a stiffness ($G' \approx 500$ Pa) comparable to that of human brain tissue could be obtained.

Subsequently, the culture of hNSC within AG73-functionalized PEG-4MAL hydrogels consistently revealed a trend for higher cell viability at day 2 and 7 of culture, for AG73 concentrations ≥ 0.5 mM. In accordance to the lower stiffness found, hydrogels functionalized with a scrambled sequence of AG73 failed to support hNSC viability, which may be related to the lower cross-linking density of these hydrogels, and, as a result, lack of a supportive matrix for hNSC anchorage Additionally, no significant differences were found regarding hNSC growth at day 7 of culture, although a trend for higher cell numbers was observed for gels modified with 1.00 mM of AG73. Altogether, these studies suggest the good cytocompatibility of the proposed matrices and point to the importance of the AG73 syndecan binding peptide in supporting hNSC viability. It is however important to highlight that a critical reduction on the number of entrapped hNSC could be found for all prepared gels at day 7 of cell culture. This might be due to issues such as the presence of several polymer inhomogeneities within the synthetic matrices (which might provide locally different mechanical stimuli that negatively influence the biological response of hNSC), as well as the fact that cell entrapment in the gels is a stress-inducing process.

At day 14 of neuronal differentiation, a higher number of hNSC-derived neurons expressing βIII-tubulin was found for PEG-4MAL gels functionalized with the highest AG73 concentrations (1.00 and 2.00 mM). These results suggest that the tethering of AG73 peptide improves hNSC neuronal differentiation, possibly by recapitulating some of the features present in neurogenic niches. Even so, the AG73-PEG-4MAL hydrogels developed so far failed to support significant neurite outgrowth, regardless of the AG73 concentration.

To overcome the high heterogeneity of the polymeric matrix caused by the fast gelation kinetics of the Michael-type addition reaction and to improve the integrity of the cell-laden hydrogels throughout the cell culture period, the gelation kinetics and the degradability of the hydrogels were subsequently optimized.

By lowering the pH of the precursor solution (to 6.5) the speed of the thiol-maleimide reaction was reduced and slower gelation rates were achieved. This resulted in more homogeneous hydrogels and in an increase in hNSC viability and metabolic activity, when compared to hydrogels prepared at a higher pH (7.4). Additionally, preliminary results have shown that the addition of a high glucose supplement to the hydrogel improves the viability of hNSC cultured within PEG-4MAL gels, independently of the pH considered. Therefore, it would be very interesting to further assess the effect of this variable on PEG-4MAL hydrogels' ability to support hNSC viability, proliferation and neuronal differentiation. On the other hand, by increasing the percentage of the non-degradable cross-linker (60:40 molar ratio of

MMP2-sensitive peptide to PEG-dithiol), hydrogels retaining their overall integrity throughout the entire culture were obtained, without negatively impacting hNSC neuronal differentiation. Interestingly, similar results were obtained when considering RGD-functionalized PEG-4MAL (2.00 mM).

The use of optimized AG73-functionalized PEG-4MAL hydrogels provided valuable insight into the effect of AG73 input concentration on hNSC response. Specifically, PEG-4MAL gels functionalized with an intermediate concentration of AG73 (1.00 mM) were shown to better support hNSC neuronal differentiation, and were the only ones permissive to neurite extension.

In light of the promising results obtained, future studies using the optimized hydrogel formulation need to be conducted to further consolidate the potential of AG73-PEG-4MAL hydrogels as a fully defined hydrogel-based system for hNSC culture and delivery. Importantly, their mechanical and structure properties should be verified to ensure that the change in pH did not impact the overall mechanical properties of PEG-4MAL hydrogels. Further studies aimed at better understanding the role of AG73-syndecan-binding peptide on the modulation of hNSC behavior/function would also be extremely relevant. In order to get insight into the contribution of syndecan-1 and -4 receptors to the response of hNSC to immobilized AG73, different studies could be performed, namely silencing the expression of the syndecan receptor using siRNA or blocking its activity using function blocking monoclonal antibodies against that syndecan receptor. On the other hand, the ability of the developed 3D platforms to support hNSC neuronal differentiation and maturation should also be assessed in long-term cultures, especially in terms of ECM remodeling, and the establishment of a functional neuronal network.

Moreover, given the ability of AG73-PEG-4MAL matrices to better mimic the 3D microenvironment found *in vivo* (comparably to common 2D culture systems), they also present the potential to be used for more fundamental studies, namely to provide insight into molecular mechanisms implicated in neurogenesis. Also, since AG73-PEG-4MAL hydrogels are able to support hNSC self-renewal, it would be interesting to explore them as biomanufacturing systems to expand hNSC for use in NSC-based therapies.

Also of interest is the functionalization of PEG-4MAL hydrogels with syndecan binding peptides derived from human laminin isoforms or even with a combination of these peptides and integrin-binding ligands. The assessment of the additive or synergistic effect of these peptides on hNSC viability, proliferation and neurite outgrowth would be of great importance to better recapitulate the laminin-rich microenvironment of neurogenic niches.

Altogether, we believe this work provided evidence of the potential of the proposed engineered matrices to be used as chemically-defined 3D platforms, for the establishment of artificial NSC niches and as temporary mimetic microenvironments to support NSC transplantation in the context of CNS regeneration and repair. Additionally, the strategy developed for hydrogel optimization resulted in the improved handling of PEG-4MAL hydrogels, as well as in the formation of more reproducible and amenable hydrogel-based matrices that can tuned to the application of interest.

APPENDICES

Appendix A

Measure-iT^{TM}Thiol Assay - Calibration Curve

In order to assess the amount of free thiol in the reaction buffers (containing AG73-PEG-4MAL precursors), a calibration curve was prepared using the Measure-iT^{TM}Thiol quantitation standard (reduced glutathione, GSH). Briefly, the thiol quantitation reagent (propanediol concentrate) is able to bind to the GSH molecules via their free sulfhydryl group (each GSH molecule only has one -SH available group), establishing disulfide bonds that can be fluorometrically detected and quantified. Figure A.1 shows the standard curve plotted as fluorescence *vs.* thiol concentration of the reduced glutathione molecules.

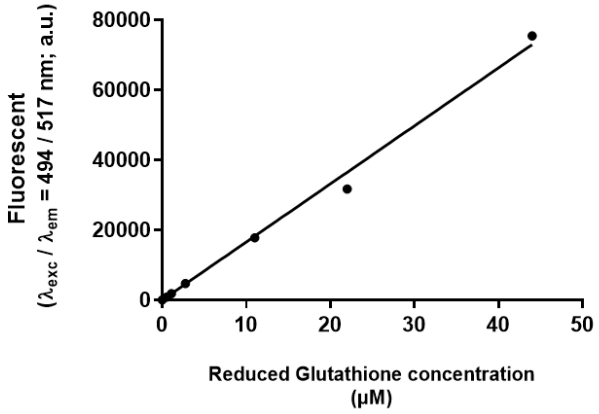

Figure A.1: Calibration curve (0 - 44 μM) used to calculate the concentration of free thiols in the reaction buffer, using the Measure-iT^{TM}Thiol Assay. Linear regression: $y = 1455.8x + 403.73$, $R^2 = 0.9965$. Results are the mean of two replicates.

Appendix B

HPLC - Calibration Curve

For peptide quantification using HPLC, a calibration curve was fisrt obtained using the AG73 peptide diluted in PBS at different concentrations (0 – 5mM). As evidenced by chromatographic data in Figure B.1, this method was not sensitive enough to detect the low thiol concentrations remaining in the supernatant. In fact, for an AG73 peptide concentration of 0.156 mM, no peak could be detected at the retention time of this peptide (as highlighted by the red circle).

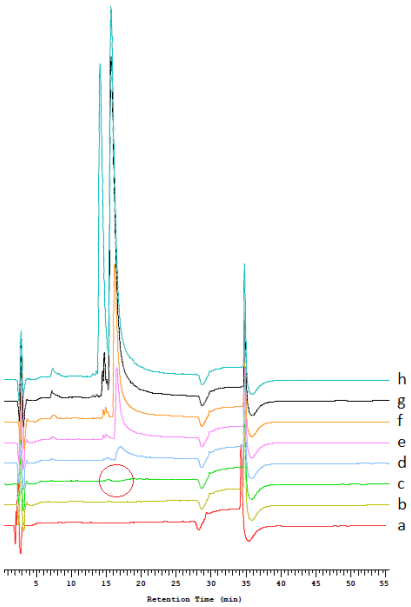

Figure B.1: HPLC chromatogram of AG73 peptide, obtained using a detection wavelength of 220nm. *a* corresponds to PBS, *b* to 0.078 mM AG73, *c* to 0.156 mM AG73, *d* to 0.313 mM AG73, *e* to 0.625 mM AG73, *f* to 1.25 mM AG73, *g* to 2.5 mM AG73 and *h* to 5mM AG73.

Appendix C

Oscillatory Amplitude Strain Sweep

The LVR of PEG-4MAL hydrogels was first determined for plain gels by oscillatory amplitude strain sweeps. This was important to choose a constant shear strain value for which tests could be carried out without destroying the structure of the sample. Given the plateau found for PEG-4MAL hydrogels, 1% shear strain was chosen for the subsequent frequency sweep studies.

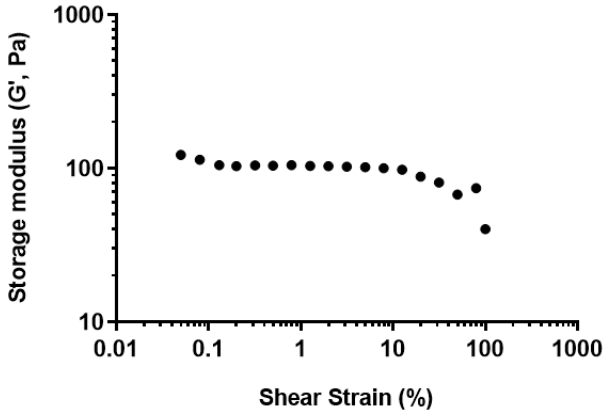

Figure C.1: Oscillatory amplitude strain sweep determined for unmodified (0.00 mM) PEG-4MAL hydrogels, at a constant frequency of 0.1 Hz. Storage Modulus (G') is presented as a function of strain (1-100%). Data represents mean of two replicates (n=2).

Appendix D

Flow cytometry analysis

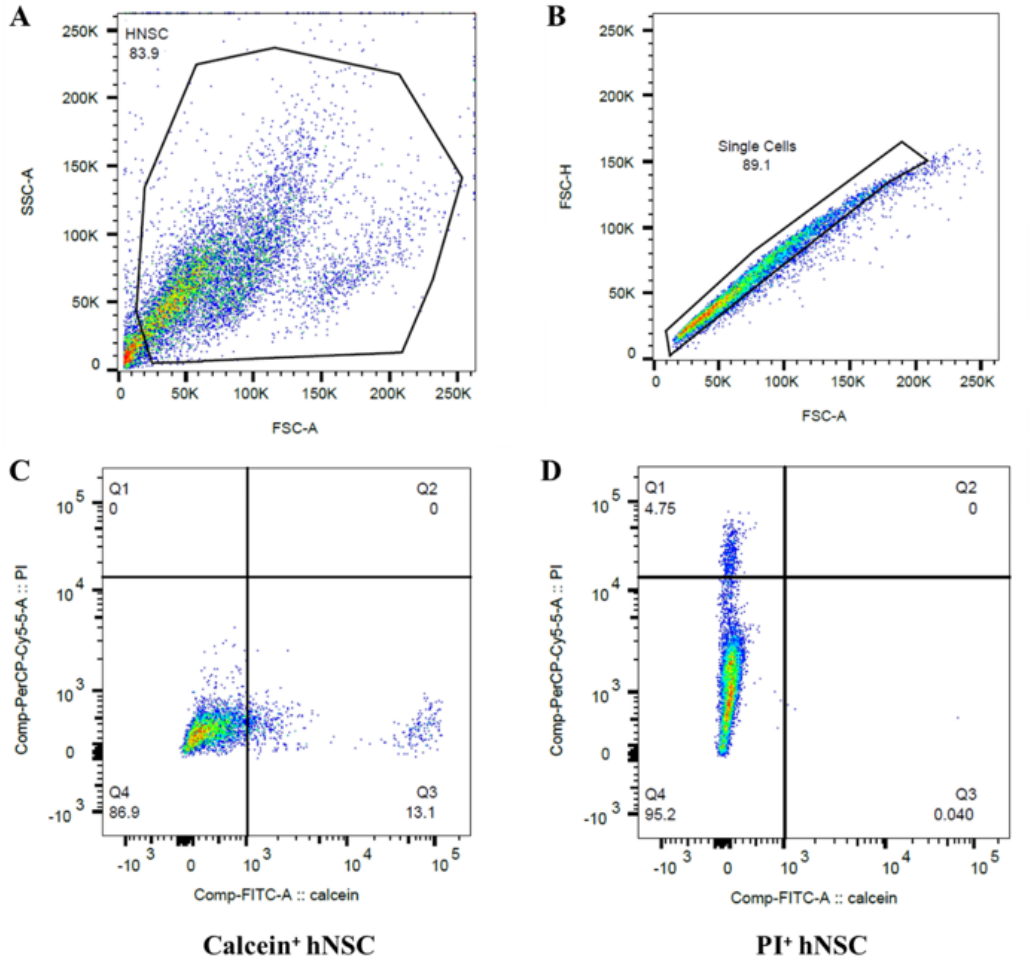

Figure D.1: **Representative scatter dot-plot images of flow cytometry for detection of viable (calcein$^+$) and dead (PI$^+$) cells.** (A) FSC/SSC, ungated - hNSC population. (B) FSC-A/FSC-H - single cell selection. (C) Calcein$^+$ cells. (D) PI$^+$ cells. All images correspond to hNSC cultured within unmodified (0.00 mM) PEG-4MAL hydrogels for 7 days under neuronal differentiation conditions.

Appendix E

Phenotypic characterization of hNSC: neurite-outgrowth

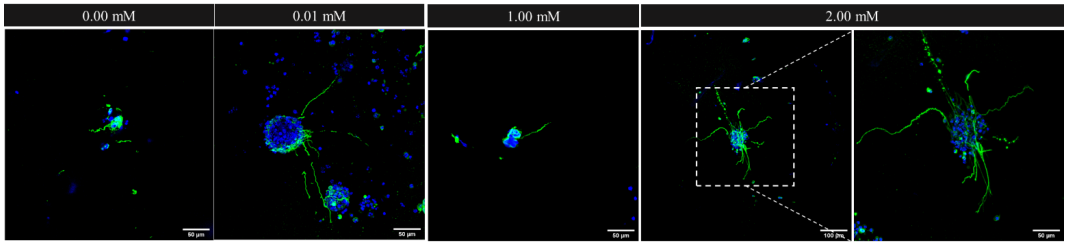

Figure E.1: Examples of neurites radially extending from floating aggregates of hNSC (neurospheres) cultured within AG73-functionalized PEG-4MAL hydrogels for 14 days, under differentiation conditions, and processed for immunofluorescence labeling of βIII-tubulin (early neuronal marker, in green). Cell nuclei were counterstained with Hoechst (blue). 2D projections of CLSM 3D stacks covering a depth of 40-150mum are shown. Scale Bar= 100 mum (20×); 50 mum (40×).

Appendix F

RGD-functionalized PEG-4MAL hydrogels

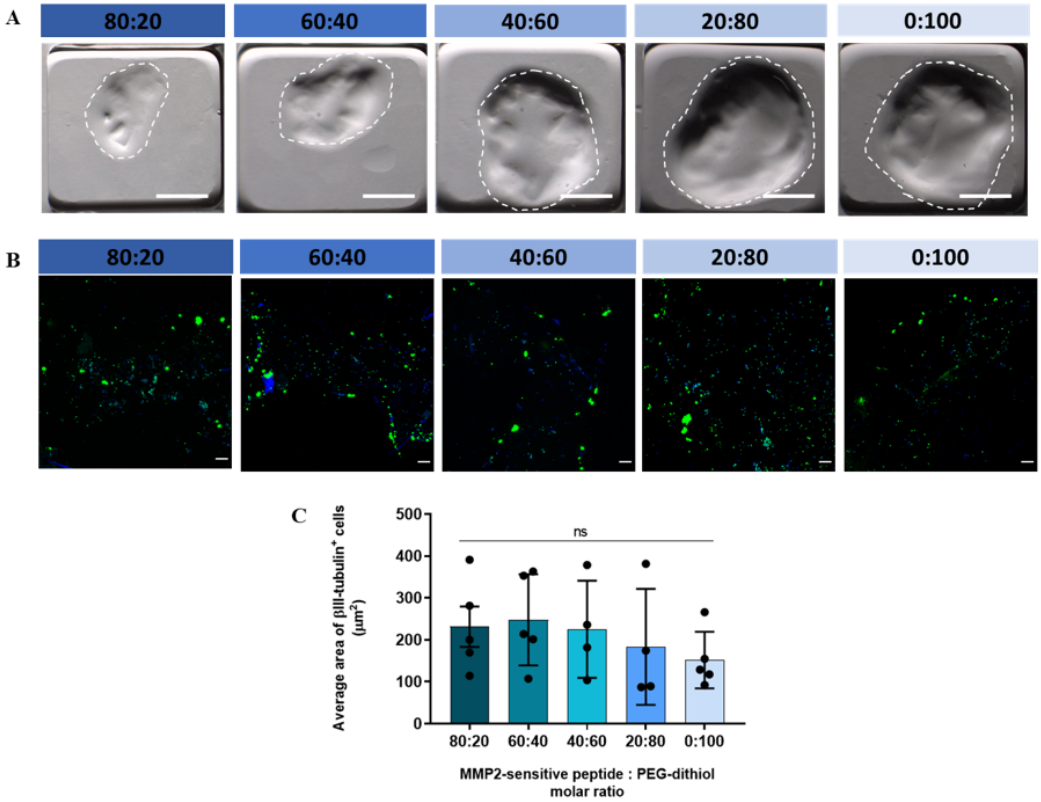

Figure F.1: **Effect of varying the molar ratio of MMP2-sensitive peptide to PEG-dithiol on hNSC neuronal differentiation cultured on RGD-functionalized PEG-4MAL gels.**(A) Macroscopic view of cell-laden hydrogels. Images were obtained using a stereo microscope (Olympus SZX10). Scale bar = 500 μm. (B) Images show representative 2D projections of CLSM 3D stack images of cell-laden gels processed for immunofluorescence labeling of βIII-tubulin (in green); cell nuclei were counterstained with Hoechst (blue). Scale Bar = 200 μm. (C) Average area occupied by βIII-tubulin$^+$ cells (mean $\pm$ SEM, n $\geq$ 3); no significant differences (*ns*) were found between conditions (p = 0.6385, One-Way ANOVA). All cell-laden RGD-PEG-4MAL hydrogels (2.00mM) were cultured for 14 days under neuronal differentiation conditions.

Bibliography

[1] S. Payne et al., *Central Nervous System*, book section 68, pp. 1199–1221. Academic Press, 3rd ed., 2019.

[2] P. Brodal, *The Central Nervous System: structure and function.* Oxford University Press, 4th ed., 2010.

[3] C. Nicholson and E. Sykova, "Extracellular space structure revealed by diffusion analysis," *Trends Neurosci*, vol. 21, no. 5, pp. 207–15, 1998.

[4] S. J. Franco and U. Muller, "Extracellular matrix functions during neuronal migration and lamination in the mammalian central nervous system," *Dev Neurobiol*, vol. 71, no. 11, pp. 889–900, 2011.

[5] Z. Redzic, "Molecular biology of the blood-brain and the blood-cerebrospinal fluid barriers: similarities and differences," *Fluids and barriers of the CNS*, vol. 8, no. 1, pp. 3–3, 2011.

[6] B. Engelhardt and L. Sorokin, "The blood–brain and the blood–cerebrospinal fluid barriers: function and dysfunction," *Seminars in Immunopathology*, vol. 31, no. 4, pp. 497–511, 2009.

[7] J. Snyder et al., *Comparative Anatomy and Histology: Nervous System.* Academic Press, 2nd ed., 2018.

[8] I. Decimo et al., "Meninges: From protective membrane to stem cell niche," *American journal of stem cells*, vol. 1, pp. 92–105, 2012.

[9] R. Rua and D. McGavern, "Advances in meningeal immunity," *Trends in Molecular Medicine*, vol. 24, 05 2018.

[10] I. Spadoni et al., "Organ-specific protection mediated by cooperation between vascular and epithelial barriers," *Nature Reviews Immunology*, vol. 17, 09 2017.

[11] X. Xiaohua et al., "Enhancing cns repair in neurological disease: challenges arising from neurodegeneration and rewiring of the network," *CNS drugs*, vol. 25, no. 7, pp. 555–573, 2011.

[12] V. Feigin and T. Vos, "Global burden of neurological disorders: From global burden of disease estimates to actions," *Neuroepidemiology*, vol. 52, no. 1-2, pp. 1–2, 2019.

[13] J. W. Fawcett, "Overcoming inhibition in the damaged spinal cord," *J Neurotrauma*, vol. 23, no. 3-4, pp. 371–83, 2006.

[14] R. Y. Tam et al., "Regenerative therapies for central nervous system diseases: a biomaterials approach," *Neuropsychopharmacology*, vol. 39, no. 1, pp. 169–88, 2014.

[15] C. Soderblom et al., "Perivascular fibroblasts form the fibrotic scar after contusive spinal cord injury," *Journal of Neuroscience*, vol. 33, no. 34, 2013.

[16] J. Silver et al., "Central nervous system regenerative failure: Role of oligodendrocytes, astrocytes, and microglia," *Cold Spring Harbor perspectives in biology*, vol. 7, 12 2014.

[17] A. M. Kaufmann et al., "Ischemic core and penumbra in human stroke," *Stroke*, vol. 30, no. 1, pp. 93–99, 1999.

[18] E. A. Huebner and S. M. Strittmatter, "Axon regeneration in the peripheral and central nervous systems," *Results and problems in cell differentiation*, vol. 48, pp. 339–351, 2009.

[19] G. Mukhopadhyay et al., "A novel role for myelin-associated glycoprotein as an inhibitor of axonal regeneration," *Neuron*, vol. 13, no. 3, pp. 757–67, 1994.

[20] M. S. Chen et al., "Nogo-a is a myelin-associated neurite outgrowth inhibitor and an antigen for monoclonal antibody in-1," *Nature*, vol. 403, no. 6768, pp. 434–9, 2000.

[21] M. T. Fitch and J. Silver, "Cns injury, glial scars, and inflammation: Inhibitory extracellular matrices and regeneration failure," *Exp Neurol*, vol. 209, no. 2, pp. 294–301, 2008.

[22] R. Sankowski, S. Mader, and S. I. Valdes-Ferrer, "Systemic inflammation and the brain: novel roles of genetic, molecular, and environmental cues as drivers of neurodegeneration," *Front Cell Neurosci*, vol. 9, p. 28, 2015.

[23] J. Altman, "Are new neurons formed in the brains of adult mammals?," *Science*, vol. 135, no. 3509, pp. 1127–8, 1962.

[24] J. Altman and G. D. Das, "Autoradiographic and histological evidence of postnatal hippocampal neurogenesis in rats," *J Comp Neurol*, vol. 124, no. 3, pp. 319–35, 1965.

[25] J. Altman, "Autoradiographic and histological studies of postnatal neurogenesis. iv. cell proliferation and migration in the anterior forebrain, with special reference to persisting neurogenesis in the olfactory bulb," *J Comp Neurol*, vol. 137, no. 4, pp. 433–57, 1969.

[26] S. David and A. J. Aguayo, "Axonal elongation into peripheral nervous system "bridges" after central nervous system injury in adult rats," *Science*, vol. 214, no. 4523, pp. 931–3, 1981.

[27] B. A. Reynolds and S. Weiss, "Generation of neurons and astrocytes from isolated cells of the adult mammalian central nervous system," *Science*, vol. 255, no. 5052, pp. 1707–10, 1992.

[28] L. J. Richards et al., "De novo generation of neuronal cells from the adult mouse brain," *Proc Natl Acad Sci U S A*, vol. 89, no. 18, pp. 8591–5, 1992.

[29] A. J. Mothe and C. H. Tator, "Proliferation, migration, and differentiation of endogenous ependymal region stem/progenitor cells following minimal spinal cord injury in the adult rat," *Neuroscience*, vol. 131, no. 1, pp. 177–87, 2005.

[30] F. Barnabe-Heider et al., "Origin of new glial cells in intact and injured adult spinal cord," *Cell Stem Cell*, vol. 7, no. 4, pp. 470–82, 2010.

[31] F. H. Gage, "Mammalian neural stem cells," *Science*, vol. 287, no. 5457, pp. 1433–8, 2000.

[32] M. S. Shoichet et al., *Frontiers in Neuroengineering: Strategies for Regeneration and Repair in the Injured Central Nervous System.* Boca Raton (FL): Taylor and Francis Group, 2008.

[33] P. K. Dash et al., "Enhanced neurogenesis in the rodent hippocampus following traumatic brain injury," *J Neurosci Res*, vol. 63, no. 4, pp. 313–9, 2001.

[34] S. G. Kernie et al., "Brain remodeling due to neuronal and astrocytic proliferation after controlled cortical injury in mice," *J Neurosci Res*, vol. 66, no. 3, pp. 317–26, 2001.

[35] S. Ramaswamy et al, "Cellular proliferation and migration following a controlled cortical impact in the mouse," *Brain Res*, vol. 1053, no. 1-2, pp. 38–53, 2005.

[36] F. Barnabé-Heider and J. Frisén, "Stem cells for spinal cord repair," *Cell Stem Cell*, vol. 3, no. 1, pp. 16–24, 2008.

[37] G. Rusanescu, "Adult spinal cord neurogenesis: A regulator of nociception," *Neurogenesis (Austin, Tex.)*, vol. 3, no. 1, pp. e1256853–e1256853, 2016.

[38] O. Lindvall and Z. Kokaia, "Neurogenesis following stroke affecting the adult brain," *Cold Spring Harb Perspect Biol*, vol. 7, no. 11, 2015.

[39] M. Donegà et al., *Systemic Neural Stem Cell-Based Therapeutic Interventions for Inflammatory CNS Disorders.* 2013.

[40] G. Martino et al., "Stem cell transplantation in multiple sclerosis: current status and future prospects," *Nat Rev Neurol*, vol. 6, no. 5, pp. 247–55, 2010.

[41] M. Pakulska et al., "Injectable hydrogels for central nervous system therapy," *Biomed Mater*, vol. 7, no. 2, p. 024101, 2012.

[42] S. U. Kim and J. de Vellis, "Stem cell-based cell therapy in neurological diseases: A review," *Journal of Neuroscience Research*, vol. 87, no. 10, pp. 2183–2200, 2009.

[43] E. Donaghue et al., "Cell and biomolecule delivery for tissue repair and regeneration in the central nervous system," *Journal of Controlled Release*, vol. 190, pp. 219–227, 2014.

[44] A. K. McAllister, "Neurotrophins and neuronal differentiation in the central nervous system," *Cell Mol Life Sci*, vol. 58, no. 8, pp. 1054–60, 2001.

[45] M. I. Romero et al., "Functional regeneration of chronically injured sensory afferents into adult spinal cord after neurotrophin gene therapy," *J Neurosci*, vol. 21, no. 21, pp. 8408–16, 2001.

[46] M. S. Ramer et al., "Functional regeneration of sensory axons into the adult spinal cord," *Nature*, vol. 403, no. 6767, pp. 312–6, 2000.

[47] S. Pezet and M. Malcangio, "Brain-derived neurotrophic factor as a drug target for cns disorders," *Expert Opinion on Therapeutic Targets*, vol. 8, no. 5, pp. 391–399, 2004.

[48] A. Misra et al., "Drug delivery to the central nervous system: a review," *J Pharm Pharm Sci*, vol. 6, no. 2, pp. 252–73, 2003.

[49] S. A. Goldman, "Stem and progenitor cell-based therapy of the central nervous system: Hopes, hype, and wishful thinking," *Cell stem cell*, vol. 18, no. 2, pp. 174–188, 2016.

[50] D. A. McCreedy and S. E. Sakiyama-Elbert, "Combination therapies in the cns: engineering the environment," *Neuroscience letters*, vol. 519, no. 2, pp. 115–121, 2012.

[51] J. Breunig, T. Haydar, and P. Rakic, "Neural stem cells: Historical perspective and future prospects," *Neuron*, vol. 70, no. 4, pp. 614–625, 2011.

[52] G. Gincberg et al., "Neural stem cells: therapeutic potential for neurodegenerative diseases," *British Medical Bulletin*, vol. 104, no. 1, pp. 7–19, 2012.

[53] H. Okano, "Neural stem cells and strategies for the regeneration of the central nervous system," *Proc Jpn Acad Ser B Phys Biol Sci*, vol. 86, no. 4, pp. 438–50, 2010.

[54] I. Pereira et al., "Filling the gap: Neural stem cells as a promising therapy for spinal cord injury," *Pharmaceuticals*, vol. 12, 04 2019.

[55] B. Olynik and M. Rastegar, "The genetic and epigenetic journey of embryonic stem cells into mature neural cells," *Frontiers in Genetics*, vol. 3, no. 81, 2012.

[56] Y. Tang et al.

[57] H. Azari and B. A. Reynolds, "In vitro models for neurogenesis," *Cold Spring Harbor perspectives in biology*, vol. 8, no. 6, p. a021279, 2016.

[58] C. Guoynes et al., "Rapid generation of sub-type, region-specific neurons and neural networks from human pluripotent stem cell-derived neurospheres," *Stem Cell Research*, vol. 15, 10 2015.

[59] S. A. Louis et al., "Methods to culture, differentiate, and characterize neural stem cells from the adult and embryonic mouse central nervous system," *Methods Mol Biol*, vol. 946, pp. 479–506, 2013.

[60] L. Conti and E. Cattaneo, "Neural stem cell systems: physiological players or in vitro entities?," *Nature Reviews Neuroscience*, vol. 11, p. 176, 2010.

[61] G. Kumagai et al., "Roles of es cell-derived gliogenic neural stem/progenitor cells in functional recovery after spinal cord injury," *PloS one*, vol. 4, p. e7706, 11 2009.

[62] S. Casarosa et al., "Neural stem cells: ready for therapeutic applications?," *Molecular and cellular therapies*, vol. 2, pp. 31–31, 2014.

[63] A. Trounson and C. McDonald, "Stem cell therapies in clinical trials: Progress and challenges," *Cell Stem Cell*, vol. 17, no. 1, pp. 11–22, 2015.

[64] B. J. Cummings et al., "Human neural stem cells differentiate and promote locomotor recovery in spinal cord-injured mice," *Proc Natl Acad Sci U S A*, vol. 102, no. 39, pp. 14069–74, 2005.

[65] H. S. Keirstead et al., "Human embryonic stem cell-derived oligodendrocyte progenitor cell transplants remyelinate and restore locomotion after spinal cord injury," *The Journal of Neuroscience*, vol. 25, no. 19, p. 4694, 2005.

[66] P. Riess et al., "Transplanted neural stem cells survive, differentiate, and improve neurological motor function after experimental traumatic brain injury," *Neurosurgery*, vol. 51, no. 4, pp. 1043–52; discussion 1052–4, 2002.

[67] S. Pluchino et al., "Neural stem cells and their use as therapeutic tool in neurological disorders," *Brain Res Brain Res Rev*, vol. 48, no. 2, pp. 211–9, 2005.

[68] J. A. Steinbeck and L. Studer, "Moving stem cells to the clinic: potential and limitations for brain repair," *Neuron*, vol. 86, no. 1, pp. 187–206, 2015.

[69] M. H. Amer et al., "Translational considerations in injectable cell-based therapeutics for neurological applications: concepts, progress and challenges," *npj Regenerative Medicine*, vol. 2, no. 1, p. 23, 2017.

[70] C. S. Bjornsson et al., "It takes a village: constructing the neurogenic niche," *Dev Cell*, vol. 32, no. 4, pp. 435–46, 2015.

[71] S. J. Morrison and A. C. Spradling, "Stem cells and niches: mechanisms that promote stem cell maintenance throughout life," *Cell*, vol. 132, no. 4, pp. 598–611, 2008.

[72] I. Kazanis et al., "Quiescence and activation of stem and precursor cell populations in the subependymal zone of the mammalian brain are associated with distinct cellular and extracellular matrix signals," *J Neurosci*, vol. 30, no. 29, pp. 9771–81, 2010.

[73] I. Decimo et al., "Neural stem cell niches in health and diseases," *Curr Pharm Des*, vol. 18, no. 13, pp. 1755–83, 2012.

[74] I. Kazanis and C. ffrench Constant, "Extracellular matrix and the neural stem cell niche," *Dev Neurobiol*, vol. 71, no. 11, pp. 1006–17, 2011.

[75] M. Aumailley et al., "A simplified laminin nomenclature," *Matrix Biol*, vol. 24, no. 5, pp. 326–32, 2005.

[76] K. J. Hamill et al., "Laminin deposition in the extracellular matrix: a complex picture emerges," *Journal of Cell Science*, vol. 122, no. 24, pp. 4409–4417, 2009.

[77] C. S. Barros et al., "Extracellular matrix: functions in the nervous system," *Cold Spring Harb Perspect Biol*, vol. 3, no. 1, p. a005108, 2011.

[78] A. Nirwane and Y. Yao, "Laminins and their receptors in the cns," *Biological Reviews*, vol. 94, no. 1, pp. 283–306, 2019.

[79] A. Domogatskaya et al., "Functional diversity of laminins," *Annu Rev Cell Dev Biol*, vol. 28, pp. 523–53, 2012.

[80] M. Aumailley, "The laminin family," *Cell Adh Migr*, vol. 7, no. 1, pp. 48–55, 2013.

[81] R. Timpl et al., "Structure and function of laminin lg modules," *Matrix Biol*, vol. 19, no. 4, pp. 309–17, 2000.

[82] A. Sonnenberg et al., "Integrin recognition of different cell-binding fragments of laminin (p1, e3, e8) and evidence that alpha 6 beta 1 but not alpha 6 beta 4 functions as a major receptor for fragment e8," *J Cell Biol*, vol. 110, no. 6, pp. 2145–55, 1990.

[83] D. Harrison et al., "Crystal structure and cell surface anchorage sites of laminin alpha1lg4-5," *The Journal of biological chemistry*, vol. 282, no. 15, pp. 11573–11581, 2007.

[84] J. Ishihara et al., "Laminin heparin-binding peptides bind to several growth factors and enhance diabetic wound healing," *Nature Communications*, vol. 9, no. 1, p. 2163, 2018.

[85] E. Hohenester and P. Yurchenco, "Laminins in basement membrane assembly," *Cell adhesion and migration*, vol. 7, 10 2012.

[86] S. Bian, *Cell Adhesion Molecules in Neural Stem Cell and Stem Cell- Based Therapy for Neural Disorders*. 2013.

[87] R. Long Katherine and B. Huttner Wieland, "How the extracellular matrix shapes neural development," *Open Biology*, vol. 9, no. 1, p. 180216, 2019.

[88] F. Mercier et al., "Anatomy of the brain neurogenic zones revisited: fractones and the fibroblast/macrophage network," *J Comp Neurol*, vol. 451, no. 2, pp. 170–88, 2002.

[89] A. Kerever et al., "Novel extracellular matrix structures in the neural stem cell niche capture the neurogenic factor fibroblast growth factor 2 from the extracellular milieu," *Stem Cells*, vol. 25, no. 9, pp. 2146–57, 2007.

[90] W. J. Tyler, "The mechanobiology of brain function," *Nature Reviews Neuroscience*, vol. 13, p. 867, 2012.

[91] J. M. Barnes et al., "Tissue mechanics regulate brain development, homeostasis and disease," *J Cell Sci*, vol. 130, no. 1, pp. 71–82, 2017.

[92] J. L. Wilson and T. C. McDevitt, *Chapter 22 - Biofunctional Hydrogels for Three-Dimensional Stem Cell Culture*, pp. 345–362. Boston: Academic Press, 2017.

[93] C. Regalado-Santiago et al., "Mimicking neural stem cell niche by biocompatible substrates," *Stem cells international*, vol. 2016, pp. 1513285–1513285, 2016.

[94] A. Farrukh et al., "Microenvironments designed to support growth and function of neuronal cells," *Frontiers in Materials*, vol. 5, no. 62, 2018.

[95] S. Kubinova, "Extracellular matrix based biomaterials for central nervous system tissue repair: the benefits and drawbacks," *Neural Regen Res*, vol. 12, no. 9, pp. 1430–1432, 2017.

[96] A. Subramanian et al., "Development of biomaterial scaffold for nerve tissue engineering: Biomaterial mediated neural regeneration," *Journal of biomedical science*, vol. 16, no. 1, pp. 108–108, 2009.

[97] R. Boni et al., "Current and novel polymeric biomaterials for neural tissue engineering," *Journal of biomedical science*, vol. 25, no. 1, pp. 90–90, 2018.

[98] H. Ghuman and M. Modo, "Biomaterial applications in neural therapy and repair," *Chinese Neurosurgical Journal*, vol. 2, 11 2016.

[99] M. J. Cooke et al., "Design of biomaterials to enhance stem cell survival when transplanted into the damaged central nervous system," *Soft Matter*, vol. 6, no. 20, pp. 4988–4998, 2010.

[100] M. W. Tibbitt and K. S. Anseth, "Hydrogels as extracellular matrix mimics for 3d cell culture," *Biotechnol Bioeng*, vol. 103, no. 4, pp. 655–63, 2009.

[101] J. Zhu and R. E. Marchant, "Design properties of hydrogel tissue-engineering scaffolds," *Expert review of medical devices*, vol. 8, no. 5, pp. 607–626, 2011.

[102] K. F. Bruggeman et al., "Harnessing stem cells and biomaterials to promote neural repair," *Br J Pharmacol*, vol. 176, no. 3, pp. 355–368, 2019.

[103] A. I. Teixeira et al., "Getting the right stuff: Controlling neural stem cell state and fate in vivo and in vitro with biomaterials," *Cell Research*, vol. 17, p. 56, 2007.

[104] N. Moriarty et al., "Encapsulation of young donor age dopaminergic grafts in a gdnf-loaded collagen hydrogel further increases their survival, reinnervation, and functional efficacy after intrastriatal transplantation in hemi-parkinsonian rats," *Eur J Neurosci*, vol. 49, no. 4, pp. 487–496, 2019.

[105] M. M. Adil et al., "Engineered hydrogels increase the post-transplantation survival of encapsulated hesc-derived midbrain dopaminergic neurons," *Biomaterials*, vol. 136, pp. 1–11, 2017.

[106] E. M. Ahmed, "Hydrogel: Preparation, characterization, and applications: A review," *Journal of Advanced Research*, vol. 6, no. 2, pp. 105–121, 2015.

[107] I. M. ElSherbiny and M. H. Yacoub, "Hydrogel scaffolds for tissue engineering: Progress and challenges," *Global cardiology science and practice*, vol. 2013, no. 3, pp. 316–342, 2013.

[108] V. A. Kornev et al., "Hydrogel-assisted neuroregeneration approaches towards brain injury therapy: A state-of-the-art review," *Computational and Structural Biotechnology Journal*, vol. 16, pp. 488–502, 2018.

[109] E. Aurand et al., "Defining and designing polymers and hydrogels for neural tissue engineering," *Neuroscience research*, vol. 72, pp. 199–213, 2011.

[110] G. Orive et al., "Biomaterials for promoting brain protection, repair and regeneration," *Nature Reviews Neuroscience*, vol. 10, p. 682, 2009.

[111] K. Saha et al., "Substrate modulus directs neural stem cell behavior," *Biophys J*, vol. 95, no. 9, pp. 4426–38, 2008.

[112] P. C. Georges et al., "Matrices with compliance comparable to that of brain tissue select neuronal over glial growth in mixed cortical cultures," *Biophys J*, vol. 90, no. 8, pp. 3012–8, 2006.

[113] N. D. Leipzig and M. S. Shoichet, "The effect of substrate stiffness on adult neural stem cell behavior," *Biomaterials*, vol. 30, no. 36, pp. 6867–78, 2009.

[114] E. Aurand et al., "Hydrogel formulation determines cell fate of fetal and adult neural progenitor cells," *Stem cell research*, vol. 12, no. 1, pp. 11–23, 2014.

[115] D. E. Discher et al., "Growth factors, matrices, and forces combine and control stem cells," *Science*, vol. 324, no. 5935, pp. 1673–7, 2009.

[116] W. Hu et al., "Advances in crosslinking strategies of biomedical hydrogels," *Biomaterials Science*, vol. 7, no. 3, pp. 843–855, 2019.

[117] S. J. Bidarra et al., "Injectable alginate hydrogels for cell delivery in tissue engineering," *Acta Biomaterialia*, vol. 10, no. 4, pp. 1646–1662, 2014.

[118] B. Niemczyk et al., "Injectable hydrogels as novel materials for central nervous system regeneration," *J Neural Eng*, vol. 15, no. 5, p. 051002, 2018.

[119] M. Gomes et al., *Chapter 6 - Natural Polymers in tissue engineering applications*, pp. 145–192. Burlington: Academic Press, 2008.

[120] R. Cruz-Acuña and A. J. García, "Synthetic hydrogels mimicking basement membrane matrices to promote cell-matrix interactions," *Matrix biology : journal of the International Society for Matrix Biology*, vol. 57-58, pp. 324–333, 2017.

[121] D. Barros, I. F. Amaral, and A. P. Pego, "Biomimetic synthetic self-assembled hydrogels for cell transplantation," *Curr Top Med Chem*, vol. 15, no. 13, pp. 1209–26, 2015.

[122] M. F. Maitz, "Applications of synthetic polymers in clinical medicine," *Biosurface and Biotribology*, vol. 1, no. 3, pp. 161–176, 2015.

[123] M. Parlato et al., "Poly(ethylene glycol) hydrogels with adaptable mechanical and degradation properties for use in biomedical applications," *Macromolecular Bioscience*, vol. 14, no. 5, pp. 687–698, 2014.

[124] J. Zhu, "Bioactive modification of poly(ethylene glycol) hydrogels for tissue engineering," *Biomaterials*, vol. 31, no. 17, pp. 4639–4656, 2010.

[125] E. A. Phelps et al., "Maleimide cross-linked bioactive peg hydrogel exhibits improved reaction kinetics and cross-linking for cell encapsulation and in situ delivery," *Adv Mater*, vol. 24, no. 1, pp. 64–70, 2, 2012.

[126] H. Li et al., "Neural stem cell encapsulation and differentiation in strain promoted crosslinked polyethylene glycol-based hydrogels," *J Biomater Appl*, vol. 32, no. 9, pp. 1222–1230, 2018.

[127] X. B. Kong et al., "Polyethylene glycol as a promising synthetic material for repair of spinal cord injury," *Neural Regen Res*, vol. 12, no. 6, pp. 1003–1008, 2017.

[128] M. J. Mahoney and K. S. Anseth, "Three-dimensional growth and function of neural tissue in degradable polyethylene glycol hydrogels," *Biomaterials*, vol. 27, no. 10, pp. 2265–74, 2006.

[129] U. Freudenberg et al., "A star-peg-heparin hydrogel platform to aid cell replacement therapies for neurodegenerative diseases," *Biomaterials*, vol. 30, no. 28, pp. 5049–60, 2009.

[130] X. Lu et al., "Polyethylene glycol in spinal cord injury repair: a critical review," *Journal of experimental pharmacology*, vol. 10, pp. 37–49, 2018.

[131] C. Lin and K. S. Anseth, "Peg hydrogels for the controlled release of biomolecules in regenerative medicine," *Pharmaceutical Research*, vol. 26, no. 3, pp. 631–643, 2009.

[132] B. D. Mather et al., "Michael addition reactions in macromolecular design for emerging technologies," *Progress in Polymer Science*, vol. 31, no. 5, pp. 487–531, 2006.

[133] S. Lin et al., "Influence of physical properties of biomaterials on cellular behavior," *Pharm Res*, vol. 28, no. 6, pp. 1422–30, 2011.

[134] N. O. Enemchukwu et al., "Synthetic matrices reveal contributions of ecm biophysical and biochemical properties to epithelial morphogenesis," *J Cell Biol*, vol. 212, no. 1, pp. 113–24, 2016.

[135] Y. S. Jo et al., "Tailoring hydrogel degradation and drug release via neighboring amino acid controlled ester hydrolysis," *Soft Matter*, vol. 5, no. 2, pp. 440–446, 2009.

[136] J. Kim et al., "Characterization of the crosslinking kinetics of multi-arm poly(ethylene glycol) hydrogels formed via michael-type addition," *Soft Matter*, vol. 12, no. 7, pp. 2076–85, 2016.

[137] S. P. Zustiak et al., "Influence of cell-adhesive peptide ligands on poly(ethylene glycol) hydrogel physical, mechanical and transport properties," *Acta Biomater*, vol. 6, no. 9, pp. 3404–14, 2010.

[138] U. Hersel et al., "Rgd modified polymers: biomaterials for stimulated cell adhesion and beyond," *Biomaterials*, vol. 24, no. 24, pp. 4385–415, 2003.

[139] S. S. Rao and J. O. Winter, "Adhesion molecule-modified biomaterials for neural tissue engineering," *Frontiers in neuroengineering*, vol. 2, pp. 6–6, 2009.

[140] J. Graf et al., "A pentapeptide from the laminin b1 chain mediates cell adhesion and binds the 67,000 laminin receptor," *Biochemistry*, vol. 26, no. 22, pp. 6896–900, 1987.

[141] K. Tashiro et al., "A synthetic peptide containing the ikvav sequence from the a chain of laminin mediates cell attachment, migration, and neurite outgrowth," *J Biol Chem*, vol. 264, no. 27, pp. 16174–82, 1989.

[142] J. Silva et al., "Fibrin functionalization with synthetic adhesive ligands interacting with $\alpha 6\beta 1$ integrin receptor enhance neurite outgrowth of embryonic stem cell-derived neural stem/progenitors," *Acta Biomaterialia V 59*, pp. 243–256, 2017.

[143] M. Nomizu et al., "Identification of cell binding sites in the laminin alpha 1 chain carboxyl-terminal globular domain by systematic screening of synthetic peptides," *J Biol Chem*, vol. 270, no. 35, pp. 20583–90, 1995.

[144] A. P. Skubitz et al., "Definition of a sequence, ryvvlpr, within laminin peptide f-9 that mediates metastatic fibrosarcoma cell adhesion and spreading," *Cancer Res*, vol. 50, no. 23, pp. 7612–22, 1990.

[145] J. C. Schense and J. A. Hubbell, "Three-dimensional migration of neurites is mediated by adhesion site density and affinity," *J Biol Chem*, vol. 275, no. 10, pp. 6813–8, 2000.

[146] P. M. Kharkar et al., "Designing degradable hydrogels for orthogonal control of cell microenvironments," *Chem Soc Rev*, vol. 42, no. 17, pp. 7335–72, 2013.

[147] E. J. Berns et al., "Aligned neurite outgrowth and directed cell migration in self-assembled monodomain gels," *Biomaterials*, vol. 35, no. 1, pp. 185–95, 2014.

[148] W. Sun et al., "Viability and neuronal differentiation of neural stem cells encapsulated in silk fibroin hydrogel functionalized with an ikvav peptide," *J Tissue Eng Regen Med*, vol. 11, no. 5, pp. 1532–1541, 2017.

[149] Y. Sun et al., "Functional self-assembling peptide nanofiber hydrogels designed for nerve degeneration," *ACS Appl Mater Interfaces*, vol. 8, no. 3, pp. 2348–59, 2016.

[150] J. Lam et al., "Hydrogel design of experiments methodology to optimize hydrogel for ipsc-npc culture," *Adv Healthc Mater*, vol. 4, no. 4, pp. 534–9, 2015.

[151] A. Bento, *Improving neurite outgrowth in 3D hydrogel matrices by mimicking cell receptor-ECM interactions occurring in neurogenic niches: an engineering approach to develop more efficient neural stem cell hydrogel carriers.* Doctoral thesis, 2018.

[152] M. Hiraoka et al., "Enhanced survival of neural cells embedded in hydrogels composed of collagen and laminin-derived cell adhesive peptide," *Bioconjugate Chemistry*, vol. 20, no. 5, pp. 976–983, 2009.

[153] T. Nakaji-Hirabayashi et al., "Improvement of neural stem cell survival in collagen hydrogels by incorporating laminin-derived cell adhesive polypeptides," *Bioconjugate Chemistry*, vol. 23, no. 2, pp. 212–221, 2012.

[154] T. Nakaji-Hirabayashi et al., "In vivo study on the survival of neural stem cells transplanted into the rat brain with a collagen hydrogel that incorporates laminin-derived polypeptides," *Bioconjug Chem*, vol. 24, no. 11, pp. 1798–804, 2013.

[155] S. Kubinova et al., "The use of superporous ac-cggasikvavs-oh-modified phema scaffolds to promote cell adhesion and the differentiation of human fetal neural precursors," *Biomaterials*, vol. 31, no. 23, pp. 5966–75, 2010.

[156] X. Li et al., "Short laminin peptide for improved neural stem cell growth," *Stem Cells Transl Med*, vol. 3, no. 5, pp. 662–70, 2014.

[157] A. Farrukh et al., "Bifunctional hydrogels containing the laminin motif ikvav promote neurogenesis," *Stem Cell Reports*, vol. 9, no. 5, pp. 1432–1440, 2017.

[158] A. Farrukh et al., "In situ, light-guided axon growth on biomaterials via photoactivatable laminin peptidomimetic ik(hanbp)vav," *ACS Applied Materials and Interfaces*, vol. 10, no. 48, pp. 41129–41137, 2018.

[159] E. M. Ovadia et al., "Designing well-defined photopolymerized synthetic matrices for three-dimensional culture and differentiation of induced pluripotent stem cells," *Biomater Sci*, vol. 6, no. 6, pp. 1358–1370, 2018.

[160] T. Zhao et al., "Tunable, injectable hydrogels based on peptide-cross-linked, cyclized polymer nanoparticles for neural progenitor cell delivery," *Biomacromolecules*, vol. 18, no. 9, pp. 2723–2731, 2017.

[161] L. A. Flanagan, L. M. Rebaza, S. Derzic, P. H. Schwartz, and E. S. Monuki, "Regulation of human neural precursor cells by laminin and integrins," *J Neurosci Res*, vol. 83, no. 5, pp. 845–56, 2006.

[162] L. E. Oikari, R. K. Okolicsanyi, A. Qin, C. Yu, L. R. Griffiths, and L. M. Haupt, "Cell surface heparan sulfate proteoglycans as novel markers of human neural stem cell fate determination," *Stem Cell Res*, vol. 16, no. 1, pp. 92–104, 2016.

[163] F. E. Poulain and H. J. Yost, "Heparan sulfate proteoglycans: a sugar code for vertebrate development?," *Development*, vol. 142, no. 20, p. 3456, 2015.

[164] M. Ford-Perriss et al., "Localisation of specific heparan sulfate proteoglycans during the proliferative phase of brain development," *Dev Dyn*, vol. 227, no. 2, pp. 170–84, 2003.

[165] Y. Choi et al., "Syndecans as cell surface receptors: Unique structure equates with functional diversity," *Matrix Biol*, vol. 30, no. 2, pp. 93–9, 2011.

[166] N. A. Afratis et al., "Syndecans - key regulators of cell signaling and biological functions," *Febs j*, vol. 284, no. 1, pp. 27–41, 2017.

[167] H. Chung et al., "Minireview: Syndecans and their crucial roles during tissue regeneration," *FEBS Lett*, vol. 590, no. 15, pp. 2408–17, 2016.

[168] D. Barros, *Engineered platforms with site-specific immobilized laminin for neural applications*. Doctoral thesis, 2019.

[169] X. Xian et al., "Syndecans as receptors and organizers of the extracellular matrix," *Cell Tissue Res*, vol. 339, no. 1, pp. 31–46, 2010.

[170] Q. Wang et al., "The niche factor syndecan-1 regulates the maintenance and proliferation of neural progenitor cells during mammalian cortical development," *PLoS One*, vol. 7, no. 8, p. e42883, 2012.

[171] L. Morizur et al., "Distinct molecular signatures of quiescent and activated adult neural stem cells reveal specific interactions with their microenvironment," *Stem Cell Reports*, vol. 11, no. 2, pp. 565–577, 2018.

[172] A. Kinnunen et al., "N-syndecan and hb-gam (heparin-binding growth-associated molecule) associate with early axonal tracts in the rat brain," *Eur J Neurosci*, vol. 10, no. 2, pp. 635–48, 1998.

[173] T. Kinnunen et al., "Neurite outgrowth in brain neurons induced by heparin-binding growth-associated molecule (hb-gam) depends on the specific interaction of hb-gam with heparan sulfate at the cell surface," *J Biol Chem*, vol. 271, no. 4, pp. 2243–8, 1996.

[174] I. M. Ethell and Y. Yamaguchi, "Cell surface heparan sulfate proteoglycan syndecan-2 induces the maturation of dendritic spines in rat hippocampal neurons," *J Cell Biol*, vol. 144, no. 3, pp. 575–86, 1999.

[175] M. P. Hoffman et al., "Laminin-1 and laminin-2 g-domain synthetic peptides bind syndecan-1 and are involved in acinar formation of a human submandibular gland cell line," *J Biol Chem*, vol. 273, no. 44, pp. 28633–41, 1998.

[176] L. N. Gama-de-Souza et al., "Adhesion and protease activity in cell lines from human salivary gland tumors are regulated by the laminin-derived peptide ag73, syndecan-1 and beta1 integrin," *Matrix Biol*, vol. 27, no. 5, pp. 402–19, 2008.

[177] N. Suzuki et al., "Syndecan binding sites in the laminin alpha1 chain g domain," *Biochemistry*, vol. 42, no. 43, pp. 12625–33, 2003.

[178] Y. Yamada et al., "Cell behavior on protein matrices containing laminin alpha1 peptide ag73," *Biomaterials*, vol. 32, no. 19, pp. 4327–35, 2011.

[179] M. P. Hoffman et al., "Cell type-specific differences in glycosaminoglycans modulate the biological activity of a heparin-binding peptide (rkrlqvqlsirt) from the g domain of the laminin alpha1 chain," *J Biol Chem*, vol. 276, no. 25, pp. 22077–85, 2001.

[180] B. L. Richard et al., "Identification of synthetic peptides derived from laminin alpha1 and alpha2 chains with cell type specificity for neurite outgrowth," *Exp Cell Res*, vol. 228, no. 1, pp. 98–105, 1996.

[181] Y. Yamada et al., "Biological activity of laminin peptide-conjugated alginate and chitosan matrices," *Biopolymers*, vol. 94, no. 6, pp. 711–20, 2010.

[182] Y. Yamada et al., "Laminin-111-derived peptide-hyaluronate hydrogels as a synthetic basement membrane," *Biomaterials*, vol. 34, no. 28, pp. 6539–47, 2013.

[183] Y. Yamada et al., "Laminin active peptide/agarose matrices as multifunctional biomaterials for tissue engineering," *Biomaterials*, vol. 33, no. 16, pp. 4118–25, 2012.

[184] Y. Yamada et al., "Cell behavior on protein matrices containing laminin alpha1 peptide ag73," *Biomaterials*, vol. 32, pp. 4327–35, 2011.

[185] K. Hozumi et al., "Mixed peptide-chitosan membranes to mimic the biological activities of a multifunctional laminin alpha1 chain lg4 module," *Biomaterials*, vol. 30, no. 8, pp. 1596–603, 2009.

[186] D. Otagiri et al., "Cell attachment and spreading activity of mixed laminin peptide–chitosan membranes," *Peptide Science*, vol. 100, no. 6, pp. 751–759, 2013.

[187] M. V. Tsurkan et al., "Defined polymer–peptide conjugates to form cell-instructive starpeg–heparin matrices in situ," *Advanced Materials*, vol. 25, no. 18, pp. 2606–2610, 2013.

[188] R. C. M. Rubinstein, *Polymer physics*. Oxford University Press, 2003.

[189] C. T. Rueden et al., "Imagej2: Imagej for the next generation of scientific image data," *BMC Bioinformatics*, vol. 18, no. 1, p. 529, 2017.

[190] J. Schindelin et al., "Fiji: an open-source platform for biological-image analysis," *Nature Methods*, vol. 9, p. 676, 2012.

[191] Sternberg, "Biomedical image processing," *Computer*, vol. 16, no. 1, pp. 22–34, 1983.

[192] D. Legland et al., "Morpholibj: integrated library and plugins for mathematical morphology with imagej," *Bioinformatics*, vol. 32, no. 22, pp. 3532–3534, 2016.

[193] F. Meyer and S. Beucher, "Morphological segmentation," *Journal of Visual Communication and Image Representation*, vol. 1, no. 1, pp. 21–46, 1990.

[194] J. N. Kapur et al., "A new method for gray-level picture thresholding using the entropy of the histogram," *Computer Vision, Graphics, and Image Processing*, vol. 29, no. 3, pp. 273–285, 1985.

[195] W. M. Han et al., "Synthetic matrix enhances transplanted satellite cell engraftment in dystrophic and aged skeletal muscle with comorbid trauma," *Sci Adv*, vol. 4, no. 8, p. eaar4008, 2018.

[196] D. Barros et al., "Engineering hydrogels with affinity-bound laminin as 3d neural stem cell culture systems," *(submitted)*, 2019.

[197] J. D. Weaver et al., "Vasculogenic hydrogel enhances islet survival, engraftment, and function in leading extrahepatic sites," *Science Advances*, vol. 3, no. 6, p. e1700184, 2017.

[198] R. Cruz-Acuña et al., "Synthetic hydrogels for human intestinal organoid generation and colonic wound repair," *Nature Cell Biology*, vol. 19, p. 1326, 2017.

[199] J. Patterson and J. A. Hubbell, "Enhanced proteolytic degradation of molecularly engineered peg hydrogels in response to mmp-1 and mmp-2," *Biomaterials*, vol. 31, no. 30, pp. 7836–45, 2010.

[200] A. R. Bento et al., "Three-dimensional culture of single embryonic stem-derived neural/stem progenitor cells in fibrin hydrogels: neuronal network formation and matrix remodelling," *J Tissue Eng Regen Med*, vol. 11, no. 12, pp. 3494–3507, 2017.

[201] T. L. Laundos et al., "Rotary orbital suspension culture of embryonic stem cell-derived neural stem/progenitor cells: impact of hydrodynamic culture on aggregate yield, morphology and cell phenotype," *J Tissue Eng Regen Med*, vol. 11, no. 8, pp. 2227–2240, 2017.

[202] D. Barros, A. J. García, I. Amaral, and A. Pêgo, "Ag73-functionalized synthetic hydrogels support neural stem cell survival, proliferation and neurite outgrowth," Under preparation.

[203] L. E. Jansen et al., "Control of thiol-maleimide reaction kinetics in peg hydrogel networks," *Acta Biomater*, vol. 70, pp. 120–128, 2018.

[204] N. Darling et al., "Controlling the kinetics of thiol-maleimide michael-type addition gelation kinetics for the generation of homogenous poly(ethylene glycol) hydrogels," *Biomaterials*, vol. 101, pp. 199–206, 2016.

[205] P. Kang et al., "Novel biomaterials to study neural stem cell mechanobiology and improve cell-replacement therapies," *Current opinion in biomedical engineering*, vol. 4, pp. 13–20, 2017.

[206] A. Banerjee et al., "The influence of hydrogel modulus on the proliferation and differentiation of encapsulated neural stem cells," *Biomaterials*, vol. 30, no. 27, pp. 4695–4699, 2009.

[207] L. A. Flanagan et al., "Neurite branching on deformable substrates," *Neuroreport*, vol. 13, no. 18, pp. 2411–5, 2002.

[208] Y. Tsou et al., "Hydrogel as a bioactive material to regulate stem cell fate," *Bioactive Materials*, vol. 1, no. 1, pp. 39–55, 2016.

[209] J. M. Stukel and R. K. Willits, "The interplay of peptide affinity and scaffold stiffness on neuronal differentiation of neural stem cells," *Biomed Mater*, vol. 13, no. 2, p. 024102, 2018.

[210] P. Sunthar, *Polymer Rheology*, pp. 171–191. New York, NY: Springer New York, 2010.

[211] S. P. Zustiak and J. B. Leach, "Hydrolytically degradable poly(ethylene glycol) hydrogel scaffolds with tunable degradation and mechanical properties," *Biomacromolecules*, vol. 11, no. 5, pp. 1348–1357, 2010.

[212] O. Okay, *General Properties of Hydrogels*, pp. 1–14. Berlin, Heidelberg: Springer Berlin Heidelberg, 2010.

[213] S. Lin-Gibson et al., "Structure-property relationships of photopolymerizable poly(ethylene glycol) dimethacrylate hydrogels," *Macromolecules*, vol. 38, no. 7, pp. 2897–2902, 2005.

[214] S. P. Zustiak et al., "Protein–hydrogel interactions in tissue engineering: Mechanisms and applications," *Tissue Engineering Part B: Reviews*, vol. 19, no. 2, pp. 160–171, 2012.

[215] S. Naficy and G. M. Spinks, *Hydrogel Network Parameters*, book section 3. Boca Raton: CRC Press, 1st ed., 2018.

[216] M. P. Lutolf and J. A. Hubbell, "Synthesis and physicochemical characterization of end-linked poly(ethylene glycol)-co-peptide hydrogels formed by michael-type addition," *Biomacromolecules*, vol. 4, no. 3, pp. 713–22, 2003.

[217] G. P. Raeber et al., "Molecularly engineered peg hydrogels: a novel model system for proteolytically mediated cell migration," *Biophysical journal*, vol. 89, no. 2, pp. 1374–1388, 2005.

[218] G. Invitrogen, "Human neural stem cells (h9 hesc-derived," *Invitrogen, Editor*.

[219] S. Suzuki et al., "The neural stem/progenitor cell marker nestin is expressed in proliferative endothelial cells, but not in mature vasculature," *The journal of histochemistry and cytochemistry : official journal of the Histochemistry Society*, vol. 58, no. 8, pp. 721–730, 2010.

[220] T. Scholzen and J. Gerdes, "The ki-67 protein: from the known and the unknown," *J Cell Physiol*, vol. 182, no. 3, pp. 311–22, 2000.

[221] N. Kee et al., "The utility of ki-67 and brdu as proliferative markers of adult neurogenesis," *J Neurosci Methods*, vol. 115, no. 1, pp. 97–105, 2002.

[222] L. P. Weiner, *Neural Stem Cells: Methods and Protocols*. 2008.

[223] X. Han et al., "Efficient and fast differentiation of human neural stem cells from human embryonic stem cells for cell therapy," *Stem Cells International*, vol. 2017, p. 11, 2017.

[224] W. Ma et al., "Cell-extracellular matrix interactions regulate neural differentiation of human embryonic stem cells," *BMC Developmental Biology*, vol. 8, no. 1, p. 90, 2008.

[225] S. Biswas et al., "Development of glial restricted human neural stem cells for oligodendrocyte differentiation in vitro and in vivo," *Scientific reports*, vol. 9, no. 1, pp. 9013–9013, 2019.

[226] J. G. Izant and J. R. McIntosh, "Microtubule-associated proteins: a monoclonal antibody to map2 binds to differentiated neurons," *Proc Natl Acad Sci U S A*, vol. 77, no. 8, pp. 4741–5, 1980.

[227] G. Huber and A. Matus, "Differences in the cellular distributions of two microtubule-associated proteins, map1 and map2, in rat brain," *J Neurosci*, vol. 4, no. 1, pp. 151–60, 1984.

[228] L. De Filippis et al., "A novel, immortal, and multipotent human neural stem cell line generating functional neurons and oligodendrocytes," *Stem Cells*, vol. 25, no. 9, pp. 2312–21, 2007.

[229] L. E. Oikari et al., "Data defining markers of human neural stem cell lineage potential," *Data in brief*, vol. 7, pp. 206–215, 2016.

[230] P. D. Yurchenco et al., "Laminin polymerization in vitro. evidence for a two-step assembly with domain specificity," *J Biol Chem*, vol. 260, no. 12, pp. 7636–44, 1985.

[231] Y. S. Cheng et al., "Self-assembly of laminin isoforms," *J Biol Chem*, vol. 272, no. 50, pp. 31525–32, 1997.

[232] K. J. Hamill et al., "Laminin deposition in the extracellular matrix: a complex picture emerges," *Journal of cell science*, vol. 122, no. Pt 24, pp. 4409–4417, 2009.

[233] T. Schwindt et al., "Effects of fgf-2 and egf removal on the differentiation of mouse neural precursor cells," *An Acad Bras Cienc*, vol. 81, no. 3, pp. 443–52, 2009.

[234] E. Bakaic et al., "Injectable hydrogels based on poly(ethylene glycol) and derivatives as functional biomaterials," *RSC Advances*, vol. 5, no. 45, pp. 35469–35486, 2015.

[235] A. J. Garcia, "Peg-maleimide hydrogels for protein and cell delivery in regenerative medicine," *Ann Biomed Eng*, vol. 42, no. 2, pp. 312–22, 2014.

[236] D. P. Nair et al., "The thiol-michael addition click reaction: A powerful and widely used tool in materials chemistry," *Chemistry of Materials*, vol. 26, no. 1, pp. 724–744, 2014.

[237] A. Metters and J. Hubbell, "Network formation and degradation behavior of hydrogels formed by michael-type addition reactions," *Biomacromolecules*, vol. 6, no. 1, pp. 290–301, 2005.

[238] R. Cruz-Acuña et al., "Peg-4mal hydrogels for human organoid generation, culture, and in vivo delivery," *Nature Protocols*, vol. 13, no. 9, pp. 2102–2119, 2018.

[239] M. P. Lutolf et al., "Systematic modulation of michael-type reactivity of thiols through the use of charged amino acids," *Bioconjugate Chemistry*, vol. 12, no. 6, pp. 1051–1056, 2001.

[240] X. Chen et al., "High glucose inhibits neural stem cell differentiation through oxidative stress and endoplasmic reticulum stress," *Stem Cells Dev*, vol. 27, no. 11, pp. 745–755, 2018.

[241] E. Mauri et al., "Evaluation of rgd functionalization in hybrid hydrogels as 3d neural stem cell culture systems," *Biomaterials Science*, vol. 6, no. 3, pp. 501–510, 2018.

[242] C. M. Madl et al., "Maintenance of neural progenitor cell stemness in 3d hydrogels requires matrix remodelling," *Nature Materials*, vol. 16, p. 1233, 2017.